2016

Reverse micelles: Functionalizing, cross-linking, entrapment and applications

Premkumar Rathinam Arivalagan
Iowa State University

Reverse micelles: Functionalizing, cross-linking, entrapment and applications

by

Premkumar Rathinam Arivalagan

A dissertation submitted to the graduate faculty

in partial fulfillment of the requirements for the degree of

DOCTOR OF PHILOSOPHY

Major: Chemistry

Program of Study Committee:

Yan Zhao, Major Professor

Levi Stanley

Brett VanVeller

Keith Woo

Wenyu Huang

Iowa State University

Ames, Iowa

2016

TABLE OF CONTENTS

ACKNOWLEDGEMENTS iii

CHAPTER 1. GENERAL INTRODUCTION 1

Dissertation Organization 1
Background 1
References 4

CHAPTER 2. INTERFACIALLY CATALYSIS OF ALDOL REACTIONS BY PROLINAMIDE SURFACTANTS IN REVERSE MICELLES 6
Abstract 6
Introduction 6
Results and discussion 8
Conclusion 19
Experimental Section 19
References 30

CHAPTER 3. PHYSICAL ENTRAPMENT OF WATER-SOLUBLE FLUORESCENT DYES BY INTERFACIALLY CROSS-LINKED REVERSE MICELLES 37
Abstract 37
Introduction 37
Results and discussion 40
Conclusion 47
Experimental Section 48
References: 64

CHAPTER 4. ENHANCEMENT OF CATALYTIC ACTIVITY AND SELECTIVITY OF MANGANESE PORPHYRIN CATALYSTS UPON ENTRAMENT IN INTERFACIALLY CROSS-LINKED REVERSE MICELLES (ICRM) 68
Abstract 68
Introduction 68
Results and discussion 70
Conclusion 77
Experimental Section 78
References 84

CHAPTER 5. ENHANCEMENT OF CATALYTIC ACTIVITY AND SELECTIVITY OF $Pt(TPPTS)_2Cl_2$ IN INTERFACIALLY CROSS-LINKED REVERSE MICELLES 86
Abstract 86
Introduction 86
Results and Discussion: 87
Conclusion 92
Experimental Section 92
References 94

ACKNOWLEDGEMENTS

First and foremost, I would like to thank my adviser, Prof. Yan Zhao for supporting and guiding me throughout my five years in his lab. Weekly meetings and preparing weekly reports helped me grow in research and to develop a strong work ethic that will be important to my career ahead. I would also like to thank Prof. Keith Woo, Prof. Wenyu Huang, Prof. Levi Stanley, and Prof. Brett VanVeller for encouraging me and being part of my POS committee. I am deeply thankful to all my lab mates and friends for supporting me. Finally, this wouldn't have been possible without the support from my parents and family.

CHAPTER 1. GENERAL INTRODUCTION

Dissertation Organization

In the first chapter, a brief background in the formation of reverse micelles and their applications was presented, followed by the formation and applications of interfacially crossed-linked reverse micelles(ICRM) in catalysis. In the second chapter, self-assembly of proline surfactants and its application in aldol reaction were discussed. Prolinamide-functionalized surfactants catalyzed aldol reaction in a nonpolar solvent in the reverse-micelle form. The reverse micelle nanostructure creates a high local concentration of prolinamide, which catalyzes aldol reaction co-operatively. In polar DMSO, the surfactants exist as individual molecules and lose their catalytic activity. In the third chapter, hydrophilic dyes were trapped in the core of the ICRM to help understand the micropolarity of the ICRM. In the fourth chapter, the site isolation of catalysts by ICRM was demonstrated for manganese porphyrins that are known to dimerize and deactivate. ICRM-entrapped catalysts showed enhanced catalytic activity than their free counterparts. In the fifth chapter, the advantage of ICRM over uncross-linked reverse micelle and its selectivity towards hydrophilic substrates were demonstrated by trapping $PtCl_2(TPPTS)_2$ in the core of the ICRM. This catalyst was used to catalyze hydration of alkynes. Since water is a reactant and can be concentrated in the core of the ICRM, the catalyst showed enhanced catalytic activity and selectivity towards hydrophilic substrates.

Background

Enzymes are the most efficient catalysts known to chemists. Enzymes use some interesting strategies for their efficient catalysis. The following are some of the important factors responsible for the catalytic activity of enzymes.

1) **Cooperative function of one or more functional groups**

The catalytic triad of trypsin contains an imidazole, a carboxylic acid and an alcohol. These three groups function cooperatively to catalyze the hydrolysis of the amide at the carboxyl side of lysine and arginine. Folding of the peptide chain brings the functional groups into proximity to function cooperatively. It is also known that enzymes lose their catalytic activity upon denaturation, which implies the importance of the superstructure of the active site.

2) **Site isolation of the active site**

The active site of an enzyme is site-isolated. This feature not only gives the enzyme selectivity but also prevents deactivation pathways such as dimerization. For instance, manganese porphyrin of cytochrome P450 is stable and selective over many catalytic cycles but the free manganese porphyrin gets deactivated quickly in solution by Mn-O-Mn μ oxo-bridge formation.

Inspired by the biological examples, scientists designed systems that incorporate these features into synthetic materials to better understand the functions of the enzymes and to achieve superior selectivity and activity in synthetic catalysts.

Cooperativity

Self-assembly is often used to introduce cooperativity to a system. Micelles, reverse micelles, and vesicles are well-known molecular self-assemblies. If the surfactant carries a functional group, self-assembling would create a high local concentration of the functional group. Concentration of a functional group often leads to properties absent in isolated functional groups.[1-2] For example, Miravet and coworkers recently reported enhanced catalysis of hydrogel formed from proline-functionalized monomers.[1-2] The monomers did not show any catalytic activity in organic solvent.

Barbas and coworkers reported catalysis of micelles formed by proline-functionalized surfactants. Micelle formation was found to enhance both the catalytic activity and enantioselectivity.[4] Inspired by these examples, three proline-functionalized surfactants were synthesized and their catalytic properties were explored upon formation of reverse micelles. Surfactants were designed to demonstrate how noncovalent interactions among the headgroups influenced their aggregation tendency and their catalytic efficiency.

Site-isolation:

Many structures could be used to site-isolate a catalyst, including macrocycles, metal organic frameworks (MOFs), and self-assembled molecules. [10] Macrocycles can encapsulate molecules in solution, but the complexes are dynamic and must be designed specifically for different guest molecules. Heterogeneous materials such as MOFs have inherent mass transfer problems when the substrate accesses the catalytic site.

Recently, the Zhao group reported the synthesis of ICRMs. They used a cross-linkable surfactant which can be polymerized under self-assembling conditions. Polymerization at the surface of the micelles yielded surface-cross-linked micelles (SCMs). With a similar strategy in nonpolar solvents, polymerization at the core of reverse micelles yielded ICRMs.[5-6] These materials were used in many applications in catalysis, sensing, and drug delivery.

Reverse micelles can solubilize hydrophilic species such as enzymes in nonpolar solvents through trapping them in their hydrophilic cores.[7-9] In my research, Organic fluorophores were trapped inside ICRMs with the intention that the location and property of the entrapped fluorophore could be studied by fluorescence spectroscopy.

After successful entrapment of hydrophilic dyes, entrapment of a catalyst in the core of the ICRM was explored. Manganese porphyrin catalysts were chosen to demonstrate site isolation of

the catalyst. It is envisioned that this catalyst upon entrapment by ICRM should show enhancement in catalytic activity when deactivation pathways are eliminated.

Selectivity:

Enzymes achieve selectivity by selectively binding the substrates. In the case of macrocycles and porous materials, selectivity was achieved by the size of the cavity and the pore. The core of the ICRM is hydrophilic. If a hydrophilic catalyst stays in the hydrophilic core, polarity-mediated selectivity can be achieved. The catalyst would be highly selective to hydrophilic substrates.

References

1. Rodriguez-Llansola, F.; Miravet, J. F.; Escuder, B., A supramolecular hydrogel as a reusable heterogeneous catalyst for the direct aldol reaction. *Chemical Communications* **2009,** (47), 7303-7305.

2. Rodríguez-Llansola, F.; Escuder, B.; Miravet, J. F., Switchable Perfomance of an l-Proline-Derived Basic Catalyst Controlled by Supramolecular Gelation. *Journal of the American Chemical Society* **2009,** *131* (32), 11478-11484.

3. Blahovec, J., [Determination of the enzymatic activity of trypsin and chymotrypsin using denatured 125I-labeled albumin]. *Veterinarni medicina* **1980,** *25* (5), 305-11.

4. Mase, N.; Nakai, Y.; Ohara, N.; Yoda, H.; Takabe, K.; Tanaka, F.; Barbas, C. F., Organocatalytic Direct Asymmetric Aldol Reactions in Water. *Journal of the American Chemical Society* **2006,** *128* (3), 734-735.

5. Zhang, S.; Zhao, Y., Facile Synthesis of Multivalent Water-Soluble Organic Nanoparticles via "Surface Clicking" of Alkynylated Surfactant Micelles. *Macromolecules* **2010,** *43* (9), 4020-4022.

6. Zhang, S.; Zhao, Y., Template Synthesis of Subnanometer Gold Clusters in Interfacially Cross-Linked Reverse Micelles Mediated by Confined Counterions. *Langmuir* **2012,** *28* (7), 3606-3613.

7. Lee, L.-C.; Zhao, Y., Interfacially Cross-Linked Reverse Micelles as Soluble Support for Palladium Nanoparticle Catalysts. *Helvetica Chimica Acta* **2012,** *95* (6), 863-871.

8. Lee, L.-C.; Zhao, Y., Room Temperature Hydroamination of Alkynes Catalyzed by Gold Clusters in Interfacially Cross-Linked Reverse Micelles. *ACS Catalysis* **2014,** *4* (2), 688-691.

9. Lee, L.-C.; Zhao, Y., Metalloenzyme-Mimicking Supramolecular Catalyst for Highly Active and Selective Intramolecular Alkyne Carboxylation. *Journal of the American Chemical Society* **2014,** *136* (15), 5579-5582.

10. Merlau, M. L.; del Pilar Mejia, M.; Nguyen, S. T.; Hupp, J. T., Artificial Enzymes Formed through Directed Assembly of Molecular Square Encapsulated Epoxidation Catalysts. *Angewandte Chemie International Edition* **2001,** *40* (22), 4239-4242.

CHAPTER 2. INTERFACIALLY CATALYSIS OF ALDOL REACTIONS BY PROLINAMIDE SURFACTANTS IN REVERSE MICELLES

A Paper published in Org. Biomol. Chem., 2015,13, 770-775.

Premkumar Rathinam Arivalagan and Yan Zhao

Abstract

L-Proline and their derivatives are one of the most important class of organic catalysts. Three prolinamide surfactants were designed and synthesized. Although the surfactants carried identical catalytic groups, their headgroups contained different functionalities that affected their ability to self-assemble under reverse micelle conditions and hydrogen-bond with the reactants. The surfactant with a zwitterionic headgroup capable of strong aggregation was found to have the highest activity. The self-association of the surfactants played critical roles in the enhanced activity. The location of the catalytic groups at the surfactant/polar solvent interface also endowed unusual selectivity in the aldol reactions catalyzed.

Introduction

Chemical reactions depend on not only inherent reactivity of the reactants but also their surrounding environments.[1]In the simplest case, a change of solvent can speed up a sluggish reaction, sometimes thousands of times or more. In biology, enzymes are powerful catalysts capable of promoting reactions that are otherwise impossible. Many times, not only the various functional groups in the active site play critical roles in the catalysis, the unique environment of the active site is also vital. In an effort to understand or mimic enzymatic catalysts, chemists have created molecular capsules to control both the reactivity and the selectivity of reactions.[2-5]Other

promising platforms include dendrimers,[6-8] star polymers,[9-10]organic and metal-organic nanocapsules,[2-5] multifunctional mesoporous materials,[11-14] and metal-organic frameworks.[15-18]

Reverse micelles (RMs) are assemblies of surfactants in nonpolar solvents. A nanometer-sized pool of a polar solvent (often water) in the center of a RM solvates the headgroups of the surfactants to help them self-assemble into spherical structures typically.[19] Because the water molecules in the RM core differ from bulk water in many aspects, chemists have examined many reactions in RM solutions.[19-22] Another usage of RMs is in template synthesis of inorganic nanomaterials.[23-24] Metal salts can be dissolved in the water pools of RMs, followed by desired chemical reactions that are modulated by the surfactant assemblies. Alternatively, inorganic precursors such as tetraethoxysilane can be dissolved in the organic phase and subsequently undergo sol–gel reactions to afford the final inorganic materials.

Our group has a long interest in the environmental control of catalysts. Amphiphilic baskets,[25-26] foldamers,[27] surface-cross-linked micelles,[28-30] and interfacially cross-linked reverse micelles[31-32] have been used to tune the polarity and other properties of the local environments around catalysts to influence their activity and selectivity. In this work, we synthesized several L-prolinamide-derived surfactants and examined their catalysis of aldol reactions in the RM configuration. The catalytic groups located at the surfactant/polar solvent interface were found to have unusual activity and selectivity. The surfactant with the strongest aggregation was the best catalyst, suggesting that the self-assembling of the surfactants was directly responsible for the enhanced catalytic activity.

Results and discussion

Catalyst Design and Synthesis

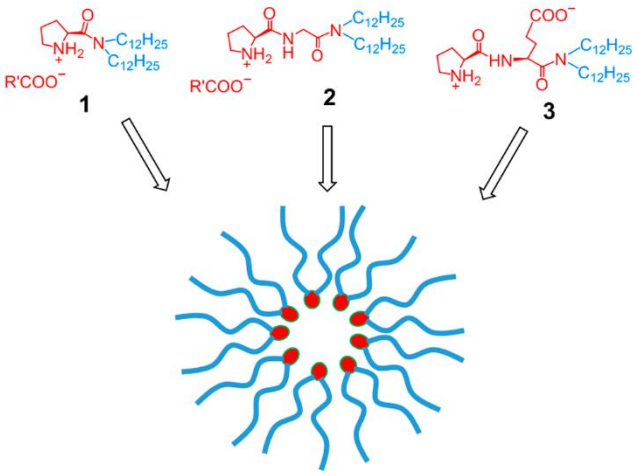

Scheme 1 Structures of prolinamide surfactants and schematic representation of their aggregation in a nonpolar solvent.

L-Proline and their derivatives are one of the most important class of organic catalysts. Having both an acid and a base catalytic group, proline can catalyze a number of important reactions including aldol, Mannich, and Michael reactions.[33-35]Its carboxylic acid is crucial to the catalysis. Converting the carboxyl into amide lowers its catalytic activity for aldol reactions[36]but, with a higher concentration of reactants (e.g., 0.5 M 4-nitrobenzaldehyde in neat acetone), prolinamides could catalyze aldol reactions effectively. Excellent ee could be obtained with prolinamides carrying vicinal hydrogen-bonding groups such as hydroxyl.[37-38]

Chemists have studied proline-catalyzed aldol reactions in surfactant assemblies very early on, interested in whether the surfactant phases could provide special benefits.[39] Although L-proline itself is catalytically ineffective in water, its derivatives with micelle-forming hydrophobic tails work well.[40-42] Polymeric micelles similarly were found to promote the reaction.[43-45]However, to our knowledge, proline-derived catalysts in the RM configuration,

particularly at the interface of surfactant/polar solvent, have not been studied. Because reactivity at the interface can be profoundly different from that in a bulk solution, we decided to synthesize surfactants with proline-derived headgroups so that their organization will place the proline group at the surfactant/polar solvent interface.

Three amphiphiles (**1**–**3**) were synthesized for this purpose, all with two dodecyl tails, resembling the common RM-forming surfactant AOT.[19]Self-assembly of a surfactant strongly depends on its critical packing parameter ($Q = v/a_0l_c$), in which v is the volume of the hydrophobic tail, a_0 the area of the hydrophilic headgroup, and l_c the average critical length of the amphiphile.[46]Two long hydrocarbon chains in **1**–**3** increase their hydrophobic volume and make them pack more easily in the RM configuration. (The long tails are also important to the solubility of the catalysts in nonpolar solvents.)

Surfactant **1** was prepared by coupling the carboxylic acid group of L-proline to didodecylamine. The synthesis involved standard protection/deprotection chemistry, with the amino group of proline protected by Boc initially and deprotected using trifluoroacetic acid after amide coupling. For the catalysis, the surfactant was used as an ammonium salt, with either acetate or benzoate as the counterion. Surfactants **2** and **3** were synthesized similarly, with **2** having a glycine and **3** having a glutamate in between proline and the didodecyl amide.

All three surfactants share the L-prolinamide catalytic functionality. Their difference lies in the potential hydrogen-bonding and electrostatic interactions among the headgroups of the surfactants. Whereas both **1** and **2** have the ammonium and carboxylate (acetate or benzoate) as counterions, surfactant **3** is a zwitterion with the counteranion in the same molecule. Unlike surfactant **1** that has a tertiary amide in the headgroup, surfactants **2** and **3** have secondary amides in the headgroup. For the latter two, the abundance of hydrogen-bond donors and

acceptors in the headgroup should provide additional driving force (in addition to solvation or hydrophobic effect) to the self-assembly of the surfactants in nonpolar solvents.[47-48]

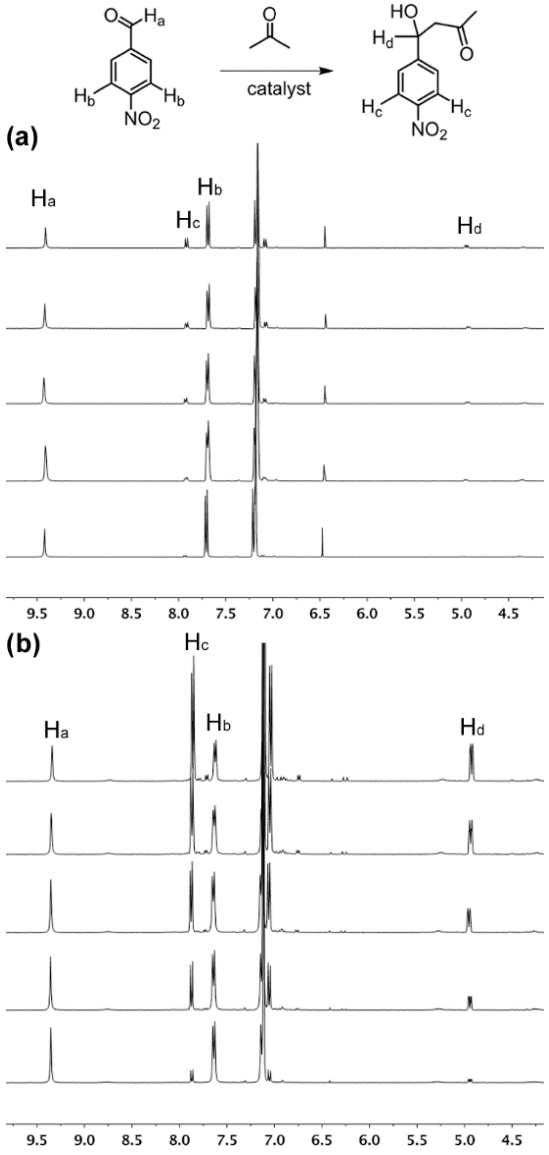

Fig. 1 ^{1}H NMR spectra of the aldol reaction between acetone and *p*-nitrobenzaldehyde catalyzed by **1** (a) and **3** (b) in DMSO-d_6/benzene-d_6 at ambient temperature. Reaction conditions: *p*-nitrobenzaldehyde (0.07 mmol), acetone (0.86 mmol), catalyst (0.007 mmol), benzene-d_6 (1.0 mL), DMSO-d_6 (2.0 μL). The spectra from bottom to top were taken at 0, 45, 100, 145 and 205 for catalysts **1** and at 10, 60, 100, 145 and 190 for catalyst **3**.

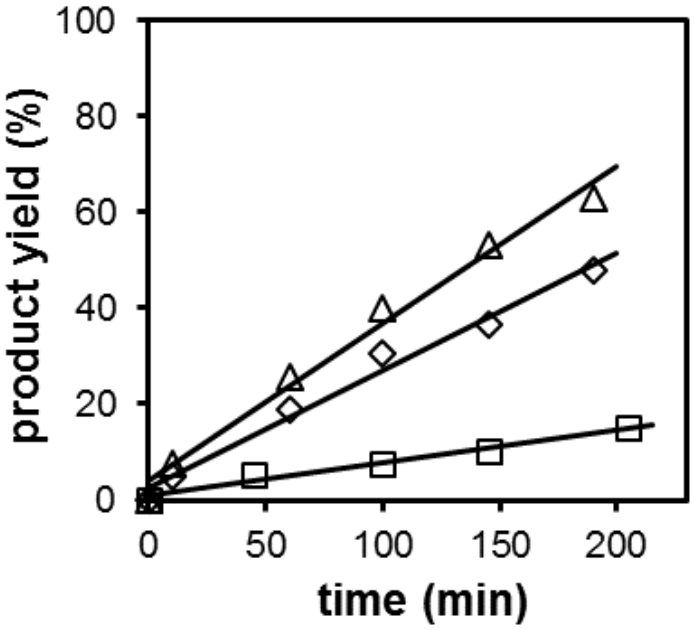

Figure 2. Reaction yields of the aldol reaction between acetone and *p*-nitrobenzaldehyde catalyzed by **1** (□), **2** (◇), and **3** (△) in DMSO-d_6/benzene-d_6 at ambient temperature. Reaction conditions: *p*-nitrobenzaldehyde (0.07 mmol), acetone (0.86 mmol), catalyst (0.007 mmol), benzene-d_6 (1.0 mL), DMSO-d_6 (2.0 μL).

Aldol reactions catalyzed by prolinamide surfactants

Aldol reactions catalyzed by proline and their derivatives are typically performed in DMSO or DMF. Nonpolar solvents such as benzene are rarely used possibly due to insolubility of the catalysts. To perform the reactions under RM conditions, however, we need a small amount of a polar solvent such as water or DMSO in a largely nonpolar mixture.[19] The polar solvent molecules solvate the headgroups of the surfactants to assist their self-assembly, with the hydrophobic tails point outward to be compatible with the nonpolar environment (Scheme 1).

To our delight, all three surfactants were readily soluble in benzene with the help of a tiny amount of polar solvent (e.g., w_0 = [DMSO or water]/[surfactant] = 5). The solution was

completely transparent, suggesting any aggregates formed must be small enough not to cause significant scattering of visible light.

Our model aldol reaction was between acetone and *p*-nitrobenzaldehyde. The reaction is commonly used by researchers in proline-catalyzed reactions.[14–16] As will be shown below, another benefit of the reactant pair is that the simplicity of their ^{1}H NMR peaks makes it straightforward to monitor the reaction progress. In the literature, a high concentration of *p*-nitrobenzaldehyde (e.g., 0.5 M) and a large excess of ketone (sometimes using the ketone as the solvent) are often used in prolinamide-catalyzed aldol reactions,[37-38] due to the low activity of prolinamide in comparison to proline. In our case, the concentration of the aldehyde was 70 mM and a ratio of [acetone]/[*p*-nitrobenzaldehyde] ≈ 12/1 was employed. The catalyst was used at 10 mol % to the aldehyde, which is also lower than many literature examples.

We did not use a huge amount of acetone for two primary reasons. First, acetone is quite polar; a large amount of it could disrupt the self-assembly of the surfactants. Second, this study was mainly aimed to identify whether catalytic groups located at the surfactant/polar solvent interface could behave differently from those in the homogeneous solution. Since the three surfactants have identical catalytic groups, we wanted to put the catalysts under challenging conditions to see their differences. A large excess of acetone (as in typical literature reactions) might overshadow the subtle differences in the catalysts' activity.

The solubility of the surfactants in deuterated DMSO/benzene mixture at $w_0 = 5$ allowed us to monitor the reactions by ^{1}H NMR spectroscopy. Figure 1 showed the progress of the aldol reaction catalyzed by surfactant **1** and **3**. (Kinetics for surfactant **2** was intermediate between those of **1** and **3** and thus not shown.) Despite the identical catalytic functionality, the three surfactants behaved very differently. Surfactant **1** showed negligible activity under our

reaction condition; the product peaks (H_c and H_d) were barely visible even at the end. With **3**, however, the product peaks quickly became major after several hours at room temperature. The activity was quite high, considering the low concentrations of the reactants and (anticipated) low activity of typical prolinamides.[37-38]

An internal standard added (i.e., bistrimethylsilylethane) allowed us to quantify the amount of product formed by integration. Figure 2 shows the yields of the three reactions as a function of time. Because the reaction was performed under pseudo-first-order conditions, good linearity was observed over much of the course of the reaction. These curves clearly show catalyst **3** as the most active and **1** as the least active catalyst. Surfactant **2** was significantly more efficient than **1** as a catalyst for the aldol reaction. Thus, the extra glycine must have helped the catalysis, directly or indirectly. The reason for the higher activity of **2** could be mechanistic. It is known that aldol reactions catalyzed by prolinamides go through an enamine intermediate and the hydrogen bond between the amide proton and the aldehyde is important to the reactivity and enantioselectivity of the reaction.[33-35] Since catalyst **1** had no amide proton being a tertiary amide, the higher activity of **2** could just be normal.

Prolinamide **3** was more active than **2**. Even though the difference in their reaction rates in Figure 2 was not huge, the results suggest that having the carboxylate in the same molecule instead of as a counteranion is beneficial. To further understand the differences in these catalysts and identify the cause for their different activity, we performed our model aldol condensation under a number of different conditions. For these studies, we generally let the reaction proceed at ambient temperature for 9 h and used the product yield as a measure for the efficiency of a catalyst.

Table 1. Reaction yields at 9 h for the aldol reaction between acetone and *p*-nitrobenzaldehyde catalyzed by the prolinamide surfactants under different conditions.[a]

entry	solvent composition	catalyst	counterion	yield
1	w_0 = 5 (DMSO)[b]	**1**	acetate	18
2	w_0 = 5 (DMSO)[b]	**2**	acetate	72
3	w_0 = 5 (DMSO)[b]	**3**	none	88
4	w_0 = 5 (DMSO)[b]	**1**	benzoate	33
5	w_0 = 5 (DMSO)[b]	**2**	benzoate	78
6	w_0 = 5 (DMSO)[b]	none	none	0
7	w_0 = 5 (water)[c]	**1**	benzoate	20
8	w_0 = 5 (water)[c]	**2**	benzoate	33
9	w_0 = 5 (water)[c]	**3**	none	78
10	DMSO/benzene = 1:9	**1**	benzoate	0
11	DMSO/benzene = 1:9	**2**	benzoate	0
12	DMSO/benzene = 1:9	**3**	none	20
13	DMSO/benzene = 9:1	**3**	none	0
14	benzene (no DMSO)	**3**	none	85

[a] Reaction conditions: catalyst (0.007 mmol), *p*-nitrobenzaldehyde (0.07 mmol), acetone (0.86 mmol). [b] Solvent = 2.0 μL DMSO + 1.0 mL benzene. [c] Solvent = 0.5 μL water + 1.0 mL benzene.

The results were illuminating. As shown in Table 1 (entries 1–2 and 4–5), the change of the counterion from acetate to benzoate in the case of **1** and **2** increased the catalytic activity

slightly when the reaction was performed in DMSO/benzene at w_0 = 5. Regardless of the counteranion, **1** and **2** had lower activity than zwitterionic **3** (entry 3). Without the prolinamide surfactants, the reaction did not occur at all, as we had anticipated (entry 6). A small amount of water in the proline-catalyzed aldol reaction is known to help the reactivity but a large amount of water is detrimental.

[33-35]Since, under the RM conditions (i.e., DMSO/benzene at w_0 = 5), the polar solvent should be concentrated near the headgroups of the surfactants in the nonpolar solvent, we were interested to know whether replacing DMSO with water would affect the activity to any significant degree.

It is possible that the high local concentration of the polar solvent could "magnify" the solvent effect near the catalytic headgroups. Indeed, as shown in entries 7–9 of Table 1, the product yields decreased for all three catalysts: from 33 to 20% for **1**, from 78 to 33% for **2**, and from 88 to 78% for **3**. As far as "water resistance" is concerned, it seems prolinamide **3** was the most robust among the three.

DMSO is often the preferred solvent for proline- or prolinamide-catalyzed aldol reactions.[33-35]The conventional thinking, thus, predicts that an increase in DMSO in our reaction mixture at least should not cause problems. On the other hand, if the formation of RM or similarly aggregated states (vide infra) for the catalytic surfactants is important to the observed activity, then the addition of the polar solvent (DMSO) would destabilize the aggregates and reduce the catalytic activity as a result.[49]

The latter turned out to be true. When the amount of DMSO was increased from 2.0 μL (i.e., w_0 = 5) to 100 μL (i.e., DMSO/benzene = 1/9), catalysts **1** and **2** became completely inactive (entries 10 and 11) and catalyst **3** lost significant activity, with the yield going down from 88%

(entry 3) to 20% (entry 12). A further increase of DMSO to DMSO/benzene = 9/1 shut down the activity of **3** entirely (entry 13).

We also found that the polar solvent DMSO was not necessary for the enhanced activity. Without any DMSO, catalyst **3** afforded 85% of the aldol product (entry 14). The yield was experimentally the same as what was observed at w_0 = 5 (entry 3). The results indicate that DMSO itself was not playing any particular roles in the reaction and most likely it was the aggregation of the surfactants that was responsible for the enhanced activity.[50]The postulation is supported by the work of Escuder, Maravet, and co-workers, who demonstrated a bisprolinamide derivative was far more catalytically active for the Henry nitroaldol reaction in the gel state than in solution.[51]The authors attributed the enhanced activity (in the gel) to the higher basicity of the proline amine in the aggregates. It is likely that a similar mechanism was enhancing the catalytic efficiency in our case. The electrostatic and hydrogen-bonding interactions among the headgroups should be the strongest in the zwitterionic **3**, making the surfactant most capable of aggregating and its amine the most basic.

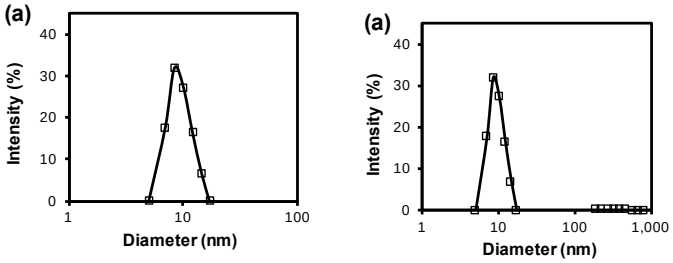

Fig. 3 Dynamic light scattering by the aggregates of **3** in (a) DMSO/heptane and (b) DMSO/benzene at w_0 = [DSMO]/[surfactant] = 5.

Dynamic light scattering (DLS) could detect surfactant aggregates easily while an individual surfactant is generally too small to be observed. To understand the aggregation of these prolinamide surfactants, we first used heptane instead of benzene as the nonpolar solvent

because its nonpolarity facilitates the RM formation.[19]The amount of DMSO was chosen to be w_0 = 5, exactly as that in our typical reactions. DLS under this condition gave poor correlation curves for surfactant **1** and **2** and no stable particles were observed. In contrast, surfactant **3** gave nanoparticles ca. 10 nm in diameter (Figure 3a), reasonable in size for typical RMs.[19]Changing the nonpolar solvent from heptane to benzene (i.e., the reaction solvent system) is expected to make RM formation more difficult. This is because, the miscibility of DMSO and benzene would make phase separation of DMSO into the central core of a RM costlier in free energy. Indeed, instead of small-sized RMs, larger particles ca. 150 nm in size were observed by DLS (Figure 3b). In 1:9 DMSO/benzene, where the activity of the catalyst was severely compromised (Table 1, entry 12), no stable particles could be identified by DLS. In benzene alone, surfactant **3** did aggregate to afford large aggregates > 500 nm in size.

The DLS study thus confirmed surfactant **3** as the one having the strongest aggregation propensity in nonpolar-dominant solvents. The aggregates apparently do not need to be exactly RMs, as the (aggregated) surfactant in benzene (Table 1, entry 14) and in DMSO/benzene at w_0 = 5 (Table 1, entry 3; Figure 3b) both showed good activity.

In addition to catalytic activity, we were interested in the effects of aggregation on other properties such as enantiomeric and substrate selectivity. Chiral HPLC showed low ee for these surfactants (~15%). The number was comparable to those reported for unactivated prolinamides in the literature.[38]Thus, no special effects were exerted by the aggregation on the enantioselectivity of the catalysts.

On the other hand, interesting substrate selectivity was clearly observed for surfactant **3**, our best catalyst (Table 2). Acetone, cyclopentanone, and cyclohexanone were all reactive, with subtle differences in reactivity. The anti/syn ratio of the products was 25/75 and 76/24 for

cyclopentanone and cyclohexanone, respectively. These numbers were comparable to those reported in the literature for other prolinamide catalysts.[52]Thus, neither enantio- nor diastereoselectivty of the reaction was significantly affected by the aggregation.[53] Cycloheptanone and the acyclic 3-pentanone were completely unreactive under the typical reaction conditions (i.e., DMSO in benzene at w_0 = 5). It is not completely clear why such a dramatic substrate effect was present. We suspect that it derives from the location of the catalytic groups at the surfactant/polar solvent interface. Both the initial iminium ion and the enamine intermediates between the ketone and the proline amine need to be formed on the surfactant headgroup in our case. It is possible that the stability of these intermediates may be quite sensitive to the size, hydrophobicity, and/or flexibility of the substrate in the tight space around the aggregated headgroups.

Table 2. Reaction yields at 9 h for the aldol reaction between different ketones and *p*-nitrobenzaldehyde catalyzed by surfactant **3** under reverse micelle conditions.[a]

entry	ketone	catalyst	counterion	yield
1	acetone	**3**	none	88
2	cyclopentanone	**3**	none	>95[b]
3	cyclohexanone	**3**	none	75[c]
4	cycloheptanone	**3**	none	0
5	3-pentanone	**3**	none	0

[a] Reaction conditions: catalyst (0.007 mmol), *p*-nitrobenzaldehyde (0.07 mmol), acetone (0.86 mmol), benzene-d_6 (1.0 mL), DMSO-d_6 (2.0 µL). [b] The anti/syn ratio was determined by ^{1}H NMR spectroscopy to be 25/75. [c] The anti/syn ratio was determined by ^{1}H NMR spectroscopy to be 76/24.

Conclusion

Aggregation of prolinamide surfactants enhanced their catalytic activity dramatically and allowed the reaction to proceed in nonpolar solvents such as benzene (with or without a small amount of DMSO). The observed catalytic activity correlated with the aggregation propensity of the surfactants in DMSO/benzene mixtures. Traditionally, chemists improve the performance of catalysts by manipulating their structures directly, whether the active metal center or the organic catalytic functionality. Nature frequently employs a different approach, by controlling the microenvironment of the catalysts. This work demonstrates that even relatively simple aggregation could enhance the activity of prolinamide dramatically and unusual selectivity could be obtained at the same time. Chemists have already recognized the importance of environmental control on the catalysis. As shown by others[1-3, 54-55] and our recent work,[10–13] there are numerous ways to manipulate the microenvironment around a catalyst and the effect can be profound. We believe that, as chemists further develop their skills in the environmental control in catalysis, unusual reactivity and selectivity seen in enzymatic catalysis can also be realized with synthetic systems.

Experimental Section

General method

All reagents and solvents were of ACS-certified grade or higher and used as received from commercial suppliers. Routine ^{1}H and ^{13}C NMR spectra were recorded on a Bruker DRX-400 or on a Varian VXR-400 spectrometer. HR-MS mass was recorded on Shimadzu LCMS-2010 mass spectrometer. Dynamic light scattering (DLS) was performed on a PD2000DLS+ dynamic light scattering detector.

General procedure for the aldol reaction under RM conditions

DMSO (2.0 µL) was added to a solution of the appropriate prolinamide catalyst (0.007 mmol) in deuterated benzene (1.0 mL) in a vial. The mixture was ultrasonicated until a clear solution was obtained. Bistrimethylsilylethane (10 µL) was added as an internal standard, followed by *p*-nitrobenzaldehyde (10 mg, 0.07 mmol) and acetone (50 µL, 0.86 mmol). The mixture was then transferred to a NMR tube and the reaction was monitored by ^{1}H NMR spectroscopy.

Reaction under normal condition:

To the solution of catalyst, **1** (2.98 mg, 0.007 mmol) and benzoic acid (0.8 mg, 0.007 mmol) was added in deuterated chloroform (1 mL) deuterated DMSO (0.10 mL) was added. P-nitrobenzaldehyde (10 mg, 0.07 mmol) and acetone (0.05 mL, 0.86 mmol) was added and the reaction was transferred to NMR tube and ^{1}H NMR was used to monitor the reaction. Bistrimethylsilylethane was added as an internal standard.

Scheme S1

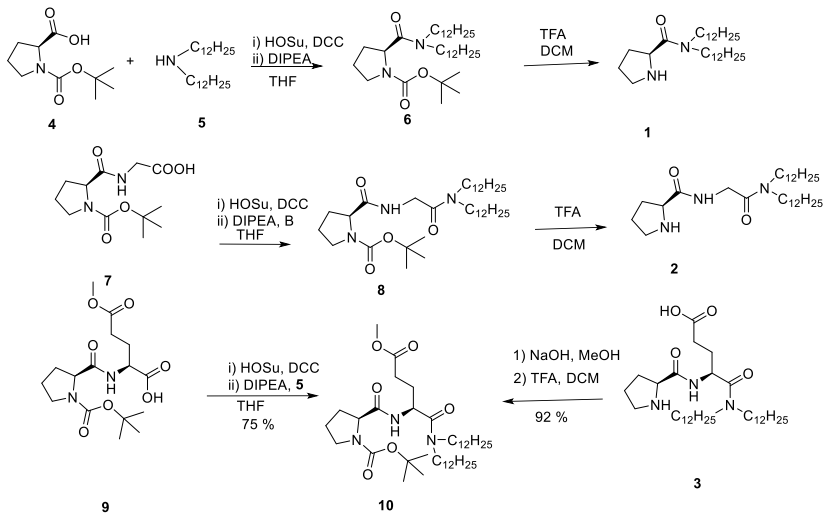

Syntheses

Syntheses of compounds 7,[56] and 9,[57,3] were previously reported. **Compound 1:** To a solution of **4** (0.30 g, 1.29 mmol) in tetrahydrofuran (10 mL), dicylcohexylcarbodiimide (0.25 g, 1.25 mmol) and N-hydroxysuccinimide (0.12 g, 1.25 mmol) were added. The reaction mixture was stirred at room temperature for 12 h. The solid precipitate was filtered off and didodecylamine (0.3 g, 0.85 mmol) and N,N-diisopropylethylamine (0.5 mL, 3.87 mmol) were added to the filtrate. After the mixture was stirred for another 12 h, the organic solvent was removed by rotary evaporation. The residue was dissolved in a minimum amount of methanol and the solution was poured into 100 mL of water. The solution was neutralized by 2 M HCl, followed by extraction with ethyl acetate (3 × 20 mL). The combined organic layers were washed with brine, dried over sodium sulfate, filtered, and concentrated in vacuo. The residue was purified by column chromatography over silica gel using hexane/EtOAc (1/0 to 20/1) as the eluent to give a colorless solid (0.36 g, 68 %). The compound was dissolved in a mixture of dichloromethane (10 mL) and trifluoroacetic acid (0.5 mL, 4.6 mmol). After 2 h at room temperature, the reaction mixture was poured into 100 mL of water and neutralized by saturated sodium carbonate, followed by extraction with ethyl acetate (3 × 20 mL). The combined organic layers were washed with brine, dried over sodium sulfate, filtered, and concentrated in vacuo. The residue was purified by column chromatography over silica gel using dichloromethane/MeOH (10/1) as the eluent to give a glassy solid (0.25 g, 86 %). ^{1}H NMR (400 MHz, $CDCl_3$, δ) 4.55-4.47 (m, 1H), 3.55–3.40 (m, 1H), 3.39–3.30 (m, 1H), 3.30–3.10 (m, 4H), 2.42–2.30 (m, 1H), 2.10–1.70 (m, 5H), 1.35–1.17 (m, 39H), 0.88 (t, J = 6.7 Hz, 6H). ^{13}C NMR (101 MHz, $CDCl_3$, δ): 172.0, 77.6, 77.3, 77.0, 57.8, 47.2, 46.0, 31.9, 31.9, 31.1, 29.7, 28.9, 27.5, 27.0,26.9, 26.0, 22.7, 14.1. HRMS (*m/z*): $[M + H]^+$ calcd for $C_{29}H_{59}N_2O$, 451.4622; found, 451.4617.

Compound 8: To a solution of **7** (0.40 g, 1.40 mmol) in THF (10 mL), dicylohexylacarbodimide (0.28 g, 1.25 mmol) and N-hydroxysuccinimide (0.12 g, 1.25 mmol) were added. The reaction mixture was stirred at room temperature for 12 h. The solid precipitate was filtered off and didodecylamine (0.40 g, 1.13 mmol) and N,N-diisopropylethylamine (0.5 mL, 3.87 mmol) were added to the filtrate. After the mixture was stirred for another 12 h, the organic solvent was removed by rotary evaporation. The residue was dissolved in a minimum amount of methanol and the solution was poured into 100 mL of water. The solution was neutralized by 2 M HCl, followed by extraction with ethyl acetate (3 × 20 mL). The combined organic layers were washed with brine, dried over sodium sulfate, filtered, and concentrated in vacuo. The residue was purified by column chromatography over silica gel using hexane/EtOAc (1/0 to 20/1) as the eluent to give a glassy solid **(**0.5 g, 73 %). ^{1}H NMR (400 MHz, Chloroform-*d*) δ 4.06 (m, 2H), 3.15 (m, 4H), 2.15 (m, 4H), 1.93 – 1.85 (m, 14H), 1.26 (d, J = 3.4 Hz, 39H), 0.88 (t, 6H). ^{13}C NMR (101 MHz, $CDCl_3$, δ): 172.94, 172.35, 167.04, 157.71, 80.17, 77.54, 76.90, 67.92, 61.09, 60.57, 48.81, 47.89, 46.17, 436.63, 33.97, 33.18, 29.76, 28.76, 27.87, 26.99, 25.6, 25.00, 24.4, 17.6, 14.12. HRMS (*m/z*): [M + H]$^{+}$ calcd for $C_{36}H_{70}N_3O_4$, 608.5361; found, 608.5359.

Compound 2: To a solution of compound **8** (0.5 g, 0.8 mmol) in dichloromethane (10 mL), trifluoroacetic acid (1.7 mL, 16 mmol) was added. After 2 h at room temperature, the reaction mixture was poured into 100 mL of water and neutralized by saturated sodium carbonate, followed by extraction with ethyl acetate (3 × 20 mL). The combined organic layers were washed with brine, dried over sodium sulfate, filtered, and concentrated in vacuo. The residue was purified by column chromatography over silica gel using dichloromethane/methanol (10/1) as the eluent to give a glassy solid **(**0.35 g, 85 %). ^{1}H NMR (400 MHz), $CDCl_3$, δ): 8.34 (s, 1H), 4.04 (dd, J = 19.1, 4.4 Hz, 2H), 3.41–3.18 (m, 4H), 3.22 – 3.08 (m, 2H), 3.01 (td, J = 6.6, 3.6 Hz, 2H), 1.53 (d, J = 7.0

Hz, 5H), 1.25 (d, *J* = 3.0 Hz, 39H), 0.88 (t, *J* = 6.7 Hz, 6H). ^{13}C NMR (101 MHz, $CDCl_3$, δ): 175.2, 167.5, 77.6, 60.5, 48.3, 47.2, 47.0, 46.2, 40.8, 32.0, 26.1, 22.7, 14.1. HRMS (*m/z*): $[M + H]^+$ calcd for $C_{30}H_{62}N_3O_2$, 508.4800; found, 508.4835.

Compound 10: To a solution of **9** (0.40 g, 1.10 mmol) in tetrahydrofuran (10 mL), dicyclohexylcarbodiimide (0.22 g, 1.10 mmol) and N-hydroxysuccinimide (0.12 g, 1.25 mmol) were added. The reaction mixture was stirred at room temperature for 12 h. The solid precipitate was filtered off and didodecylamine (0.30 g, 0.56 mmol) and N,N-diisopropylethylamine (0.5 mL, 3.87 mmol) were added to the filtrate. After the mixture was stirred for another 12 h, the organic solvent was removed by rotary evaporation. The residue was dissolved in a minimum amount of methanol and the solution was poured into 100 mL of water. The solution was neutralized by 2 M HCl, followed by extraction with ethyl acetate (3 × 20 mL). The combined organic layers were washed with brine, dried over sodium sulfate, filtered, and concentrated in vacuo. The residue was purified by column chromatography over silica gel using hexane/EtOAc (1/0 to 20/1) as the eluent to give a glassy solid (0.50 g, 64 %). ^{1}H NMR (400 MHz), $CDCl_3$, δ): 6.88 (s, 1H), 4.81–4.74 (m, 1H), 4.16 (m, 1H), 3.67 (s, 3H), 3.33-3.05 (m, 4H), 2.32-2.07 (m, 3H), 2.04-1.44 (m, 17H), 1.27 (s, 39H), 0.89 (t, *J* = 6.7 Hz, 6H). ^{13}C NMR (101 MHz, $CDCl_3$, δ): 173.12, 172.57, 171.99, 17.50, 155.03, 109.99, 80.29, 61.01, 51.62, 47.97, 46.91, 46.05, 33.91, 31.86, 29.59, 28.25, 27.56, 26.92, 24.60, 23.70, 22.03, 14.07. HRMS (*m/z*): $[M + H]^+$ calcd for $C_{40}H_{76}N_3O_6$, 694.5729; found, 694.5709.

Compound 3: Compound **10** (0.5 g, 0.72 mmol) was dissolved in MeOH (5mL). A solution of 1 N NaOH (1.0 mL, 1.0 mmol) was added over a period of 30 min. After 2 h, another batch of 1 N NaOH (0.3 mL, 0.3 mmol) was added. After 1 h of stirring, the reaction mixture was poured into water (100 mL) and then neutralized with 2 M HCl. The aqueous solution was extracted with

EtOAc (2 × 25 mL). The combined organic solution was washed with brine, dried over sodium sulfate, and concentrated in vacuo. The residue was dissolved in a mixture of dichloromethane (10 mL) and triflouroacetic acid (1.7 mL, 16 mmol). After 2 h at room temperature, the reaction mixture was poured into 100 mL of water and neutralized by saturated sodium carbonate, followed by extraction with ethyl acetate (3 × 20 mL). The combined organic layers were washed with brine, dried over sodium sulfate, filtered, and concentrated in vacuo. The residue was purified by column chromatography over silica gel using dichlormethane/MeOH (10/1) as the eluent to give a glassy solid (0.30 g, 88 %). ^{1}H NMR (400 MHz, Methanol-d_4, δ): 7.88 (s, 1H), 4.81–4.74 (m, 1H), 4.04 (m, 1H), 3.63-3.47 (m, 2H), 3.33-3.05 (m, 4H), 2.32-2.07 (m, 3H), 2.04-1.44 (m, 6H), 1.27 (s, 39H), 0.89 (t, J = 6.7 Hz, 6H). ^{13}C NMR (101 MHz, Methanol-d_4, δ): 179.33, 171.90, 171.60, 130.98, 129.47, 67.62, 59.48, 49.26, 47.22, 47.02, 46.22, 40.83, 38.761, 24.35, 23.56, 22.67, 22.39, 13.10. HRMS (*m/z*): $[M + H]^+$ calcd for $C_{34}H_{66}N_3O_4$, 580.5048; found, 580.5053.

^{1}H and ^{13}C NMR spectra

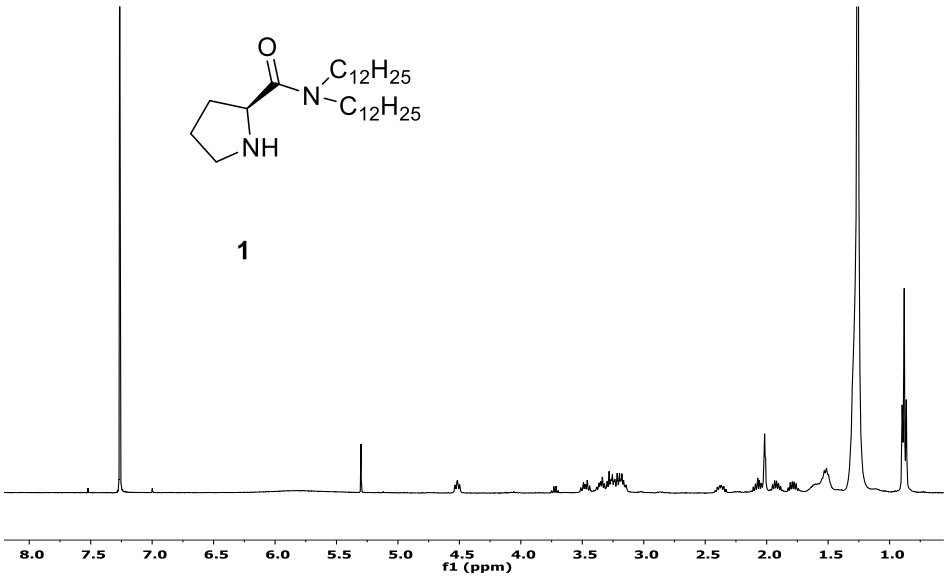

1

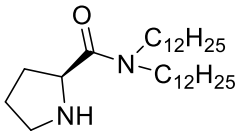

1

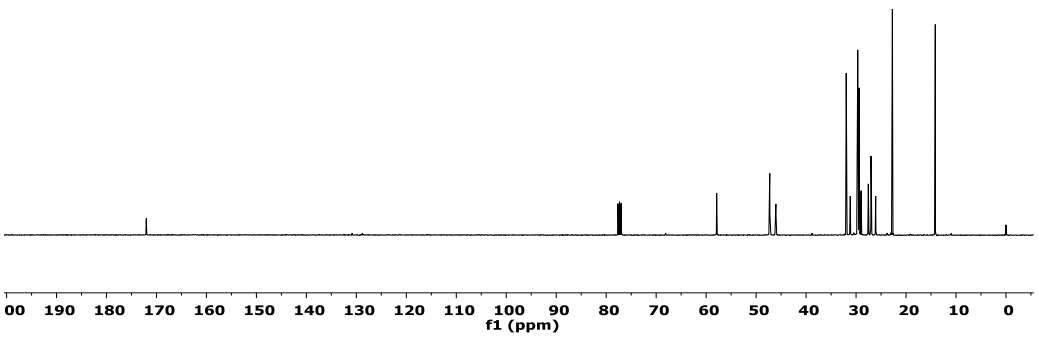

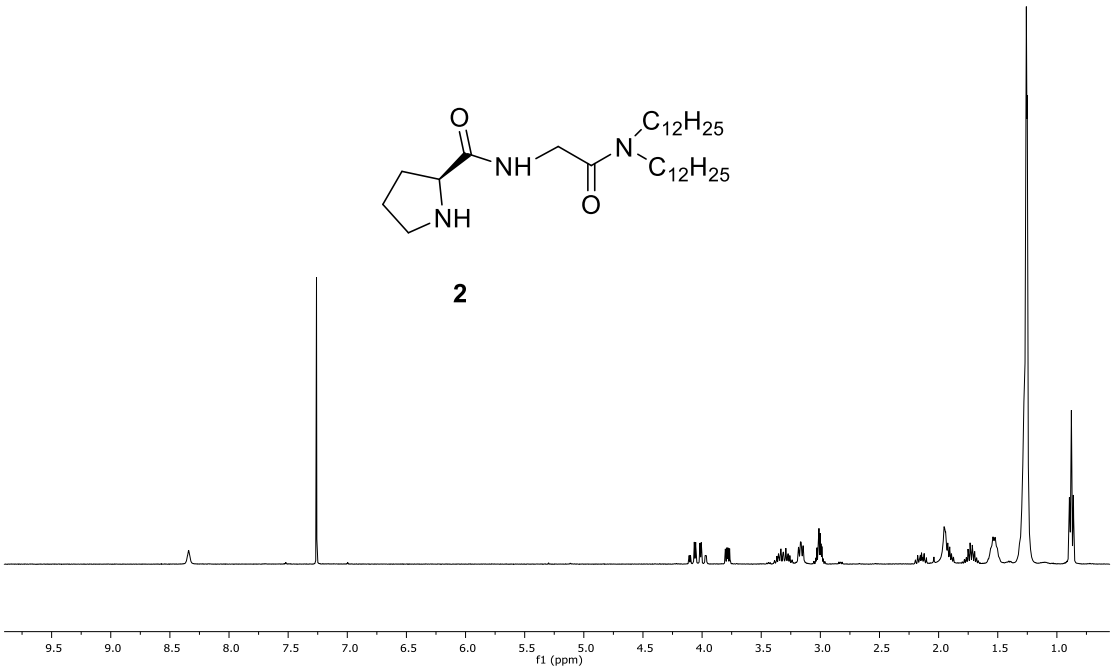

2

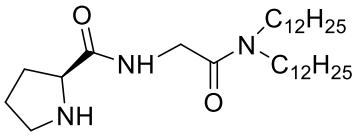

2

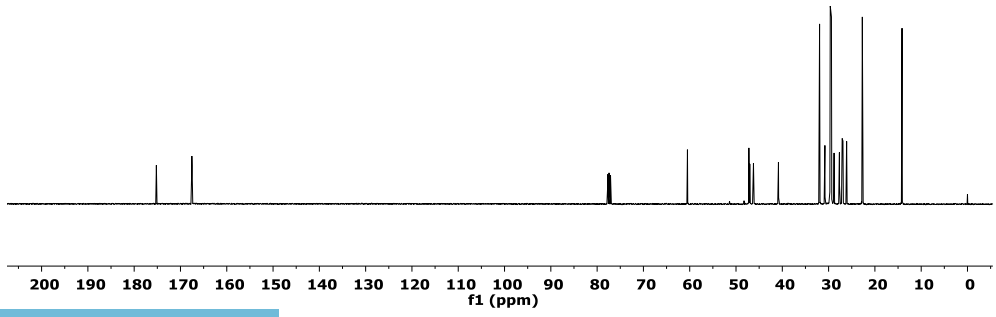

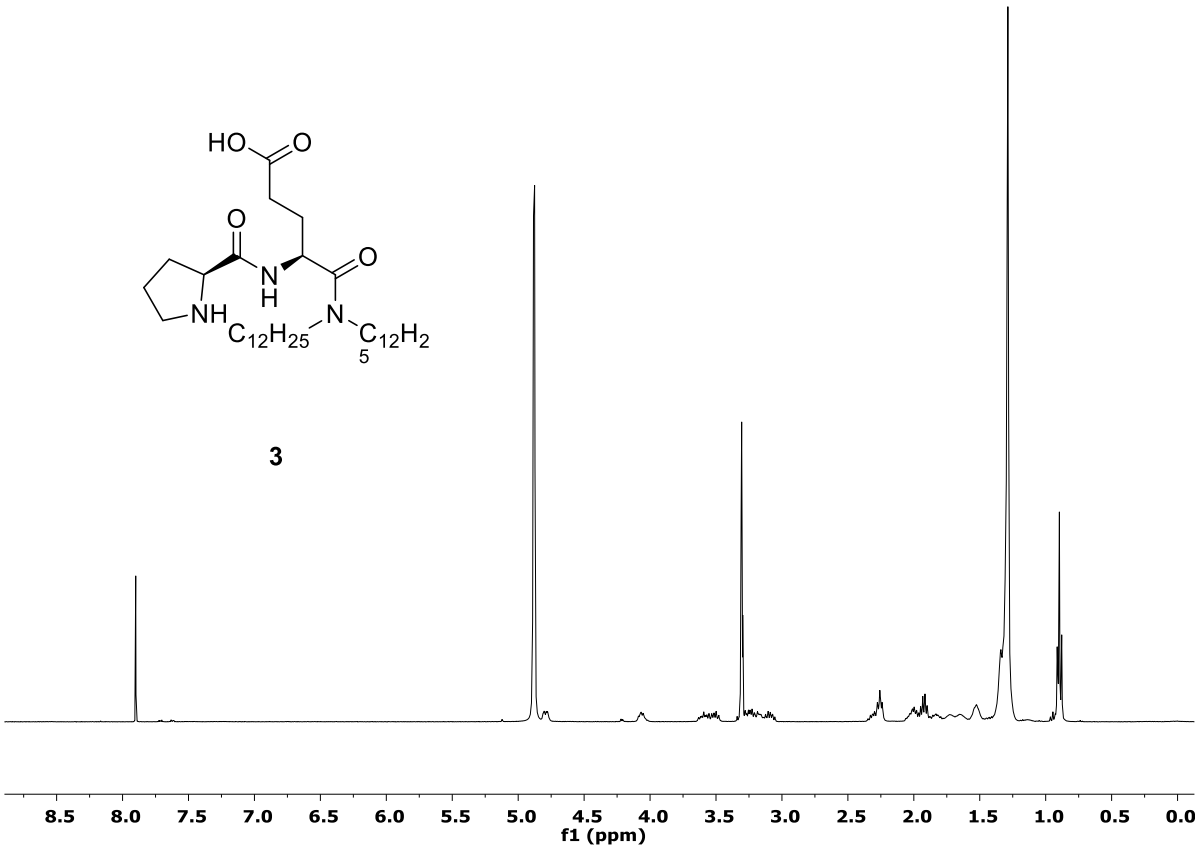

3

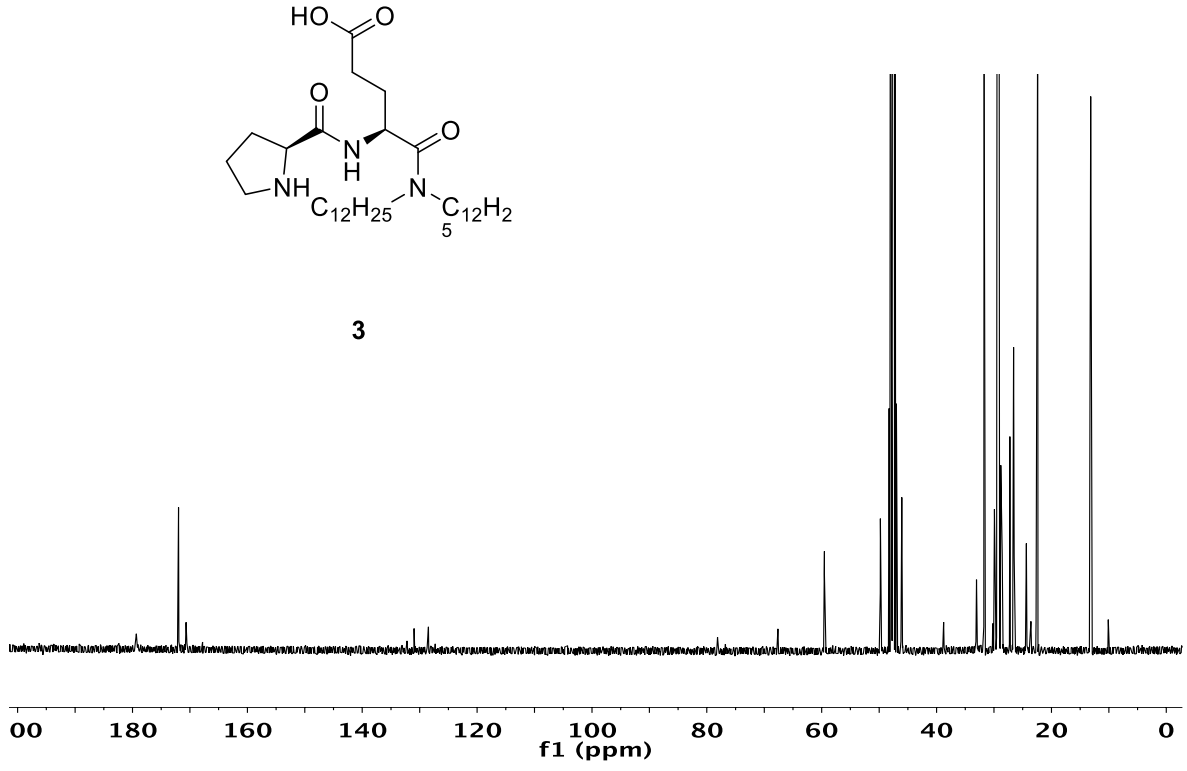

3

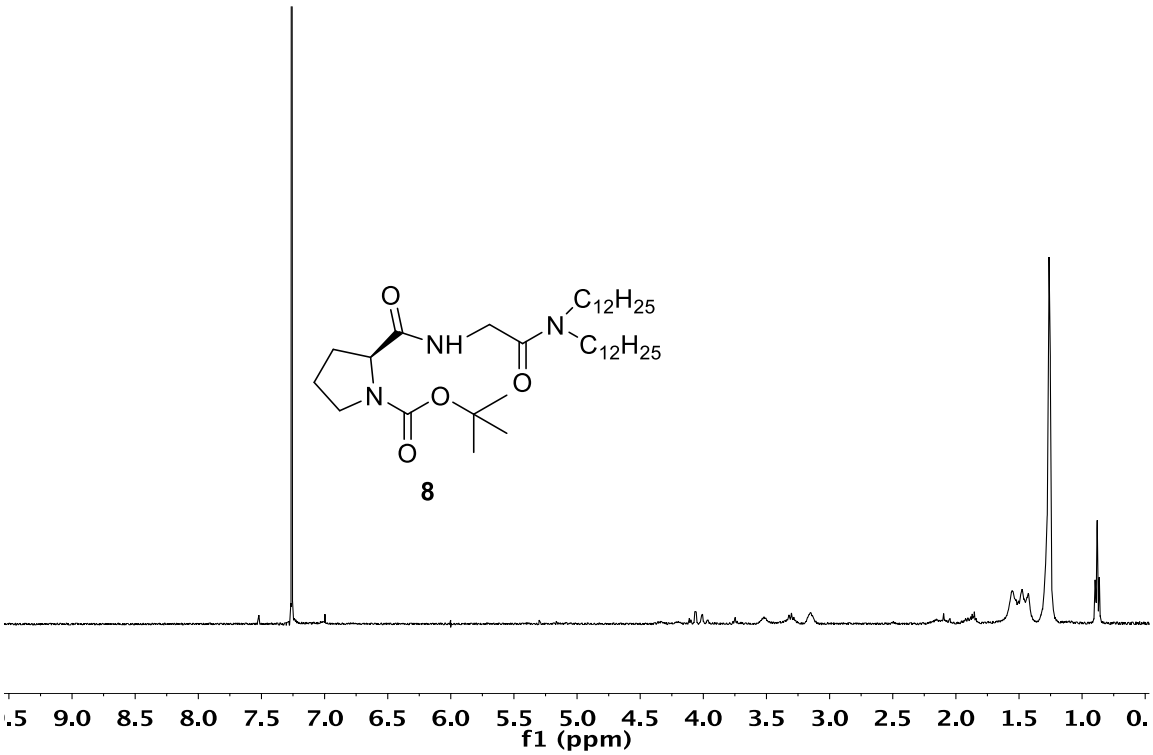

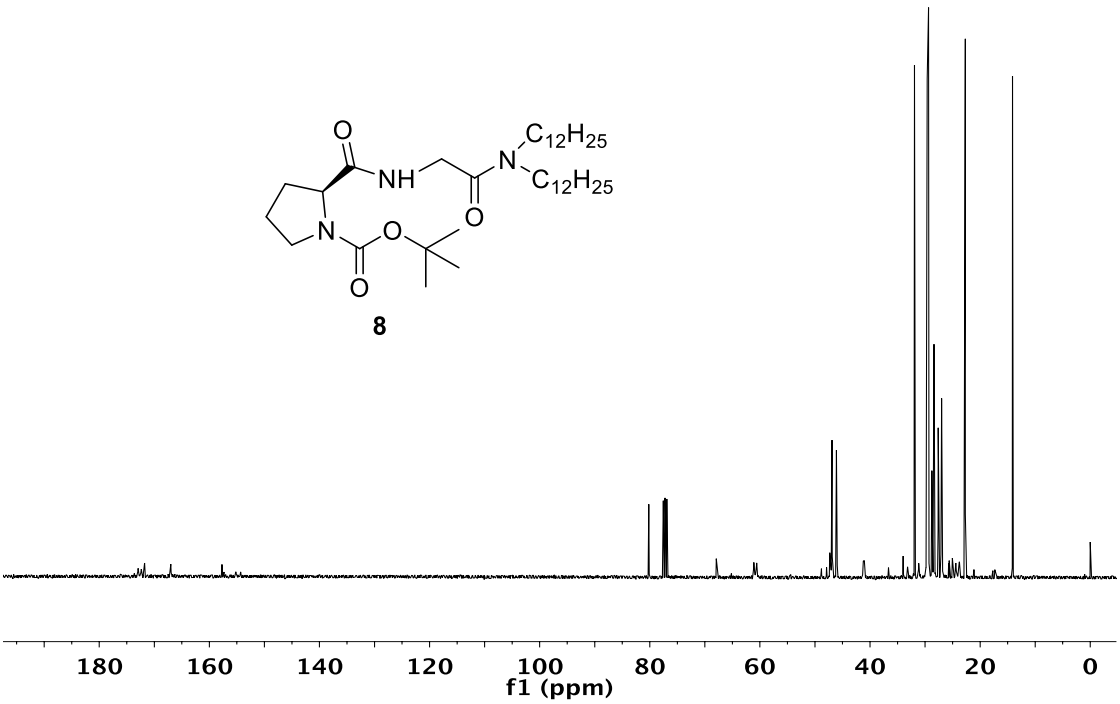

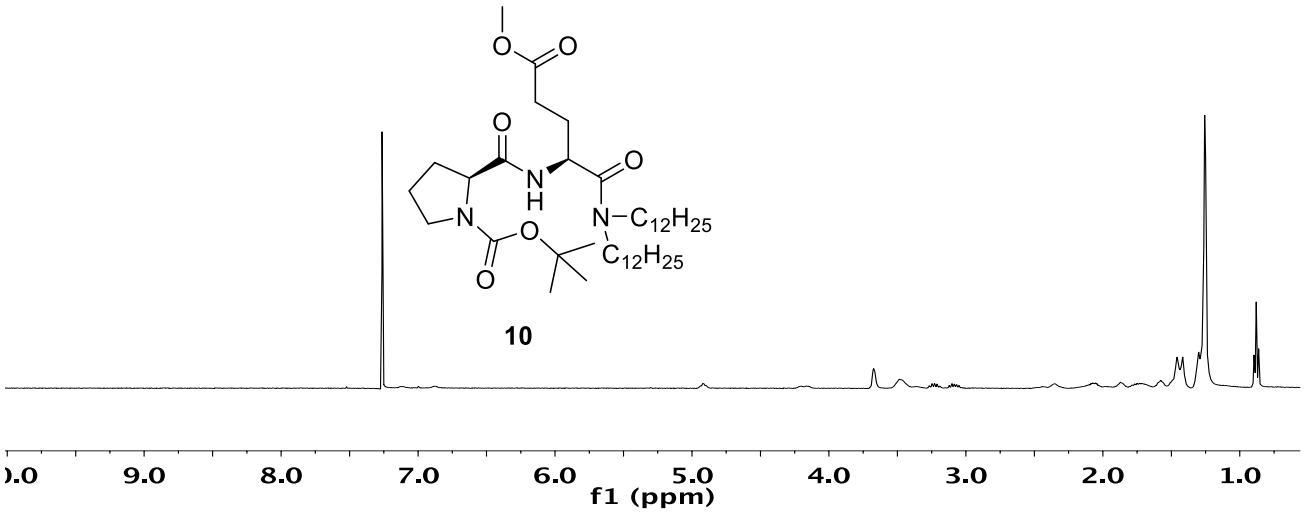

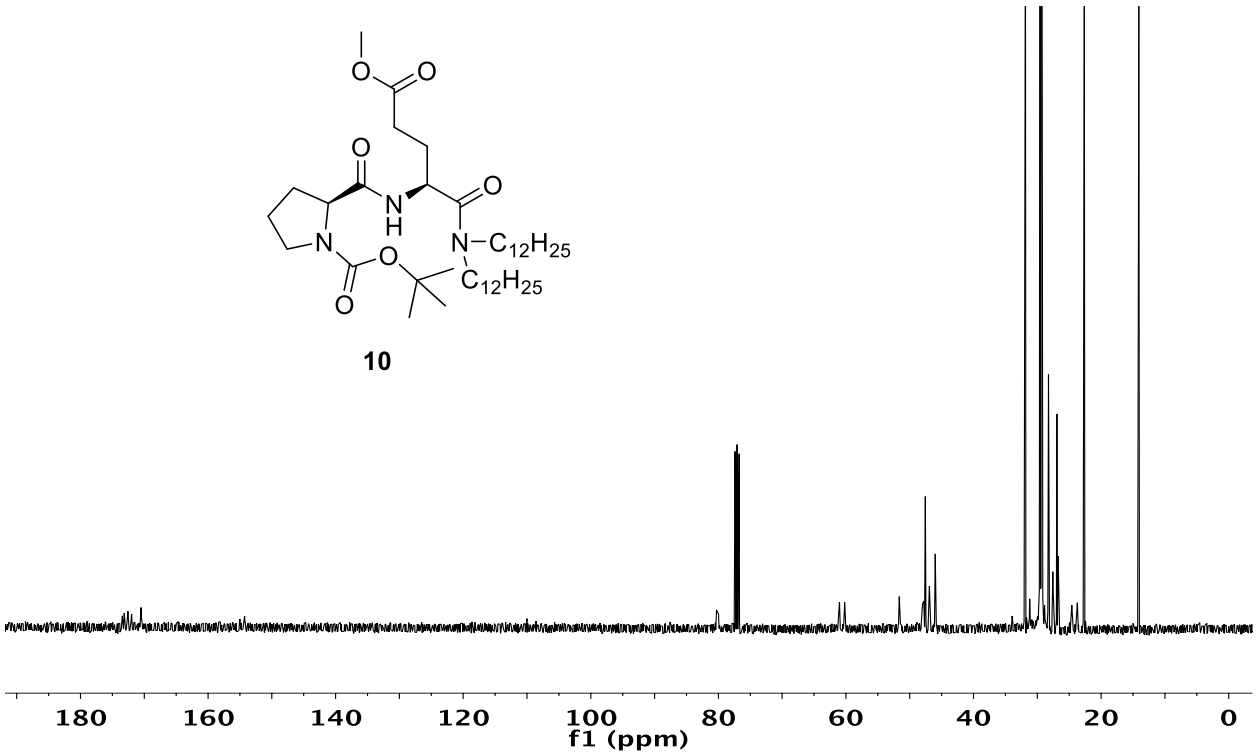

References

1. Das, S.; Brudvig, G. W.; Crabtree, R. H., Molecular recognition in homogeneous transition metal catalysis: a biomimetic strategy for high selectivity. *Chem. Commun.* **2008,** (4), 413-424.

2. Fiedler, D.; Leung, D. H.; Bergman, R. G.; Raymond, K. N., Selective Molecular Recognition, C−H Bond Activation, and Catalysis in Nanoscale Reaction Vessels. *Acc. Chem. Res.* **2004,** *38* (4), 349-358.

3. Vriezema, D. M.; Aragones, M. C.; Elemans, J.; Cornelissen, J.; Rowan, A. E.; Nolte, R. J. M., Self-assembled nanoreactors. *Chem. Rev.* **2005,** *105* (4), 1445-1489.

4. Rebek, J., Simultaneous Encapsulation: Molecules Held at Close Range. *Angew. Chem. Int. Ed.* **2005,** *44* (14), 2068-2078.

5. Yoshizawa, M.; Klosterman, J. K.; Fujita, M., Functional Molecular Flasks: New Properties and Reactions within Discrete, Self-Assembled Hosts. *Angew. Chem. Int. Ed.* **2009,** *48* (19), 3418-3438.

6. Crooks, R. M.; Zhao, M. Q.; Sun, L.; Chechik, V.; Yeung, L. K., Dendrimer-encapsulated metal nanoparticles: Synthesis, characterization, and applications to catalysis. *Acc. Chem. Res.* **2001,** *34* (3), 181-190.

7. Zhao, M.; Crooks, R. M., Homogeneous Hydrogenation Catalysis with Monodisperse, Dendrimer-Encapsulated Pd and Pt Nanoparticles. *Angew. Chem. Int. Ed.* **1999,** *38* (3), 364-366.

8. Somorjai, G. A.; Li, Y. M., Selective Nanocatalysis of Organic Transformation by Metals: Concepts, Model Systems, and Instruments. *Top. Catal.* **2010,** *53* (13-14), 832-847.

9. Chi, Y. G.; Scroggins, S. T.; Frechet, J. M. J., One-pot multi-component asymmetric cascade reactions catalyzed by soluble star polymers with highly branched non-interpenetrating catalytic cores. *J. Am. Chem. Soc.* **2008,** *130* (20), 6322-6323.

10. Rodionov, V.; Gao, H.; Scroggins, S.; Unruh, D. A.; Avestro, A.-J.; Fréchet, J. M. J., Easy Access to a Family of Polymer Catalysts from Modular Star Polymers. *J. Am. Chem. Soc.* **2010,** *132* (8), 2570-2572.

11. Corma, A., From Microporous to Mesoporous Molecular Sieve Materials and Their Use in Catalysis. *Chem. Rev.* **1997,** *97* (6), 2373-2420.

12. Huh, S.; Chen, H.-T.; Wiench, J. W.; Pruski, M.; Lin, V. S. Y., Cooperative Catalysis by General Acid and Base Bifunctionalized Mesoporous Silica Nanospheres. *Angew. Chem. Int. Ed.* **2005,** *44* (12), 1826-1830.

13. Hudson, S.; Cooney, J.; Magner, E., Proteins in Mesoporous Silicates. *Angew. Chem. Int. Ed.* **2008,** *47* (45), 8582-8594.

14. Thomas, J. M.; Raja, R., Exploiting Nanospace for Asymmetric Catalysis: Confinement of Immobilized, Single-Site Chiral Catalysts Enhances Enantioselectivity. *Acc. Chem. Res.* **2008,** *41* (6), 708-720.

15. Ma, L.; Abney, C.; Lin, W., Enantioselective catalysis with homochiral metal-organic frameworks. *Chem. Soc. Rev.* **2009,** *38* (5), 1248-1256.

16. Corma, A.; García, H.; Llabrés i Xamena, F. X., Engineering Metal Organic Frameworks for Heterogeneous Catalysis. *Chem. Rev.* **2010,** *110* (8), 4606-4655.

17. Lee, J.; Farha, O. K.; Roberts, J.; Scheidt, K. A.; Nguyen, S. T.; Hupp, J. T., Metal-organic framework materials as catalysts. *Chem. Soc. Rev.* **2009,** *38* (5), 1450-1459.

18. Farrusseng, D.; Aguado, S.; Pinel, C., Metal-Organic Frameworks: Opportunities for Catalysis. *Angew. Chem. Int. Ed.* **2009,** *48* (41), 7502-7513.

19. Pileni, M. P., *Structure and Reactivity in Reverse Micelles*. Elsevier: Amsterdam, 1989.

20. Menger, F. M.; Donohue, J. A.; Williams, R. F., Catalysis in Water Pools. *J. Am. Chem. Soc.* **1973,** *95* (1), 286-288.

21. Menger, F. M.; Yamada, K., Enzyme Catalysis in Water Pools. *J. Am. Chem. Soc.* **1979,** *101* (22), 6731-6734.

22. Luisi, P. L.; Giomini, M.; Pileni, M. P.; Robinson, B. H., Reverse Micelles as Hosts for Proteins and Small Molecules. *Biochim. Biophys. Acta* **1988,** *947* (1), 209-246.

23. Pileni, M. P., Nanosized particles made in colloidal assemblies. *Langmuir* **1997,** *13* (13), 3266-3276.

24. Pileni, M. P., The role of soft colloidal templates in controlling the size and shape of inorganic nanocrystals. *Nat. Mater.* **2003,** *2* (3), 145-150.

25. Ryu, E.-H.; Cho, H.; Zhao, Y., Catalyzing Methanolysis of Alkyl Halides in the Interior of an Amphiphilic Molecular Basket. *Org. Lett.* **2007,** *9* (25), 5147-5150.

26. Zhou, Y. B.; Ryu, E.-H.; Zhao, Y.; Woo, L. K., Solvent-responsive metalloporphyrins: Binding and catalysis. *Organometallics* **2007,** *26* (2), 358-364.

27. Cho, H.; Zhong, Z.; Zhao, Y., A DMAP-functionalized oligocholate foldamer for solvent-responsive catalysis. *Tetrahedron* **2009,** *65* (35), 7311-7316.

28. Zhang, S.; Zhao, Y., Artificial metalloenzymes via encapsulation of hydrophobic transition-metal catalysts in surface-crosslinked micelles (SCMs). *Chem. Commun.* **2012,** *48* (80), 9998-10000.

29. Chadha, G.; Zhao, Y., Histidine-functionalized water-soluble nanoparticles for biomimetic nucleophilic/general-base catalysis under acidic conditions. *Org. Biomol. Chem.* **2013,** *11* (39), 6849-6855.

30. Chadha, G.; Zhao, Y., Environmental control of nucleophilic catalysis in water. *Chem. Commun.* **2014,** *50* (21), 2718-2720.

31. Lee, L.-C.; Zhao, Y., Room Temperature Hydroamination of Alkynes Catalyzed by Gold Clusters in Interfacially Cross-Linked Reverse Micelles. *ACS Catalysis* **2014**, 688-691.

32. Lee, L.-C.; Zhao, Y., Metalloenzyme-Mimicking Supramolecular Catalyst for Highly Active and Selective Intramolecular Alkyne Carboxylation. *J. Am. Chem. Soc.* **2014,** *136* (15), 5579-5582.

33. List, B., Proline-catalyzed asymmetric reactions. *Tetrahedron* **2002,** *58* (28), 5573-5590.

34. List, B., Enamine Catalysis Is a Powerful Strategy for the Catalytic Generation and Use of Carbanion Equivalents. *Acc. Chem. Res.* **2004,** *37* (8), 548-557.

35. Notz, W.; Tanaka, F.; Barbas, C. F., Enamine-based organocatalysis with proline and diamines: The development of direct catalytic asymmetric Aldol, Mannich, Michael, and Diels-Alder reactions. *Acc. Chem. Res.* **2004,** *37* (8), 580-591.

36. Sakthivel, K.; Notz, W.; Bui, T.; Barbas, C. F., Amino Acid Catalyzed Direct Asymmetric Aldol Reactions: A Bioorganic Approach to Catalytic Asymmetric Carbon−Carbon Bond-Forming Reactions. *J. Am. Chem. Soc.* **2001,** *123* (22), 5260-5267.

37. Tang, Z.; Jiang, F.; Yu, L.-T.; Cui, X.; Gong, L.-Z.; Mi, A.-Q.; Jiang, Y.-Z.; Wu, Y.-D., Novel Small Organic Molecules for a Highly Enantioselective Direct Aldol Reaction. *J. Am. Chem. Soc.* **2003,** *125* (18), 5262-5263.

38. Tang, Z.; Jiang, F.; Cui, X.; Gong, L.-Z.; Mi, A.-Q.; Jiang, Y.-Z.; Wu, Y.-D., Enantioselective direct aldol reactions catalyzed by l-prolinamide derivatives. *Proc. Natl. Acad. Sci. U. S. A.* **2004,** *101* (16), 5755-5760.

39. Peng, Y. Y.; Ding, Q. P.; Li, Z. C.; Wang, P. G.; Cheng, J. P., Proline catalyzed aldol reactions in aqueous micelles: an environmentally friendly reaction system. *Tetrahedron Lett* **2003,** *44* (19), 3871-3875.

40. Mase, N.; Nakai, Y.; Ohara, N.; Yoda, H.; Takabe, K.; Tanaka, F.; Barbas, C. F., Organocatalytic direct asymmetric aldol reactions in water. *J. Am. Chem. Soc.* **2006,** *128* (3), 734-735.

41. Lo, C. M.; Chow, H. F., Structural Effects on the Catalytic, Emulsifying, and Recycling Properties of Chiral Amphiphilic Dendritic Organocatalysts. *J. Org. Chem.* **2009,** *74* (15), 5181-5191.

42. He, T.; Li, K.; Wu, M.-Y.; Wu, M.-B.; Wang, N.; Pu, L.; Yu, X.-Q., Water promoted enantioselective aldol Reaction by proline-cholesterol and -diosgenin based amphiphilic organocatalysts. *Tetrahedron* **2013,** *69* (25), 5136-5143.

43. Doyagüez, E. G.; Corrales, G.; Garrido, L.; Rodríguez-Hernández, J.; Gallardo, A.; Fernández-Mayoralas, A., Linear Copolymers of Proline Methacrylate and Styrene as Catalysts for Aldol Reactions in Water: Effect of the Copolymer Aggregation on the Enantioselectivity. *Macromolecules* **2011,** *44* (16), 6268-6276.

44. Lu, A.; Cotanda, P.; Patterson, J. P.; Longbottom, D. A.; O'Reilly, R. K., Aldol reactions catalyzed by l-proline functionalized polymeric nanoreactors in water. *Chem. Commun.* **2012,** *48* (78), 9699-9701.

45. Zayas, H. A.; Lu, A.; Valade, D.; Amir, F.; Jia, Z.; O'Reilly, R. K.; Monteiro, M. J., Thermoresponsive Polymer-Supported l-Proline Micelle Catalysts for the Direct Asymmetric Aldol Reaction in Water. *ACS Macro Lett.* **2013,** *2* (4), 327-331.

46. Israelachvili, J. N., *Intermolecular and surface forces: with applications to colloidal and biological systems*. Academic Press: London, 1985.

47. Leydet, A.; Boyer, B.; Lamaty, G.; Roque, J. P.; Catlin, K.; Menger, F. M., Nitrogen Analogs of AOT. Synthesis and Properties. *Langmuir* **1994,** *10* (4), 1000-1002.

48. Shenhar, R.; Rotello, V. M., Nanoparticles: Scaffolds and building blocks. *Acc. Chem. Res.* **2003,** *36* (7), 549-561.

49. Another way of verifying the importance of aggregation to the catalysis is to employ non-RM-forming prolinamides such as those missing the long alkyl tails and compare their performance with that of 3 under our RM conditions. Such catalysts, however, are expected to be insoluble in nonpolar solvents used under RM conditions and thus their syntheses were not attempted.

50. The headgroups of the zwitterionic surfactants could not be solvated properly by nonpolar solvents such as benzene and need to aggregate (or "self-solvate") to make the surfactants soluble in the nonpolar solvent.

51. Rodriguez-Llansola, F.; Escuder, B.; Miravet, J. F., Switchable Perfomance of an L-Proline-Derived Basic Catalyst Controlled by Supramolecular Gelation. *J. Am. Chem. Soc.* **2009,** *131* (32), 11478-11484.

52. Kong, Y.; Tan, R.; Zhao, L. L.; Yin, D. H., L-Proline supported on ionic liquid-modified magnetic nanoparticles as a highly efficient and reusable organocatalyst for direct asymmetric aldol reaction in water. *Green Chem.* **2013,** *15* (9), 2422-2433.

53. As mentioned earlier, aggregation most likely accelerated the reaction by enhancing basicity of the amine in the catalysts. Enantio- and diastereoselectivity, on the other hand, probably depended more on the "intimate" interactions between individual substrates and their

corresponding catalysts and thus were not affected as much by other (uninvolved) catalysts in the aggregate.

54. Koblenz, T. S.; Wassenaar, J.; Reek, J. N. H., Reactivity within a confined self-assembled nanospace. *Chem. Soc. Rev.* **2008,** *37* (2), 247-262.

55. Rakowski DuBois, M.; DuBois, D. L., The roles of the first and second coordination spheres in the design of molecular catalysts for H2 production and oxidation. *Chem. Soc. Rev.* **2009,** *38* (1), 62-72.

56. Morisue, M.; Haruta, N.; Kalita, D.; Kobuke, Y., Efficient Charge Injection from the S2 Photoexcited State of Special-Pair Mimic Porphyrin Assemblies Anchored on a Titanium-Modified ITO Anode. *Chemistry – A European Journal* **2006,** *12* (31), 8123-8135.

57. Zhang, S. Y.; Zhao, Y., Rapid Release of Entrapped Contents from Multi-Functionalizable, Surface Cross-Linked Micelles upon Different Stimulation. *J Am Chem Soc* **2010,** *132* (31), 10642-10644.

CHAPTER 3. PHYSICAL ENTRAPMENT OF WATER-SOLUBLE FLUORESCENT DYES BY INTERFACIALLY CROSS-LINKED REVERSE MICELLES

Premkumar Rathinam Arivalagan and Yan Zhao

Abstract

Reverse micelles of triallylammonium-functionalized surfactants were cross-linked by dithiothreitol (DTT) through the thiol–ene free radical addition to afford interfacially cross-linked reverse micelles (ICRMs). ICRM-entrapped metal cluster catalysts were previously shown to display unusual properties. These core–shell organic nanoparticles in this work were shown to encapsulate water-soluble fluorescent dyes in the hydrophilic core. The quantum yield of the entrapped fluorophore may decrease or increase, depending on the fluorophore itself and the properties of the ICRMs. Fluorescence quenching revealed that the entrapped dyes were located at the surfactant/water interface and accessible to both hydrophilic and hydrophobic molecules.

Introduction

Surfactant molecules like to work as a community instead of as individuals. By self-assembling into different mesophases, they can solubilize nonpolar substance in water, serve as a hydrophobic barrier for water-soluble molecules, or coat polar or nonpolar surfaces. Reverse micelles (RMs) are spherical aggregates of surfactants formed in nonpolar solvent. The headgroups of surfactants in a RM point inward, solvated by a pool of water (or other polar solvent) in the center.[1] Having both water and organic solvent in the mixture, a RM solution can be used as a medium for chemical and biological reactions.[1-4] Because the self-assembled surfactants can modulate the crystal

growth, size, and morphology of inorganics, RMs are also frequently used as templates for inorganic nanomaterials.[5-6]

There has been long standing interest in capturing surfactant mesophases by polymerization.[7-11] Once stabilized by covalent bonds, a surfactant mesophase can enable applications not possible with its noncovalent counterpart. However, because the exchange of surfactants among different RMs is nearly diffusion-controlled, it is difficult to confine polymerization within individual micelles.[12-13]

The Zhao group recently employed the highly efficient thiol–ene click reaction to cross-link RMs at the surfactant/water interface.[14] These interfacially cross-linked RMs (ICRMs) joined those reported by McQuade and co-workers[15-16] as the first examples of covalently captured RMs. Subsequently, they also found that ICRMs could also be prepared by free radical polymerization at the water/surfactant interface and was also able to produce interfacially cross-linked RMs (ICRMs).[17]

ICRMs are core–shell organic nanoparticles (4–5 nm in size) with diverse applications.[14, 17-19] As highly unusual templates, they allowed the preparation of luminescent Au_4, Au_8, and Au_{13}–Au_{23} clusters, as well as gold nanoparticles several nanometers in size, simply by using different amounts of gold precursor and reducing conditions.[14, 18] The metal clusters/nanoparticles were physically encapsulated by the ICRMs and displayed interesting catalytic activities. Colloidal gold, for example, normally displays no catalytic activity in the intermolecular hydroamination of alkynes.[20] When deposited on a chitosan–silica support, gold nanoparticles could catalyze the reaction but require rather harsh conditions (100 °C for 22 h). With ICRM-trapped gold clusters (i.e., Au_n@ICRM), the reaction happened readily at room temperature.[21] Not only so, functional groups on the ICRM shell could be used to "pull" substrates (e.g., 4-pentynoic acid) toward the

encapsulated Au cluster. As the binding functionality (carboxyl) was converted (in an intramolecular alkyne carboxylation to lactone), the nonpolar product was rapidly ejected into the environment, making Au_n@ICRM behave like a "catalytic nanomachine". As a result, catalyst loading was reduced by 30–100-fold in comparison to typical levels reported in the literature.[17]

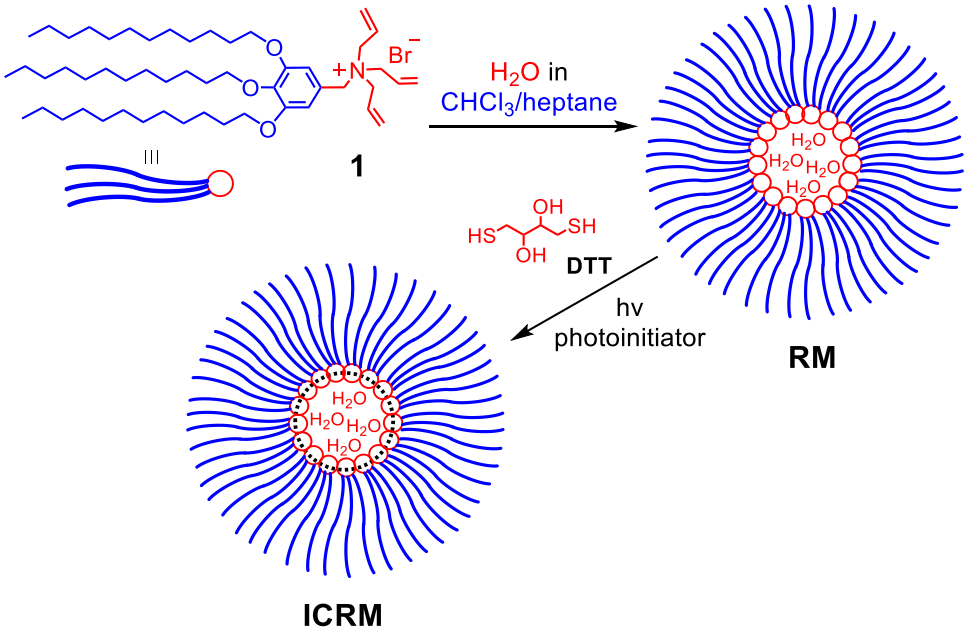

Scheme 1 Preparation of ICRM by photocross-linking of **1** with DTT in the RM configuration.

In this work, we trapped water-soluble fluorescent dyes within the hydrophilic core of ICRM. The motivation for the research is two-fold. First, supramolecular photonic materials are useful in sensing, light-harvesting, and photocatalysis.[22] Since the dye molecules can be organized by the surfactant assemblies and covalent capture could fix the structures, we can easily obtain ordered photonic materials.[23] Second, fluorescence spectroscopy can be used to probe the location of the fluorophore.[24] Since it is difficult to directly measure the mass transfer of different substrates to catalysts in the ICRM core, we can use physically entrapped fluorophore as mock catalysts and test their accessibility by different molecules. In this way, we have an indirect way of knowing the location of entrapped catalysts, especially if their charge and polarity are similar to those of the

fluorescent dye. Such learning is expected to be invaluable to the future design of ICRM-based catalytic systems.

Results and discussion

Synthesis of dye-containing ICRMs

Self-assembly of a surfactant strongly depends on its critical packing parameter ($Q = v/a_0l_c$), in which v is the volume of the hydrophobic tail, a_0 the area of the hydrophilic headgroup, and l_c the average critical length of the amphiphile.[25] To make surfactant pack more easily in the RM configuration, we chose to use triple-tailed **1** with a large hydrophobic volume (Scheme 1). The triallylammonium headgroup put a high local concentration of alkene at the surfactant/water interface. The water-soluble dithiol cross-linker, dithiothreitol (DTT) was concentrated in the internal water pool. UV irradiation of photoinitiator 2,2-dimethoxy-2-phenylacetophenone triggered the highly efficient thiol–ene radical addition, further facilitated by the high local concentration of the reactive groups.

We reasoned that, to be trapped physically inside the hydrophilic core of an ICRM, the dye had to carry multiple anionic charges, similar to our gold clusters protected by bromide anions.[17-18] Fluorophore **2** fulfills this criterion. Having three carboxylates, it should readily ion-pair with three surfactants in nonpolar solvents. The compound is similar to dansyl in structure, whose fluorescence is well-known to be sensitive to environmental polarity. Its emission, thus, should help us understand the local environment around the probe.

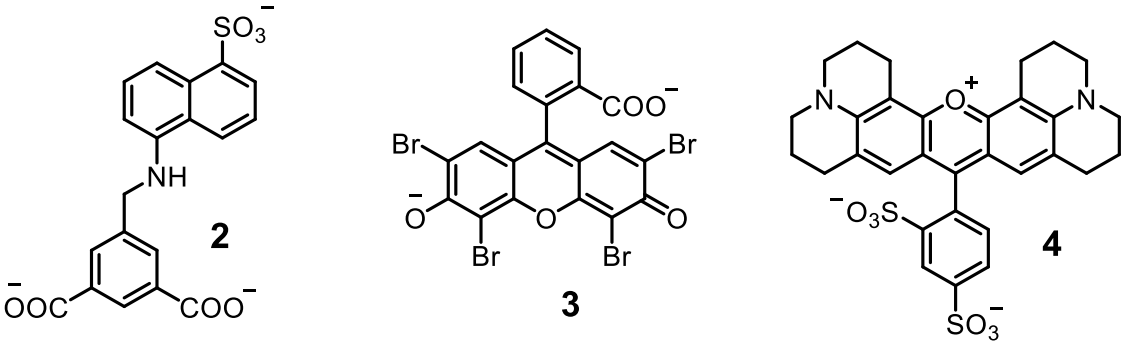

Figure 1. Structures of dyes **2**, **3**, and **4**.

The same ICRM synthesis worked well for the preparation of dye-entrapped ICRMs. Detailed procedures are reported in the Experimental Section. Typically, a clear RM solution was formed with the appropriate amounts of the dye, Millipore water, and cross-linkable surfactant **1** in a mixture of heptane and chloroform. Interfacial cross-linking was achieved following our standard procedures for all three fluorophores (**2**–**4**). The dye-entrapped ICRMs were generally isolated after the reaction by precipitation from acetone and washed with mixtures of methanol/acetone. Since the supernatant remained nearly colorless during repeated washing while the ICRMs retained the distinctive color of the dye, the fluorophores were apparently trapped physically inside the ICRMs.

Characterization of Dye-Containing ICRMs

^{1}H NMR spectroscopy may be used to monitor cross-linking of the ICRMs. As shown in Figure 2, the olefinic protons from the ally groups disappeared after cross-linking. For the nonreactive protons, those close to the cross-linked headgroups also disappeared (e.g., H_a). As the protons move away from the cross-linked core, they become more visible, e.g., H_b and H_f. In particular, the methyl protons (H_b) are sharp and well-resolved. These results are consistent with the cross-linking at the allyl groups in the RM configuration, since the movement of the protons in the cross-linked ICRM core is expected to by very restricted but protons at the dodecyl tail

end should remain mobile. The aromatic region of the ^{1}H NMR spectra did not show any protons from the entrapped aromatic dye. This result, however, is fully expected due to the low mobility of the dye in the ICRM core and low dye to surfactant ratio.

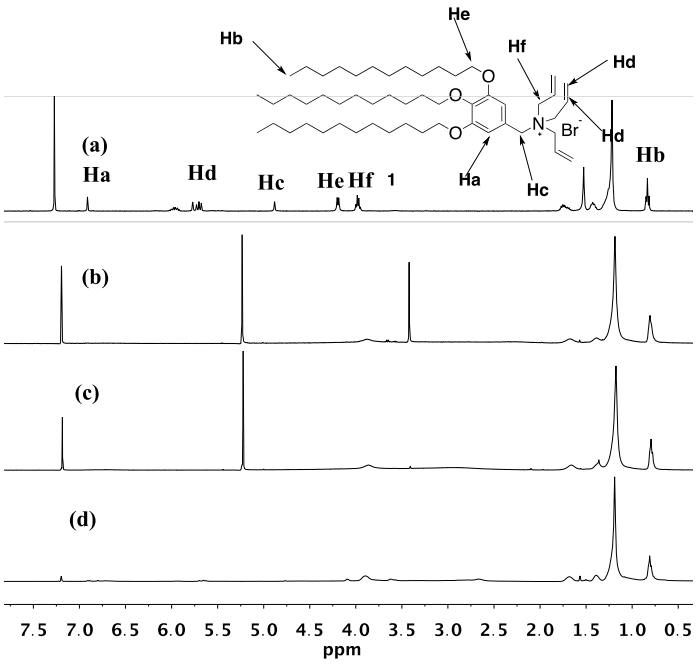

Figure 2. ^{1}H NMR spectra of (a) surfactant **1** and (b) **2**@ICRM in $CHCl_3$ (c) **3**@ICRM and (d) **4@**ICRM. 4/100 fluorophore/surfactant.

The size of the dye-containing ICRMs was determined by dynamic light scattering (DLS). The DLS size was confirmed earlier by transmission electron microscopy (TEM).[14] As shown in figure 4, the ICRMs are typically 4–5 nm in diameter. The size is similar to that of uncross-linked RMs and regular ICRMs. Apparently, dye-entrapment did not change the size of the ICRM.

Photophysical properties of entrapped dyes

Figure 3 shows the absorption and emission spectra of compound **2**, in the free form and as entrapped inside the ICRM (Figure 3a and 3b). Property of micropolarity can be tuned by

changing the parameters such as surfactant/fluorophore ratio and w_0. These changes in parameters are also expected to tune the photophysical properties of the fluorophores. Dye **2** is known to exhibit solvatochromic effect, which means its photo physical properties can be tuned by different solvents. From the Figure 3 and Table 1**,** it can be inferred that dyes retained its identity upon entrapment with small spectral shifts.

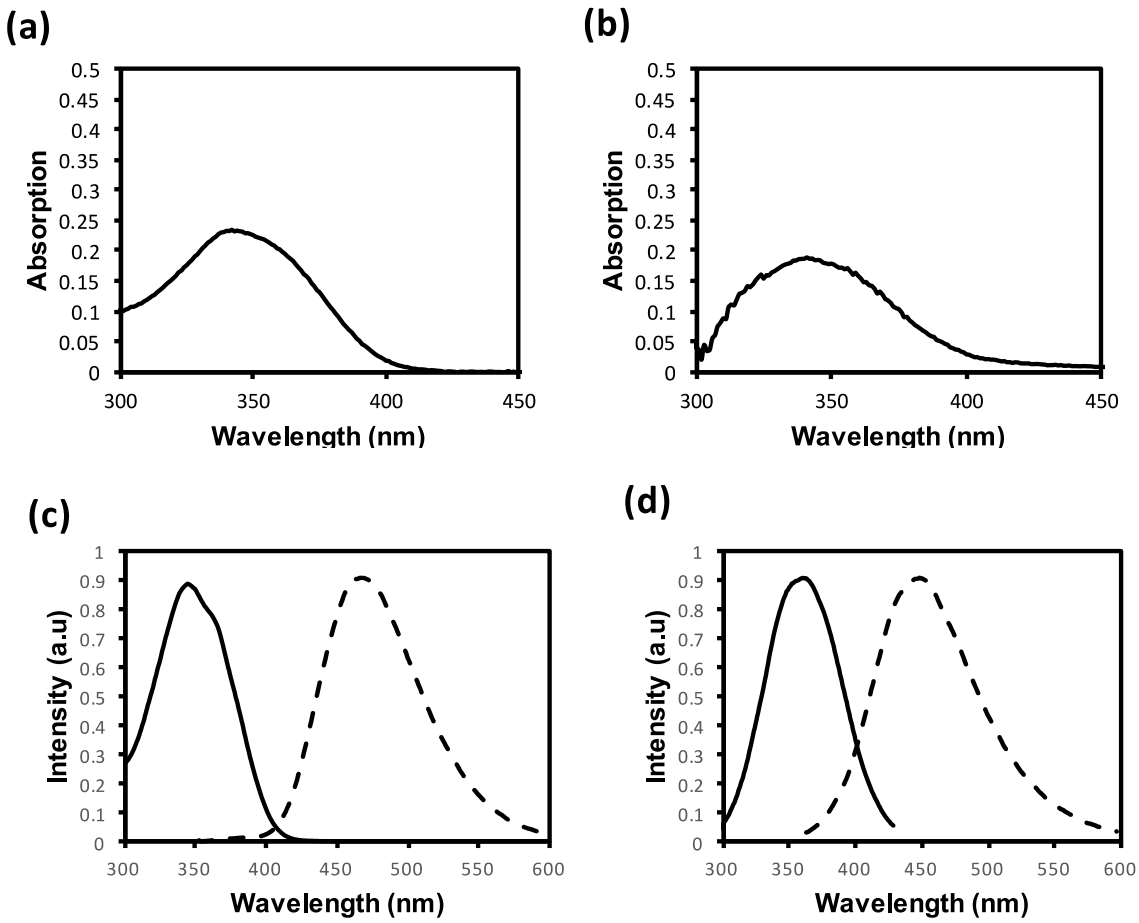

Figure 3. Absorption spectra of (a) in methanol [**2**] = 46 μM and (b) 4%@ICRM in chloroform. w_0 = [H2O]/[surfactant] = 5. [**2**] = 0.184 mM. Emission (solid lines) and excitation (dashed lines) spectra of (c) **2** in methanol and (d) 4%@ICRM in chloroform. w_0 = [H_2O]/[surfactant] = 5.

Table 1. Comparison of ICRM-entrapped dyes and dyes dissolved in methanol.

entry	dye	loading[a]	w_0	λ_{ab} (nm)	λ_{ex} (nm)	λ_{em} (nm)	QY[b]
1	**2**	1%	5	340	360	490	0.40
2	**2**	2%	5	340	360	490	0.31
3	**2**	4%	5	340	360	448	0.19
4	**2**	1%	10	340	360	448	0.15
5	**2**	1%	2.5	340	360	448	0.12
6	**2**	In methanol[c]		342	342	460	0.16
7	**3**	1%	5	545	552	564	0.18
8	**3**	2%	5	545	552	564	0.31
9	**3**	4%	5	545	552	564	0.27
10	**3**	1%	10	545	552	564	0.16
11	**3**	1%	2.5	545	552	564	0.22
12	**3**	In methanol[c]		525	525	542	0.44
13	**4**	1%	5	582	582	595	0.33
14	**4**	2%	5	582	582	595	0.42
15	**4**	4%	5	582	582	595	0.45
16	**4**	1%	10	582	582	595	0.27
17	**4**	1%	2.5	582	582	595	0.30
18	**4**	In methanol[c]		578	578	598	0.96

[a] Loading is the molar ratio of the dye to cross-linkable surfactant in the ICRM preparation. [b] Quantum yields were determined using quinine sulfate in 0.05 M H_2SO_4 as a standard for **2**, by the excitation at 343 nm. Dye **3** and **4** were used as standards for themselves, using literature-reported quantum yields. he quantum yields were calculated according to equation $\Phi = \Phi_S \times (I/I_S) \times (OD_S/OD) \times (\eta^2/\eta_S^2)$, in which Φ is the quantum yield, I is the integrated intensity, η is the refractive index ($\eta^2 = \eta_S^2$ as water was used for both systems), and OD is the optical density. The subscript S refers to the standard. [c] The photophysical properties were for the dye dissolved in methanol. [dye] = 0.005 mM.

Effect of Surfactant/fluorophore ratio

By changing the ratio of surfactant to dye in the ICRM synthesis, we can tune the number of dye molecules per ICRM. From the DLS experiments, the number of surfactant per ICRM was found to be approximately 50. Increasing the fluorophore/surfactant ratio increases the number of fluorophores per ICRM. Such a change should have a marked effect on the photo physical properties due to the increase in the probability of fluorophore-fluorophore interactions among fluorophores within the ICRM core.

For the dye **2,** the UV-vis λ_{max} was found to be 345 nm in both the free and entrapped state at all the three ratios. But fluorescence spectra showed a red shift around 30 nm from the free state when the surfactant ratio was 100/1 and 50/1. There was a blue shift around 10 nm for the ratio 25/1.

For dyes **3** and **4,** a red shift around 20 nm was observed in emission, excitation, and absorption spectra for all the three ratios. The fluorescence quantum yield is the measure of efficiency for a fluorophore to convert absorbed light into fluorescence. Confinement in the microenvironment should influence fluorescence quenching pathways and result in enhancement or decrease of fluorescence. When the surfactant/dye ratio was changed from 100/1 to 50/1 to 25/1, the quantum yield decreased, possibly due to self-quenching of dyes when the number of fluorophores per ICRM became higher. Overall the quantum yield for the ICRM entrapped dyes was lower compared to those of the free fluorophores. Surprisingly, the quantum yield of dye **2** increased from 0.16 to 0.40 for 100/1 but then decreased to 0.31 and 0.19 for 50/1 and 25/1, respectively. This could be due to changes of property of micropolar environment. For the fluorophores **3** and **4**, the fluorescence quantum yield decreased upon trapping at all three ratios.

Effect of w_0

w_0 is the ratio of water to surfactant in the reverse micelle. It is well known in the literature that water in the reverse micelle has properties different from that of the bulk water and, at high w_0, the water in the RM core will approach the bulk water in property.[26] For the ICRMs, w_0 was changed from 2.5 to 10, while keeping surfactant/fluorophore ratio at 100/1. For fluorophores **3** and **4,** the change in w_0 did not have any significant effect in the UV-vis and fluorescence spectra or on the quantum yield. For the fluorophore **2,** the emission λ_{max} changed from 460 nm to 448 nm when w_0 changed from 5 to 10 and 5 to 2.5. Fluorescent quantum yields decreased from 0.40 to 0.12 to 0.16 in the meantime. Again this could be a result of change of micropolarity and solvatochromic property of fluorophore **2.**[27] At lower w_0 = 2.5, the fluorophore at the surfactant/water interface can be influenced by the bulk solvent, which is hydrophobic. This could be reason for the blue shift.

Table 2. Quenching studies of dyes **1**, **2**, and **3**.

entry	dye	medium	TEMPO	TBAI
			k_q $mM^{-1}s^{-1}$	
1	**1**	Methanol	0.024	0.003
2		ICRM	0.018	0.029
3	**2**	Methanol	0.035	-
4		ICRM	0.005	0.002
5	**3**	Methanol	0.098	0.008
6		ICRM	0.067	0.045

Fluorescence Quenching of ICRM-Trapped Dyes

We chose two quenchers, tetrabutyl ammonium iodide and TEMPO. Iodide quenches fluorescence by promoting intersystem crossing due to the heavy atom effect.[28] TEMPO

quenches the fluorescence by excited-state collisional dynamic quenching.[29] Since the dyes are expected to be in the hydrophilic interface, they would be more accessible to TBAI than to TEMPO. Quenching efficiencies can be quantified by Stern-volmer quenching constants. A hydrophobic quencher TEMPO can easily penetrate through the hydrophobic shell of ICRM. If the fluorophore is located at the interface, it should be easily quenched. For a hydrophilic quencher, there is higher partition tendency for it to go to the ICRM core. Enhanced quenching should result from a high local concentration. TEMPO quenched all the fluorophores, whether they were free or entrapped inside ICRMs . Free fluorophores were quenched slightly better than the trapped dyes. Apparently, the trapped dyes were somewhat protected by the surfactant hydrophobic tails. Hydrophilic quencher TBAI quenched the fluorescence of the dyes better under trapped condition than the free condition. This is again due to high local concentration of the quencher at the interface. From these quenching studies it was very clear that the dyes were located at the interface, but accessible to both hydrophobic and hydrophilic quenchers.

Conclusion

In this work, dyes were encapsulated and their photophysical properties were compared with those of the free dyes in methanol. Photophysical properties were retained upon entrapment. Quantum yield of fluorescence increased for dye **2** and decreased for dyes **3** and **4**. Dyes were located in the hydrophilic core but were accessible to both the hydrophilic and hydrophobic quencher. The properties bode well for the applications of ICRMs in catalysis because the entrapped catalysts need to be readily accessible to substrates of different kinds.

Experimental Section

General Method

All reagents and solvents were of ACS-certified grade or higher and used as received from commercial suppliers. Routine ^{1}H and ^{13}C NMR spectra were recorded on a Bruker DRX-400 or on a Varian VXR-400 spectrometer. HR-MS mass was recorded on Shimadzu LCMS-2010 mass spectrometer. Dynamic light scattering (DLS) was performed on a PD2000DLS+ dynamic light scattering detector.

Syntheses

Scheme S1

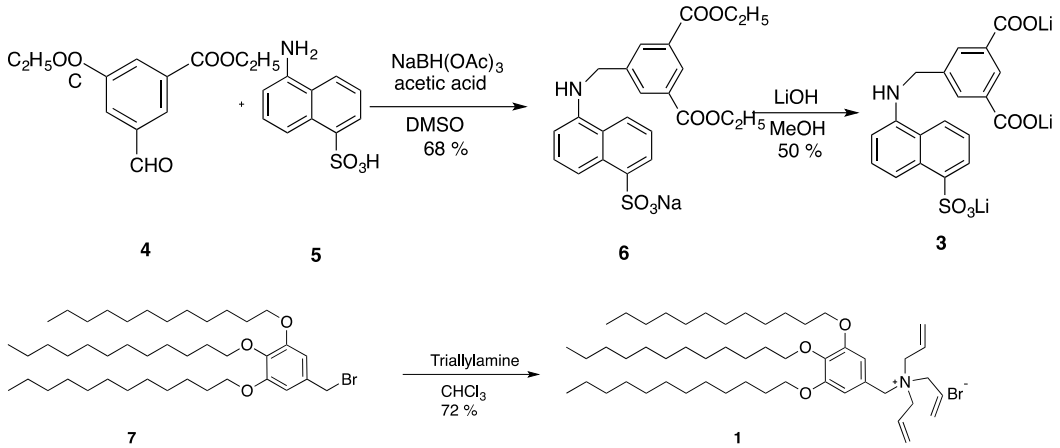

Syntheses of compounds **5**,[30] and **7**,[2] were previously reported.

Compound 6. To a solution of **5** (0.30 g, 1.29 mmol) and **6** in DMSO (10 mL), sodium triacetoxyborohydride (0.5 g, 2.3 mmol) and acetic acid (0.4 mL, 6.66 mmol) were added. The reaction mixture was stirred at room temperature for 24 h. The reaction mixture was poured into brine water (500 mL) and the product was removed by vacuum filtration. Then the product was collected from the column by eluting with methanol/ EtOAc (1: 10) and the solvents were removed by rotary evaporation. The residue was purified by column chromatography over silica gel using

EtOAc /methanol (20/1 to 13/1 to 20/1) as the eluent to give a glassy solid **6** (0.20 g, 68 %). ^{1}H NMR (400 MHz, Methanol-d_4, δ): 8.48 (s, 1H), 8.30 (m, 3H), 8.15 (m, 3H), 7.44 (m, 1H), 7.27 (m, 1H), 6.45 (m, 1H), 4.65 (m, 2H), 4.35 (qd, 7.1, 1.0 Hz, 4H), 1.35 (t, J = 6.7 Hz, 6H). ^{13}C NMR (101 MHz, Methanol-d_4, δ): 165.70, 156.13, 143.53, 141.65, 140.29, 131.96, 130.79, 130.01, 129.25, 128.42, 126.98, 125.42, 124.37, 124.20, 122.32, 120.21, 115.16, 104.70, 79.41, 61.15, 47.69, 47.48, 47.27, 47.05, 46.53, 27.76, 13.27. HRMS (*m/z*): $[M + H]^+$ calcd for $C_{23}H_{22}NNaO_7S$, 480.1087; found, 480.1094.

Compound 5. Compound **6** (0.2 g, 0.47 mmol) was dissolved in MeOH (5mL). A solution of LiOH (0.057 g, 1.39 mmol) in 0.2 mL water was added over a period of 30 minutes and the reaction mixture was allowed to stir for 12 h. Then 100 mL of methanol was added to the reaction mixture and the solution was dried by anhydrous sodium sulfate. The solvent was removed by rotary evaporation and the residue was purified by preparative TLC using EtOAc /methanol (6/4) to give a glassy solid. (0.1 g, 50 %). ^{1}H NMR (400 MHz, Methanol-d_4, δ): 8.88 (s, 1H), 8.62 (d, J = 8.4 Hz, 1H), 8.44 (q, J = 5.8, 5.2 Hz, 4H), 7.67 (dtd, J = 43.4, 7.9, 5.0 Hz, 2H), 6.92 (d, J = 7.1 Hz, 1H), 4.89 (d, J = 4.7 Hz, 2H).

Compound 1. Triallylamine (1.8 mL, 10.36 mmol) was slowly added to a solution of 3, 4, 5-tris(dodecyloxy)benzyl bromide **7** (7.4 g, 10.27 mmol) in $CHCl_3$. After 3 d at room temperature, $CHCl_3$ was removed *in vacuo* and the crude product was washed with acetone (2 mL) to give a white solid (6.4 g, 72 %). ^{1}H NMR (400 MHz, $CDCl_3$, δ): 6.9 (s, 2H), 5.99-5.94 (m, 3H), 5.76-5.67 (m, 6H), 4.89 (s, 2H), 4.19(d, 6H).99-3.97 (m, 6H), 1.8-126 (m, 60H), 0.88 (t, 9H). ^{13}C NMR (400 MHz, $CDCl_3$, δ): 153.51, 140.00, 128.38, 125.30, 122.04, 111.53, 73.50, 69.61, 64.42, 61.89, 54.43, 31.95, 30.39, 29.79, 29.77, 29.75, 29.70, 29.68, 29.64, 29.62, 29.53, 29.44, 29.43, 29.42,

29.40, 26.20, 26.13, 22.71, 14.14. HR-MS (*m/z*) $[M-Br]^+$ for calcd $C_{52}H_{94}NO_3^+$, 780.7228; found, 780.7228.

Preparation of fluoro@ICRM

Millipore water (1.8 μL) was added to a solution of **1** (20 mg, 0.02 mmol), **2** (0.019 mg, 0.00002 mmol) in heptane (10 mL) and $CHCl_3$ (0.5 mL). The mixture was hand shaken and sonicated at room temperature for 4 min to give an optically clear solution. After addition of DTT (5.30 mg, 0.03 mmol) and 2-hydroxy-4′(2-hydroxyethoxy)-2-methylpropiophenone (0.5 mg, 0.002 mmol) the mixture was irradiated in a Rayonet photoreactor for ca. 2 h until most alkenic protons were consumed. The organic solvents were removed by rotary evaporation. The residue was dissolved in 0.3 mL chloroform and precipitated upon addition of 10 ml of acetone. It was centrifuged and the residue was washed with methanol/acetone (4 mL/6 mL) 3 times and dried to give 18 mg (75 %) and used for photophysical experiments.

Millipore water (1.8 μL) was added to a solution of **1** (20 mg, 0.02 mmol), Sulpharhodamine **4** (0.14 mg, 0.00002 mmol) in heptane (10 mL) and $CHCl_3$ (0.5 mL). The mixture was hand shaken and sonicated at room temperature for 4 min to give an optically clear solution. After addition of DTT (5.30 mg, 0.03 mmol) and 2-hydroxy-4′(2-hydroxyethoxy)-2-methylpropiophenone (0.5 mg, 0.002 mmol) the mixture was irradiated in a Rayonet photoreactor for ca. 2 h until most alkenic protons were consumed. The organic solvents were removed by rotary evaporation. The residue was dissolved in 0.3 mL chloroform and precipitated upon addition of 10 ml of acetone. It was centrifuged and the residue was washed with methanol/acetone (4 mL/6 mL) 3 times and dried to give 18 mg (75 %) and used for photophysical experiment.

Millipore water (1.8 μL) was added to a solution of **1** (20 mg, 0.02 mmol), Eosin y **3** (0.16 mg, 0.00002 mmol) in heptane (10 mL) and $CHCl_3$ (0.5 mL). The mixture was hand shaken and

sonicated at room temperature for 4 min to give an optically clear solution. After addition of DTT (5.30 mg, 0.03 mmol) and 2-hydroxy-4′(2-hydroxyethoxy)-2-methylpropiophenone (0.5 mg, 0.002 mmol) the mixture was irradiated in a Rayonet photoreactor for ca. 2 h until most alkenic protons were consumed. The organic solvents were removed by rotary evaporation. The residue was dissolved in 0.3 mL chloroform and precipitated upon addition of 10 ml of acetone. It was centrifuged and the residue was washed with methanol/acetone (4 mL/6 mL) 3 times and dried to give 18 mg (75 %) and used for photo physical experiments.

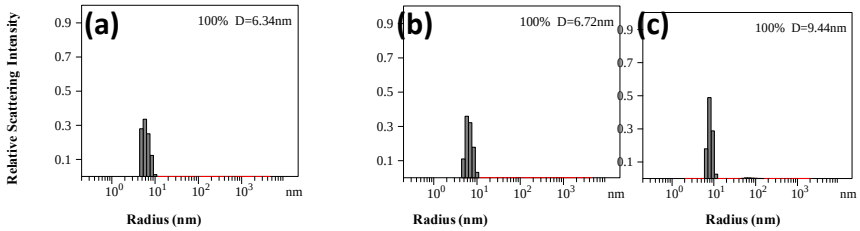

Figure 4. Hydrodynamic Diameters of **2**@ ICRMs determined by DLS at w_0 = (a) 2.5 (b) 5 and (c) 10 in heptane/chloroform (10:0.5). The diameter was calculated using the viscosity and refractive index of heptane.

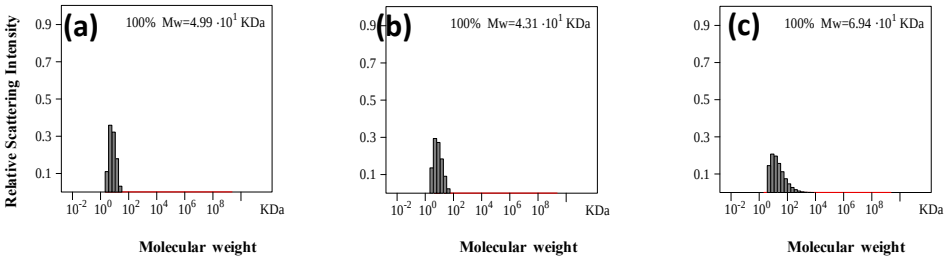

Figure 5. Distribution of the molecular weights of the **2**@ICRMs (a) w_0 = 2.5 (b) 5 and (c) 10 and the correlation curve for DLS. The molecular weight distribution was calculated by the PRECISION DECONVOLVE program assuming the intensity of scattering is proportional to the mass of the particle squared. (a) If each unit of building block for the **2**@ICRM is assumed to

contain one molecule of compound **1** (MW = 863 g/mol), 1.5 molecules of DTT (MW = 156 g/mol), and 5molecules of water (MW = 18 g/mol), the molecular weight of the fluoro@ICRM translates to **43** [= 49900/(863+1.5×156+2.5×18)] of such units. (b) If each unit of building block for the **2**@ICRM is assumed to contain one molecule of compound **1** (MW = 863 g/mol), 1.5 molecules of DTT (MW = 156 g/mol), and 5molecules of water (MW = 18 g/mol), the molecular weight of the fluoro@ICRM translates to **36** [= 43100/(863+1.5×156+5×18)] of such units.(c) If each unit of building block for the **2**@ICRM is assumed to contain one molecule of compound **1** (MW = 863 g/mol), 1.5 molecules of DTT (MW = 156 g/mol), and 5molecules of water (MW = 18 g/mol), the molecular weight of the fluoro@ICRM translates to **155** [= 69400/(863+1.5×156+10×18)] of such units.

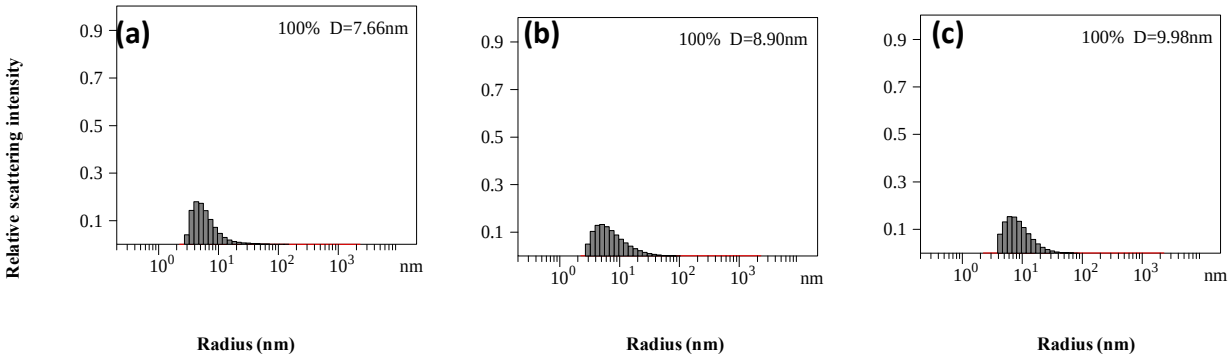

Figure 6. Hydrodynamic Diameters of **3**@ ICRMs determined by DLS at w_0 = (a) 2.5 (b) 5 and (c) 10 in heptane/chloroform (10:0.5). The diameter was calculated using the viscosity and refractive index of heptane.

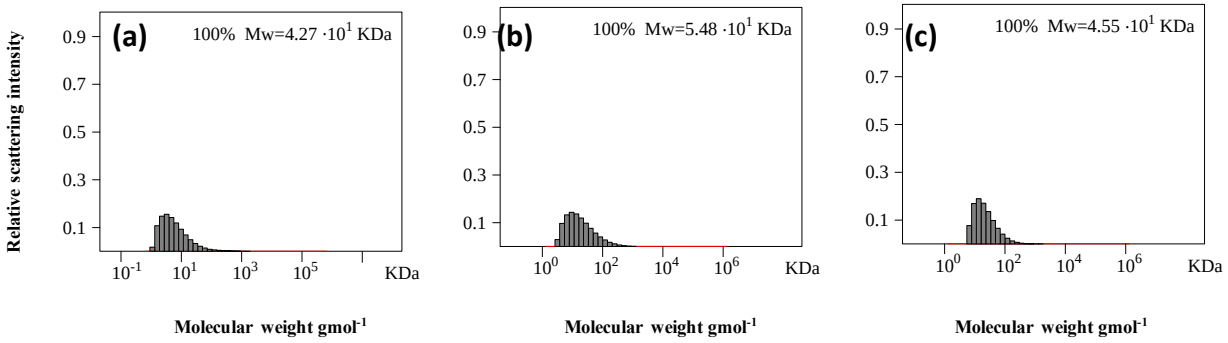

Figure 7. Distribution of the molecular weights of the **3**@ICRMs (a) w_0 = 2.5 (b) 5 and (c) 10 and the correlation curve for DLS. The molecular weight distribution was calculated by the PRECISION DECONVOLVE program assuming the intensity of scattering is proportional to the mass of the particle squared. (a) If each unit of building block for the **3**@ICRM is assumed to contain one molecule of compound **1** (MW = 863 g/mol), 1.5 molecules of DTT (MW = 156 g/mol), and 5molecules of water (MW = 18 g/mol), the molecular weight of the fluoro@ICRM translates to **37** [= 42700/(863+1.5×156+2.5×18)] of such units. (b) If each unit of building block for the **3**@ICRM is assumed to contain one molecule of compound **1** (MW = 863 g/mol), 1.5 molecules of DTT (MW = 156 g/mol), and 5molecules of water (MW = 18 g/mol), the molecular weight of the fluoro@ICRM translates to **46** [= 548000/(863+1.5×156+5×18)] of such units. (c) If each unit of building block for the **3**@ICRM is assumed to contain one molecule of compound **1** (MW = 863 g/mol), 1.5 molecules of DTT (MW = 156 g/mol), and 5molecules of water (MW = 18 g/mol), the molecular weight of the fluoro@ICRM translates to **36** [= 45500/(863+1.5×156+10×18)] of such units.

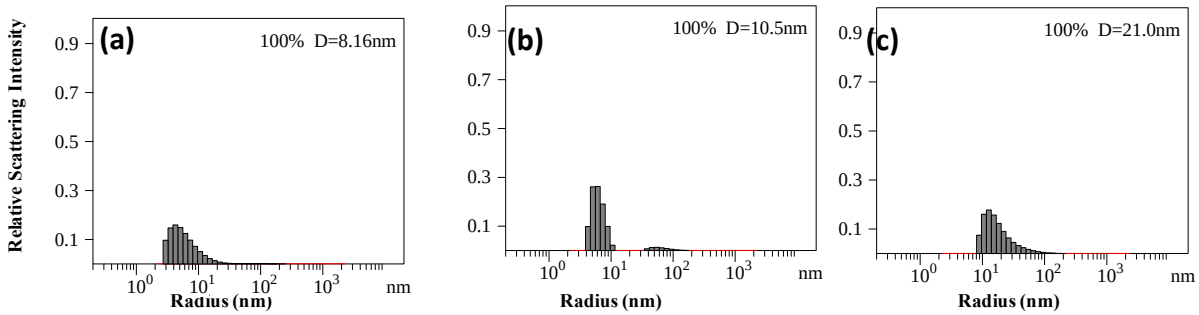

Figure 8. Hydrodynamic Diameters of **4**@ ICRMs determined by DLS at W_0= (a) 2.5 (b) 5 and (c) 10 in heptane/chloroform (10:0.5). The diameter was calculated using the viscosity and refractive index of heptane.

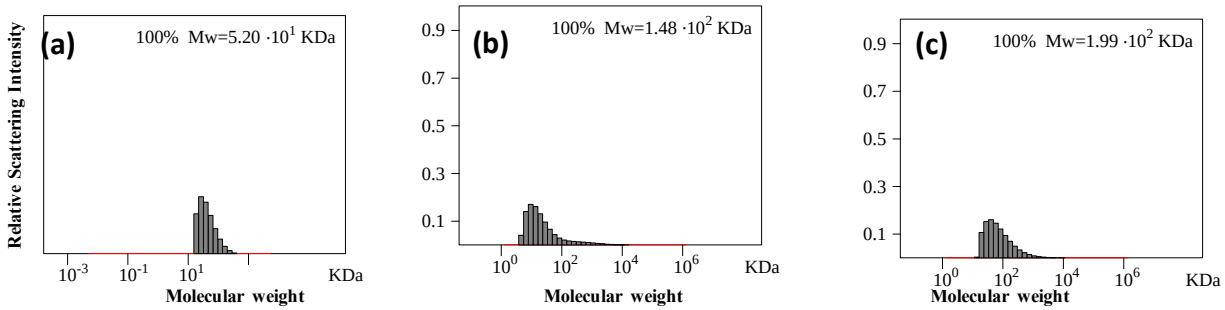

Figure 9. Distribution of the molecular weights of the 4@ICRMs (a) w_0 = 2.5 (b) 5 and (c) 10 and the correlation curve for DLS. The molecular weight distribution was calculated by the PRECISION DECONVOLVE program assuming the intensity of scattering is proportional to the mass of the particle squared. (a) If each unit of building block for the **4**@ICRM is assumed to contain one molecule of compound **1** (MW = 863 g/mol), 1.5 molecules of DTT (MW = 156 g/mol), and 5molecules of water (MW = 18 g/mol), the molecular weight of the fluoro@ICRM translates to **45** [= 52000/(863+1.5×156+2.5×18)] of such units. (b) If each unit of building block for the **4**@ICRM is assumed to contain one molecule of compound **1** (MW = 863 g/mol), 1.5 molecules of DTT (MW = 156 g/mol), and 5molecules of water (MW = 18 g/mol), the molecular weight of the fluoro@ICRM translates to **120** [= 66300/(863+1.5×156+5×18)] of such units. (c) If each unit of building block for the **4**@ICRM is assumed to contain one molecule of compound **1**

(MW = 863 g/mol), 1.5 molecules of DTT (MW = 156 g/mol), and 5molecules of water (MW = 18 g/mol), the molecular weight of the fluoro@ICRM translates to **160** [= 199000/(863+1.5×156+10×18)] of such units.

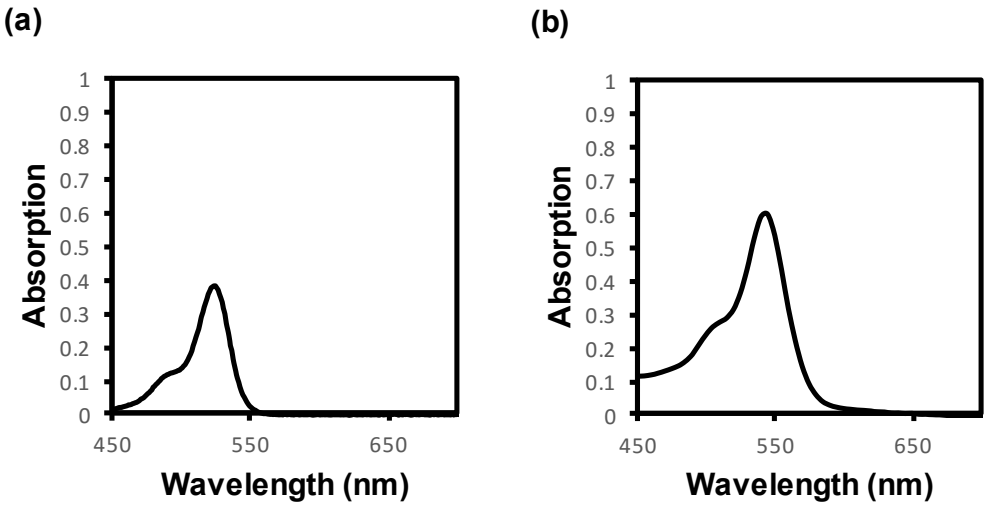

Figure 10. Absorption spectra of fluorophore [**3**]. (a) methanol [**3**] =11.2 μM and (b) ICRM (25/1) w_0 = 5 in Chloroform [**3**] = 46 μM.

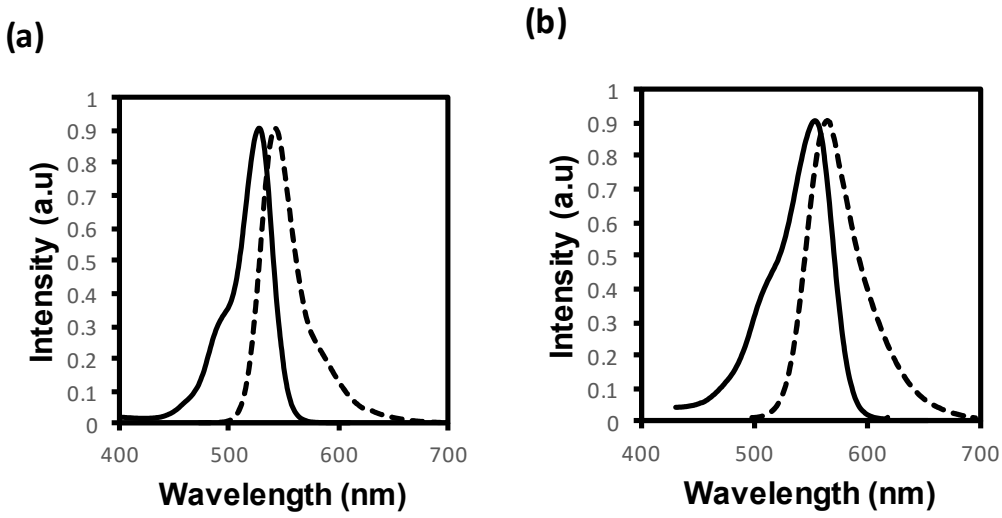

Figure 11. Normalized Emission and excitation spectra of fluorophore **[3]** = 4.6 μM (a) methanol and (b) ICRM (100/1) w_0 = 5 in chloroform.

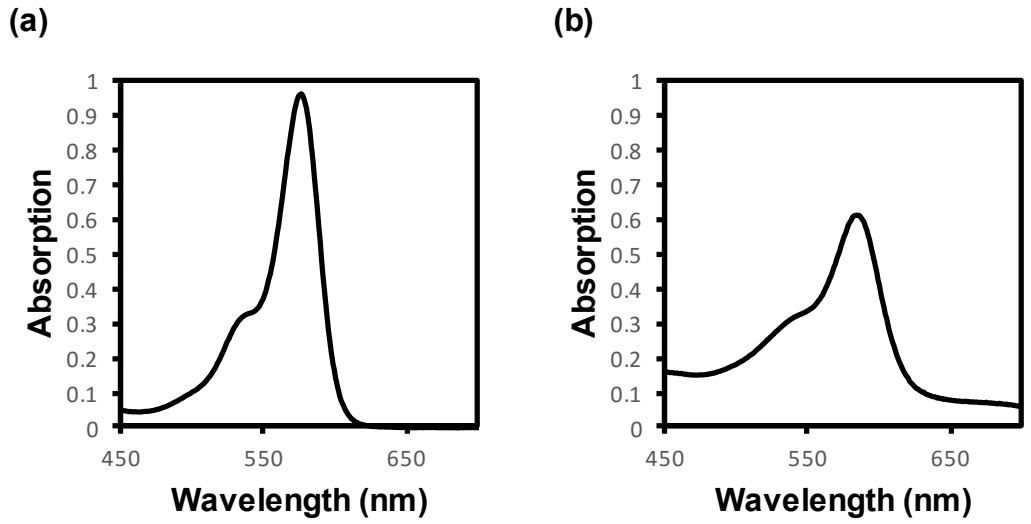

Figure 12. Absorption spectra of fluorophore [**4**]. (a) methanol [**4**] =11.2 μM and (b) ICRM (25/1) $w_0 = 5$. [**4**] = 46 μM in chloroform.

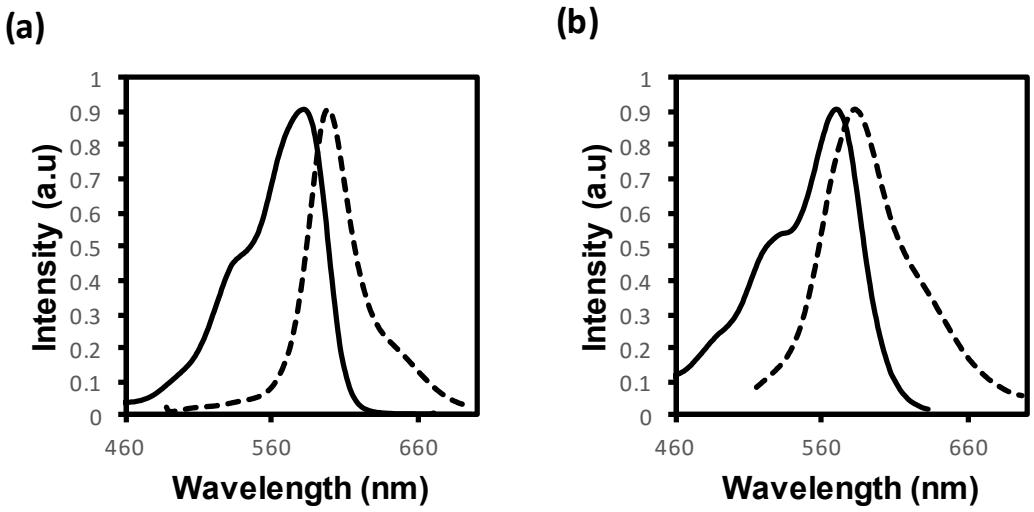

Figure 13. Normalized Emission and excitation spectra of fluorophore [**4**] = 4.6 μM (a) methanol and (b) ICRM (100/1) $w_0 = 5$ in chloroform.

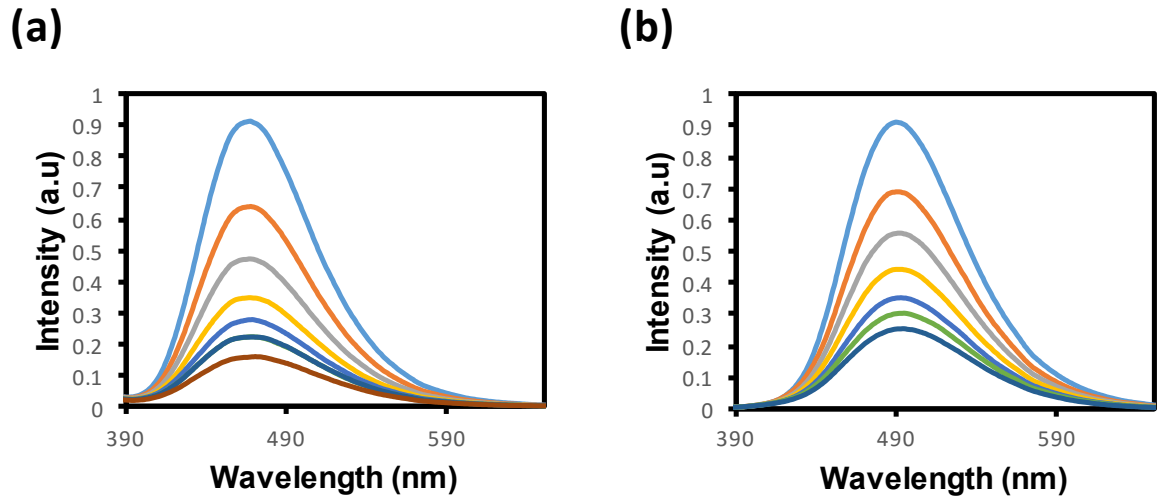

Figure 14. Emission spectra of fluorophore [**2**] = 2.5 μM in the presence of different concentrations of TEMPO. (a) methanol and (b) ICRM (100/1) w_0 = 5 in chloroform.

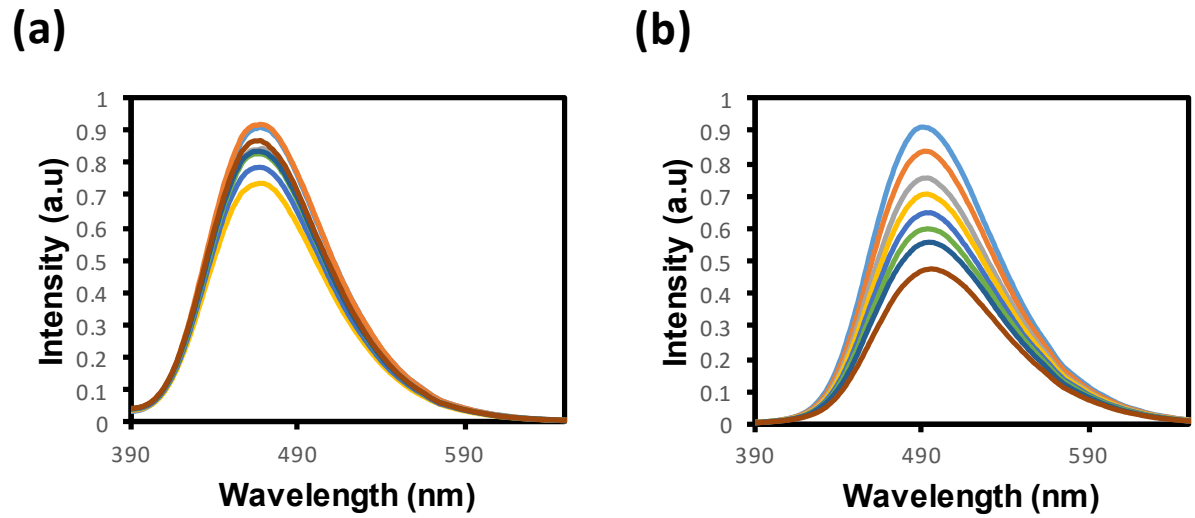

Figure 15. Emission spectra of fluorophore [**2**] = 2.5 μM in the presence of different concentrations of Tetrabutylammonium Iodide. (a) methanol and (b) ICRM (100/1) w_0 = 5 in chloroform.

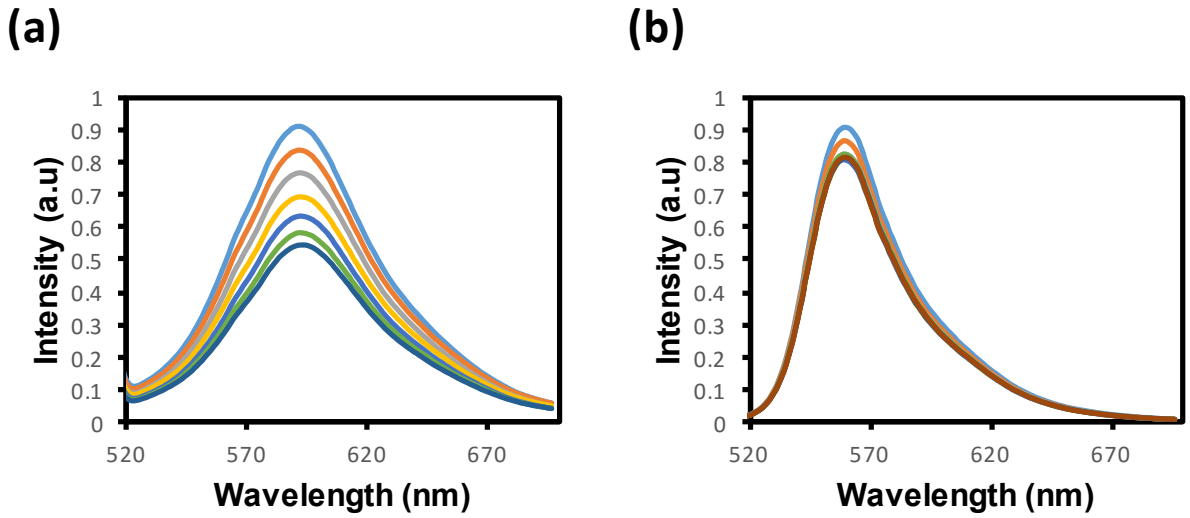

Figure 16. Emission spectra of fluorophore [**4**] = 4.6 μM in the presence of different concentrations of TEMPO. (a) methanol and (b) ICRM (100/1) w_0 = 5 in chloroform.

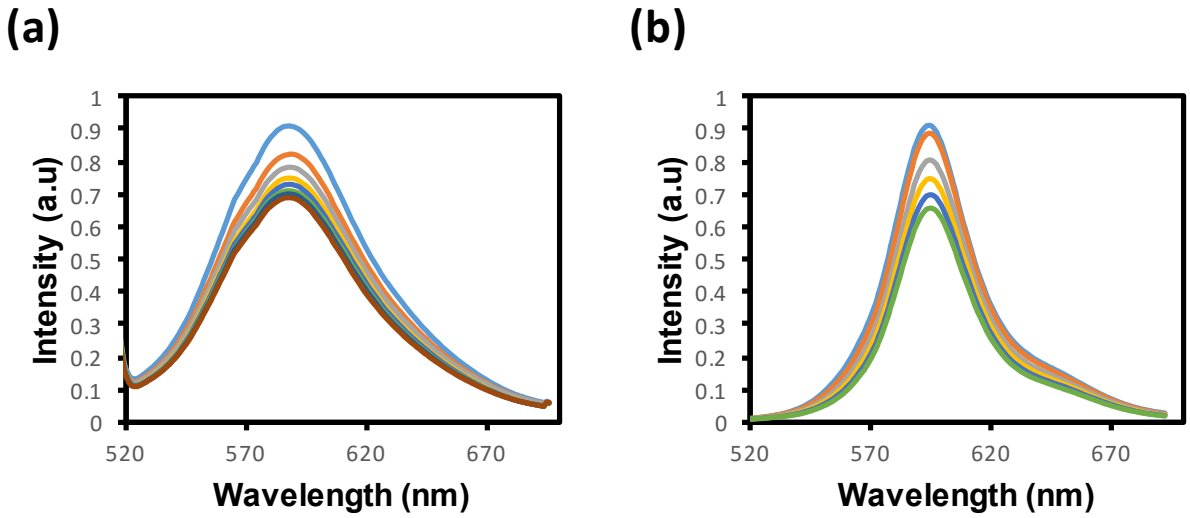

Figure 17. Emission spectra of fluorophore [**4**] = 4.6 μM in the presence of different concentrations of Tetrabutylammonium Iodide. (a) methanol and (b) ICRM (100/1) w_0 = 5 in chloroform.

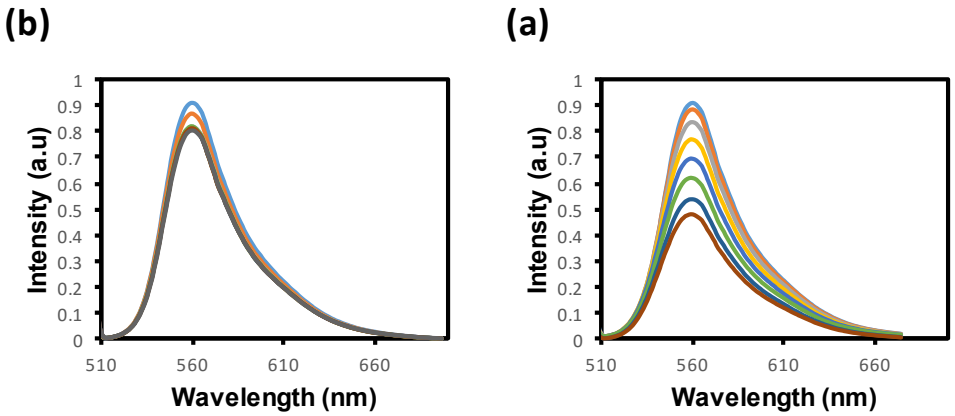

Figure 18. Emission spectra of fluorophore **3** in ICRM [**3**] =11.2 μM in the presence of different concentrations of (a) TEMPO (b) TBAI in chloroform.

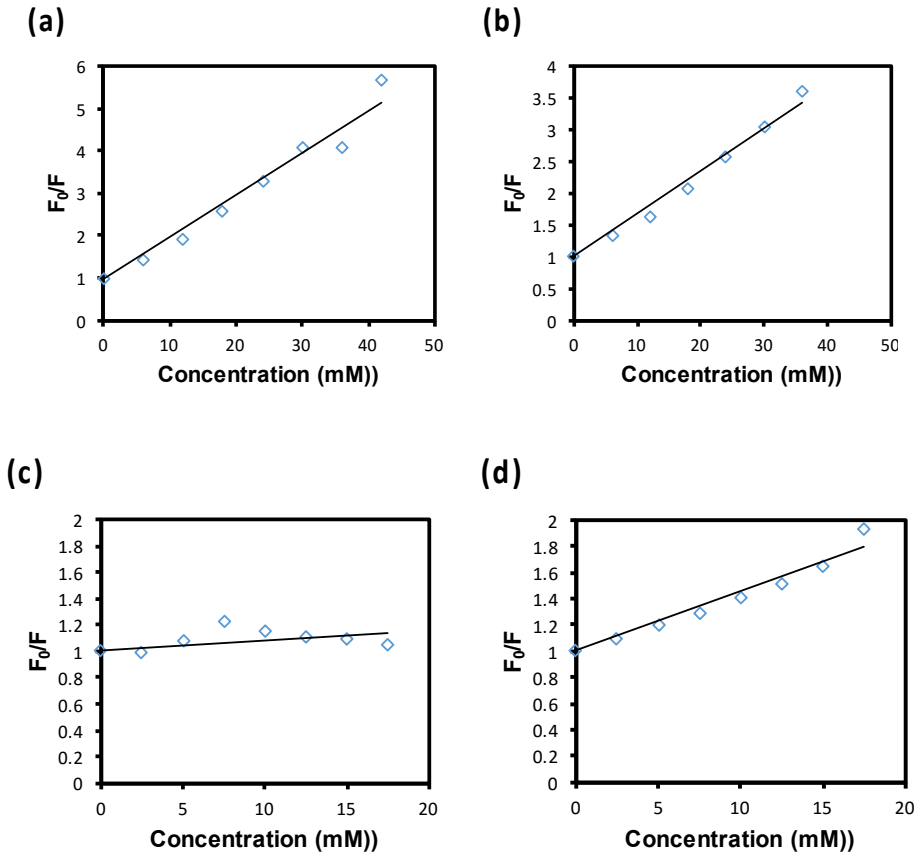

Figure 19. Stern-Volmer Plot of quenching of fluorophore **2** by (a) Tempo in methanol, (b) Tempo in ICRM, (c) TBAI in methanol and (d) TBAI in ICRM in chloroform.

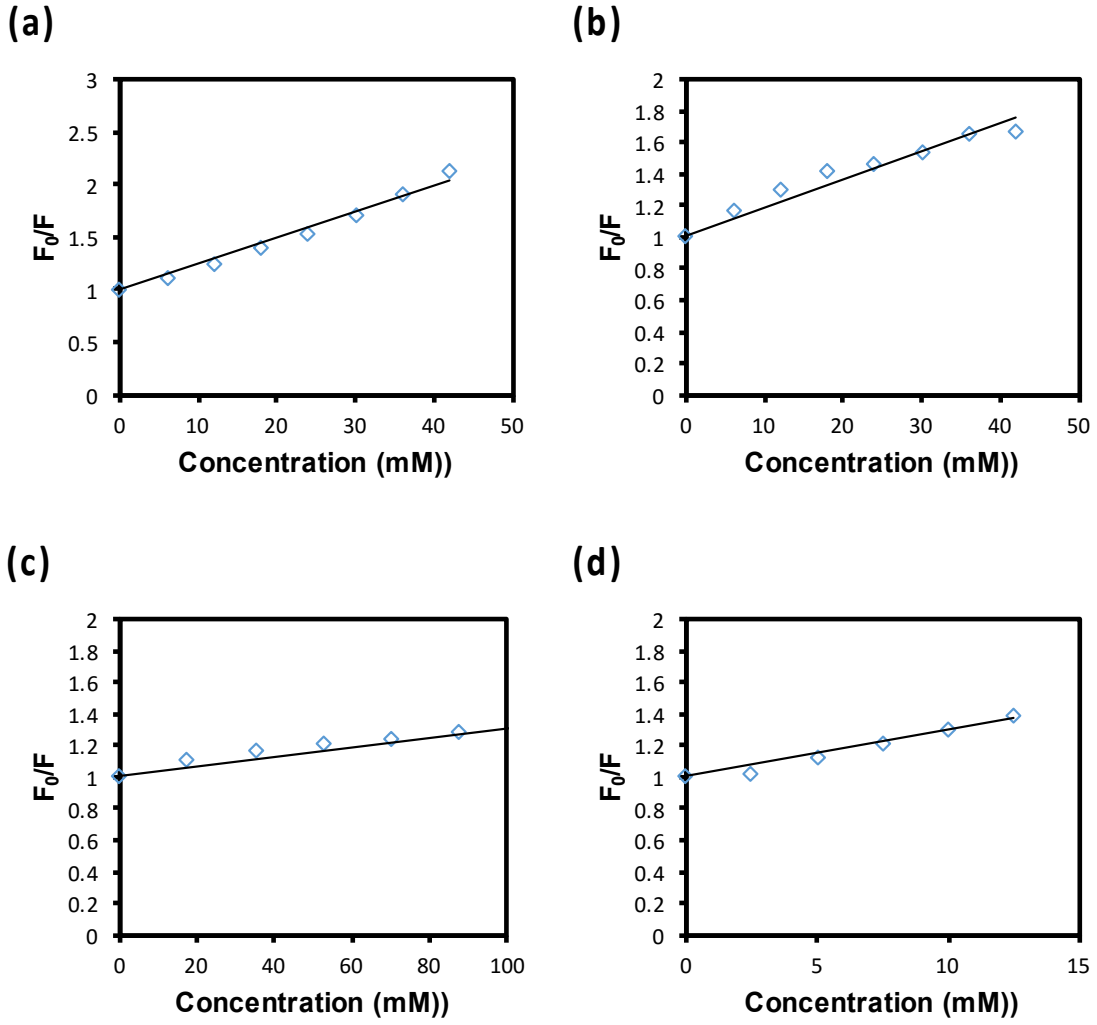

Figure 20. Stern-Volmer Plot of quenching of fluorophore **4** by (a) Tempo in methanol, (b) Tempo in ICRM, (c) TBAI in methanol and (d) TBAI in ICRM.

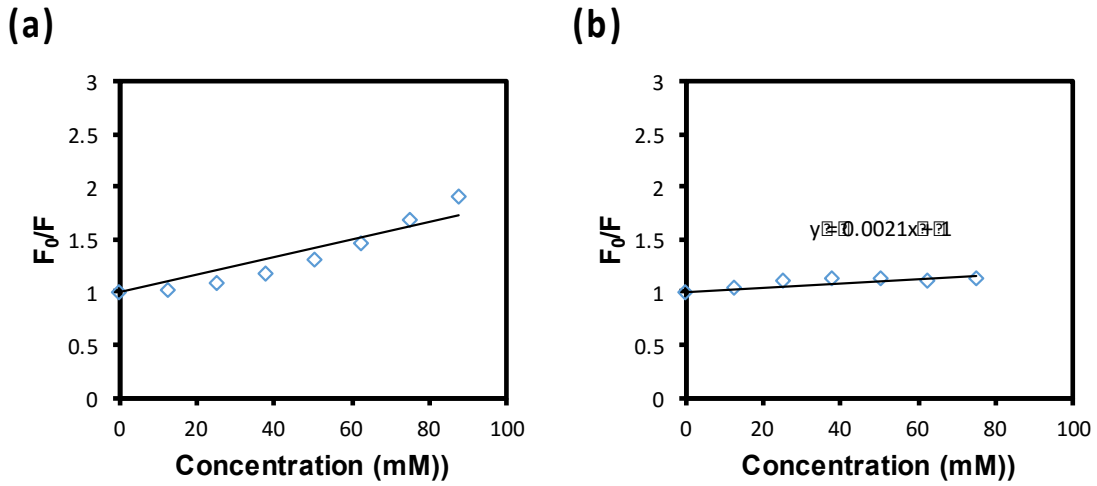

Figure 21. Stern-Volmer plot of fluorophore **3** in ICRM [**3**] =11.2 μM in the presence of different concentrations of (a) TEMPO (b) TBAI.

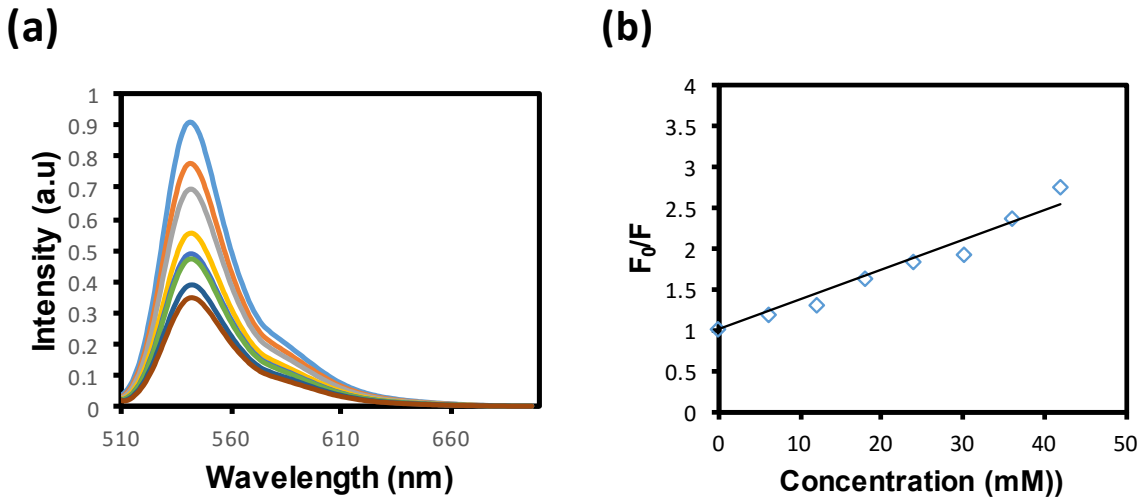

Figure 22. (a) Emission spectra of flourophore [**3**] in the presence of different concentrations of TEMPO. [**3**] =11.2 μM in methanol and (b) Stern-Volmer plot.

^{1}H and ^{13}C NMR spectra

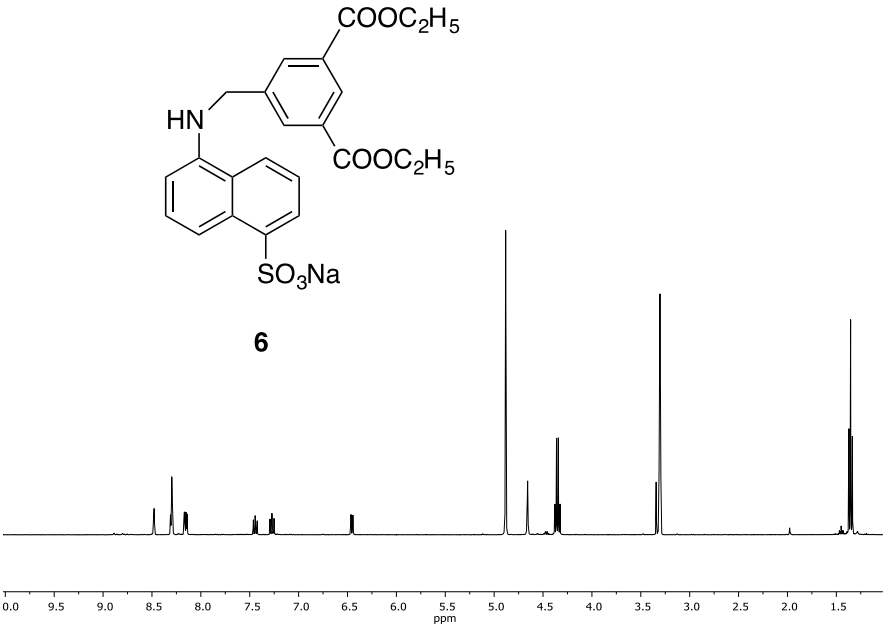

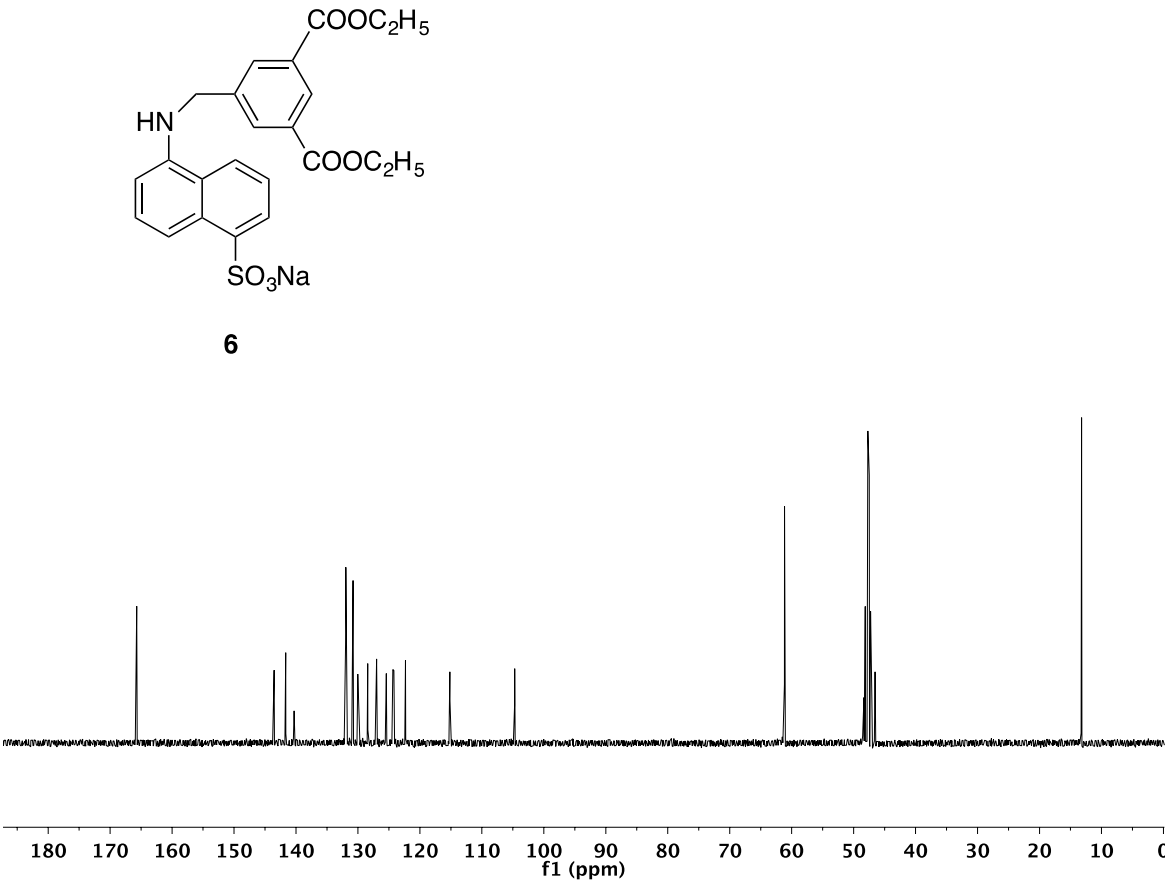

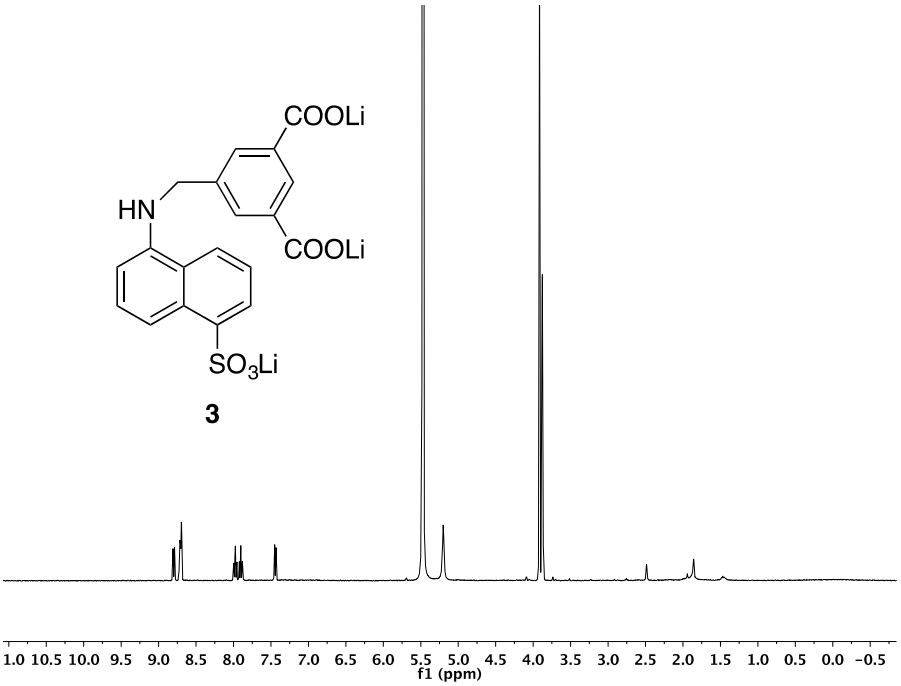

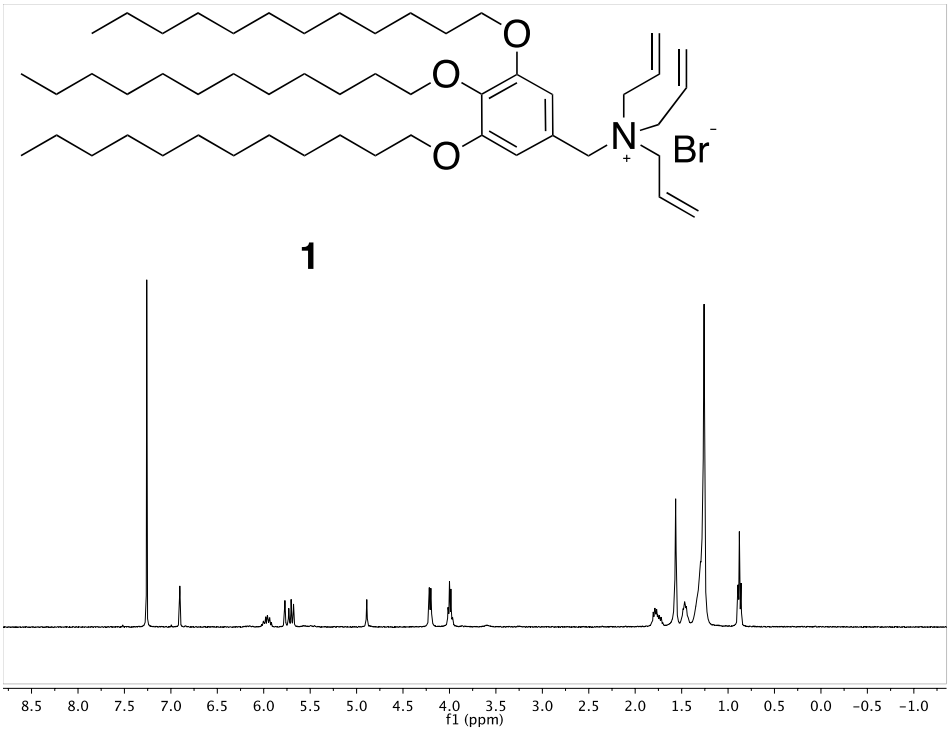

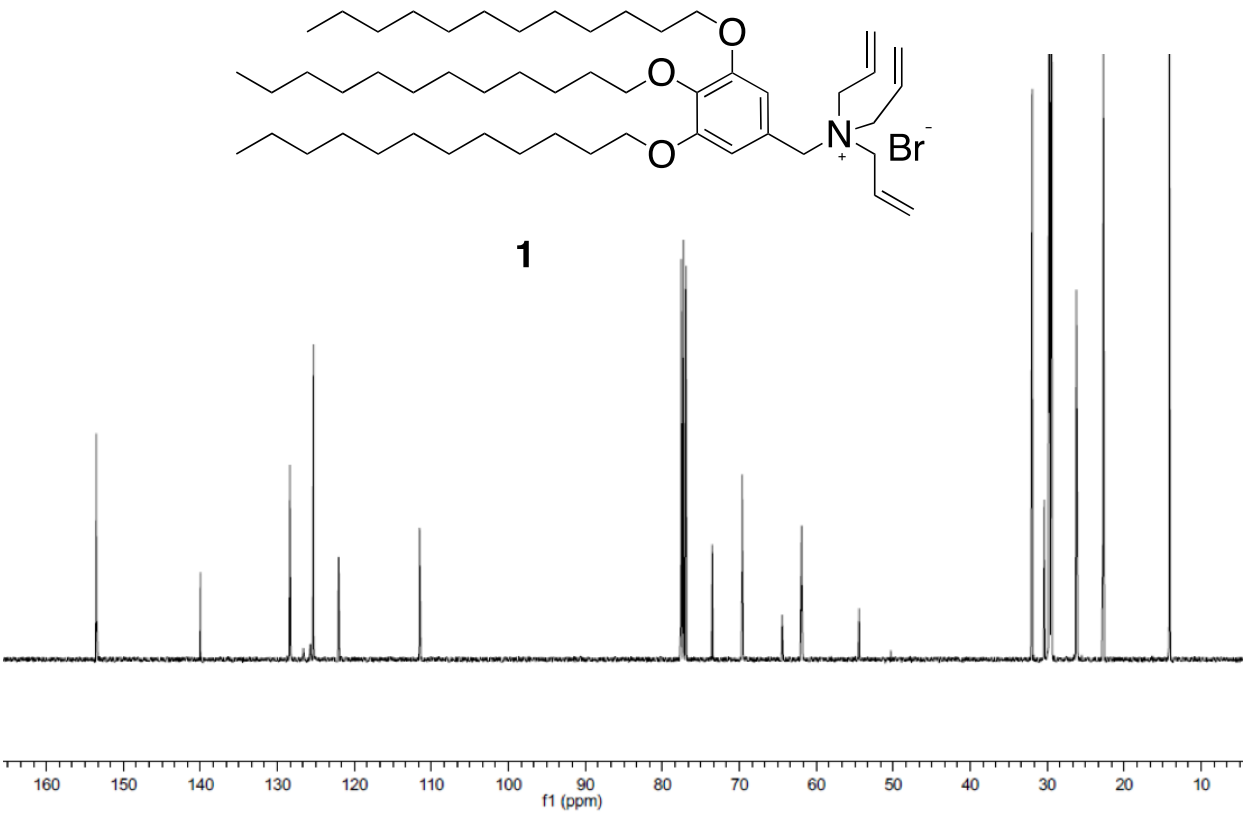

References:

1. Pileni, M. P., *Structure and Reactivity in Reverse Micelles*. Elsevier: Amsterdam, 1989.

2. Menger, F. M.; Donohue, J. A.; Williams, R. F., Catalysis in Water Pools. *J. Am. Chem. Soc.* **1973,** *95* (1), 286-288.

3. Menger, F. M.; Yamada, K., Enzyme Catalysis in Water Pools. *J. Am. Chem. Soc.* **1979,** *101* (22), 6731-6734.

4. Luisi, P. L.; Giomini, M.; Pileni, M. P.; Robinson, B. H., Reverse Micelles as Hosts for Proteins and Small Molecules. *Biochim. Biophys. Acta* **1988,** *947* (1), 209-246.

5. Pileni, M. P., Nanosized particles made in colloidal assemblies. *Langmuir* **1997,** *13* (13), 3266-3276.

6. Pileni, M. P., The role of soft colloidal templates in controlling the size and shape of inorganic nanocrystals. *Nat. Mater.* **2003,** *2* (3), 145-150.

7. Mueller, A.; O'Brien, D. F., Supramolecular materials via polymerization of mesophases of hydrated amphiphiles. *Chem. Rev.* **2002,** *102* (3), 727-757.

8. Gin, D. L.; Gu, W.; Pindzola, B. A.; Zhou, W. J., Polymerized lyotropic liquid crystal assemblies for materials applications. *Acc. Chem. Res.* **2001,** *34* (12), 973-980.

9. Eastoe, J.; Summers, M.; Heenan, R. K., Control over phase curvature using mixtures of polymerizable surfactants. *Chem. Mater.* **2000,** *12* (12), 3533-3537.

10. Yan, F.; Texter, J., Polymerization of and in mesophases. *Adv. Colloid Interface Sci.* **2006,** *128-130*, 27-35.

11. Tajima, K.; Aida, T., Controlled polymerizations with constrained geometries. *Chem. Commun.* **2000,** (24), 2399-2412.

12. Voortmans, G.; Verbeeck, A.; Jackers, C.; Deschryver, F. C., Polymerization of N,N-Didodecyl-N-Methyl-N-(2-(Methacryloyloxy)Ethyl)Ammonium Chloride, an Inverse Micelle Forming Detergent. *Macromolecules* **1988,** *21* (7), 1977-1980.

13. Voortmans, G.; De Schryver, F. C., Polymerization in and of Inverse Micelles. In *Structure and reactivity in reverse micelles*, Pileni, M. P., Ed. Elsevier: Amsterdam, 1989.

14. Zhang, S.; Zhao, Y., Facile Preparation of Organic Nanoparticles by Interfacial Cross-Linking of Reverse Micelles and Template Synthesis of Subnanometer Au−Pt Nanoparticles. *ACS Nano* **2011,** *5* (4), 2637-2646.

15. Jung, H. M.; Price, K. E.; McQuade, D. T., Synthesis and characterization of cross-linked reverse micelles. *J. Am. Chem. Soc.* **2003,** *125* (18), 5351-5355.

16. Price, K. E.; McQuade, D. T., A cross-linked reverse micelle-encapsulated palladium catalyst. *Chem. Commun.* **2005,** (13), 1714-1716.

17. Lee, L.-C.; Zhao, Y., Metalloenzyme-Mimicking Supramolecular Catalyst for Highly Active and Selective Intramolecular Alkyne Carboxylation. *J. Am. Chem. Soc.* **2014,** *136* (15), 5579-5582.

18. Zhang, S.; Zhao, Y., Template Synthesis of Subnanometer Gold Clusters in Interfacially Cross-Linked Reverse Micelles Mediated by Confined Counterions. *Langmuir* **2012,** *28* (7), 3606-3613.

19. Lee, L.-C.; Zhao, Y., Size-Selective Phase-Transfer Catalysis with Interfacially Cross-Linked Reverse Micelles. *Org. Lett.* **2012,** *14* (3), 784-787.

20. Corma, A.; Gonzalez-Arellano, C.; Iglesias, M.; Navarro, M. T.; Sanchez, F., Synthesis of bifunctional Au-Sn organic-inorganic catalysts for acid-free hydroamination reactions. *Chem. Commun.* **2008,** (46), 6218-6220.

21. Lee, L.-C.; Zhao, Y., Room Temperature Hydroamination of Alkynes Catalyzed by Gold Clusters in Interfacially Cross-Linked Reverse Micelles. *ACS Catalysis* **2014**, 688-691.

22. Peng, H. Q.; Niu, L. Y.; Chen, Y. Z.; Wu, L. Z.; Tung, C. H.; Yang, Q. Z., Biological Applications of Supramolecular Assemblies Designed for Excitation Energy Transfer. *Chem. Rev.* **2015,** *115* (15), 7502-7542.

23. Peng, H.-Q.; Chen, Y.-Z.; Zhao, Y.; Yang, Q.-Z.; Wu, L.-Z.; Tung, C.-H.; Zhang, L.-P.; Tong, Q.-X., Artificial Light-Harvesting System Based on Multifunctional Surface-Cross-Linked Micelles. *Angew. Chem. Int. Ed.* **2012,** *51* (9), 2088-2092.

24. Lakowicz, J. R., *Principles of fluorescence spectroscopy*. 2nd ed.; Kluwer Academic/Plenum: New York, 1999.

25. Israelachvili, J. N., *Intermolecular and surface forces: with applications to colloidal and biological systems*. Academic Press: London, 1985.

26. Moilanen, D. E.; Fenn, E. E.; Wong, D.; Fayer, M. D., Water dynamics in large and small reverse micelles: From two ensembles to collective behavior. *The Journal of Chemical Physics* **2009,** *131* (1), 014704.

27. Fletcher, K. A.; Storey, I. A.; Hendricks, A. E.; Pandey, S.; Pandey, S., Behavior of the solvatochromic probes Reichardt's dye, pyrene, dansylamide, Nile Red and 1-pyrenecarbaldehyde within the room-temperature ionic liquid bmimPF. *Green Chemistry* **2001,** *3* (5), 210-215.

28. Chmyrov, A.; Sandén, T.; Widengren, J., Iodide as a Fluorescence Quencher and Promoter—Mechanisms and Possible Implications. *The Journal of Physical Chemistry B* **2010,** *114* (34), 11282-11291.

29. Zhu, P.; Clamme, J.-P.; Deniz, A. A., Fluorescence Quenching by TEMPO: A Sub-30 Å Single-Molecule Ruler. *Biophysical Journal* **2005,** *89* (5), L37-L39.

30. Zhang, S. Y.; Zhao, Y., Rapid Release of Entrapped Contents from Multi-Functionalizable, Surface Cross-Linked Micelles upon Different Stimulation. *J Am Chem Soc* **2010,** *132* (31), 10642-10644.

CHAPTER 4. ENHANCEMENT OF CATALYTIC ACTIVITY AND SELECTIVITY OF MANGANESE PORPHYRIN CATALYSTS UPON ENTRAMENT IN INTERFACIALLY CROSS-LINKED REVERSE MICELLES (ICRM)

Premkumar Rathinam Arivalagan and Yan Zhao

Abstract

Manganese porphyrins were successfully encapsulated in the core of interfacial cross-linked reverse micelles. The catalytic efficiency was investigated in the epoxidation reactions of various olefins. The catalysts showed enhanced catalytic activity upon encapsulation compared to their free counterparts. In the free state catalyst, the porphyrin was easily deactivated by the formation of oxo-bridged Mn-O-Mn dimer. Upon encapsulation, this deactivation pathway was eliminated and the catalysts showed enhanced activity. Substrate scope of the catalysts was also investigated with various olefins.

Introduction

Site isolation potentially offers preservation of both structure and activity of a catalyst that is sensitive to solvent or other chemical species present in the bulk solution.[1] Site isolation renders unusual properties like enhanced fluorescent quantum yield, catalytic activity, and unusual stability.[2-3] Many materials can be used for site isolation such as mesoporous silica,[4] dendrimers,[5] starpolymers,[1] metal organic framework,[6] and their applications in multistep catalysis have been reported in the literature.[1, 4-6]

One of the most important applications of site isolation is in multistep catalysis. A more specific application is in "wolf and lamb reactions".[1] Acids and bases can be site isolated and

programmed to catalyze multistep reactions in a sequential manner without being deactivated by each other. Another application is in the manganese porphyrin-catalyzed epoxidation. Even though manganese porphyrins are similar to the iron heme moiety present in the active site of cytochrome P450, the catalyst in the loses its activity by the formation of a Mn-O-Mn dimer. Irreversible oxidation of the catalyst by the oxidant is another pathway of catalytic deactivation. In the native enzyme, the iron heme is isolated in the active site which precludes the formation of oxo-bridged Fe-O-Fe dimer.

Although many strategies have been reported in the literature, on the site-isolation of Mn-porphyrin complexes, none of these examples illustrate the site-isolation homogeneously in the solution phase.[7] Homogeneous catalysis has the advantage over heterogeneous catalysis in that the catalyst is easily accessible to the substrates. Having recognized this importance, our group used interfacially crosslinked reverse micelles as a soluble support for Pd nanoparticles for catalytic Heck reactions. The catalyst maintained its activity in multiple runs. The ICRM approach was used to encapsulate gold clusters and used to catalyze room temperature hydroamination reactions. Recently, ICRM was used not only as a support but also as an affinity site in cyclization of 4-pentynoic acid.[8-13] In that work, hydrophilic cationic core of ICRM was used to bring the negatively charged substrate to the catalytic site. Once the reaction was completed, the hydrophobic product was ejected from the active site, completing the catalytic cycle. After achieving considerable benefits of encapsulating nanoparticles, we explored the encapsulation of hydrophilic moieties. In the previous chapter, I reported the encapsulation of hydrophilic fluorophores and investigated their location in the core using fluorescence quenching studies. The study showed that entrapped fluorophores are at the interface and accessible to both hydrophilic and hydrophobic quenchers. In this chapter, we explore the encapsulation of hydrophilic

manganese porphyrin catalysts and demonstrate the benefit of such site isolation.

Results and discussion

Trapping of the catalysts:

The synthesis of catalyst@ICRM was similar to the synthesis of fluorophore@ICRM as described in the previous chapter. We chose surfactant **1** for the synthesis of catalyst@ICRM which can be crosslinked by free radical polymerization. We chose two catalysts, 5,10,15,20-tetrakis(4-sulfonatophenyl)porphine manganese(III) chloride **4** and manganese(III) 5,10,15,20-tetra(4-pyridyl)porphine chloride **5**, for encapsulation. Catalyst **4** was trapped using the similar strategy as reported in the previous work of encapsulating hydrophilic fluorophores. Catalyst **4** was anionic and can be solubilized in the cationic core of a reverse micelle which was subsequently polymerized by free radical polymerization. Encapsulation was estimated to be complete, as there was no leaching of the catalyst during washing using water and methanol.

Catalyst **5** was basic and trapped using p-vinyl benzoic as the co-surfactant to solubilize it in the core. Its encapsulation in the hydrophilic core was not as efficient as catalyst **4** since the catalyst **5** is slightly more hydrophobic. However, encapsulation was quantified by UV-visible spectroscopic measurements of the washings, which contained about 20 % of the catalyst. This means about 80 % of the catalyst was encapsulated. The catalyst/surfactant ratio of 1/25 was chosen.

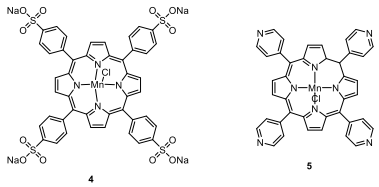

Fig. 1. Structures of catalyst **4** and **5.**

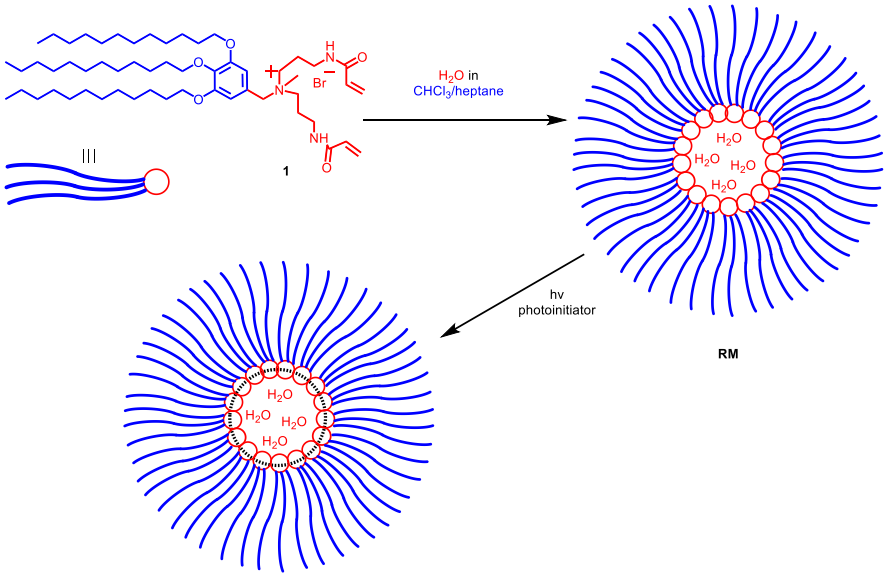

Scheme 1. Schematic representation of synthesis of ICRM.

Characterization

The ICRMs were characterized by ^{1}H NMR spectroscopy and dynamic light scattering (DLS) experiments and UV-vis spectroscopy. Figure 4 shows the ^{1}H NMR of surfactant **1** and catalyst@ICRM. Apparently, the olefinic protons disappeared upon photo cross-linking. Figure 6 and Figure 8 show the particle size distribution profiles of catalyst@ICRM obtained from DLS. The particles size was in the range of 4-10 nm. The aggregation number was obtained by DLS from which the number of metalloporphyrins per ICRM were deduced. The average aggregation number was found to be 50 at $w_0 = 5$. For the surfactant/catalyst ratio 50/1 there is one catalyst for every ICRM. The UV-visible spectra of the encapsulated catalysts were similar to their free counterparts (Fig. 3).

Epoxidation reactions:

Two oxidants, diacetoxyiodobenzene and iodosobenzene were used for epoxidation reactions and styrene was used as the model substrate. Both the entrapped catalysts with

(diacetoxyiodo)benzene showed similar activity compared to their free counterparts. This suggested that catalysts did not dimerize under free condition with (diaectoxyiodo)benzene. This oxidant was used to optimize the catalyst preparation and investigate the substrate scope of the trapped catalysts. With iodosobenzene, catalyst **5** was deactivated by irreversible oxidation of porphyrin ligand and catalyst **4** was deactivated by both reversible dimerization and irreversible oxidation. This oxidant was used to demonstrate the site isolation benefits of ICRM.

Optimization of the catalyst 4@ICRM

Our initial aim was to optimize the catalyst **4** for the best reaction conditions. Table 1 summarizes the reaction yields of epoxidation of styrene, under different conditions after 2 h for catalyst **4**. (diacetoxyiodo)benzene was used as the oxidant, since the catalyst did not undergo dimerization under this oxidation condition. we investigated the effect of solvents, w_0 and catalyst loading on the reaction yields.

Effect of solvents:

Solvents play significant roles in a reaction by stabilizing or destabilizing the transition state, increasing or decreasing the free energy of the reactants or the products. A solvent can have two effects in the case of an ICRM-entrapped catalyst. One is on the substrate's partition in a nonpolar solvent. For example, polar substrates prefer to migrate to the hydrophilic core. Another is a generic solvent effect on the reaction as mentioned above. Since styrene is a hydrophobic substrate, partition would not play any significant role in the reaction. But the location of the catalyst would have a significant effect on the reaction. To unravel these effects, a chloroform/methanol mixture with different compositions was used as the solvent. As the chloroform/methanol ratio was changed from 1/0 to 1/1 gradually, the reaction yield increased from 50% to 96%. This is a generic solvent effect, as the free catalyst also showed a similar trend (results not reported here). This

again supports our previous conclusion that catalyst is at the interface of the ICRM and solvents could have a significant impact on the catalysis.

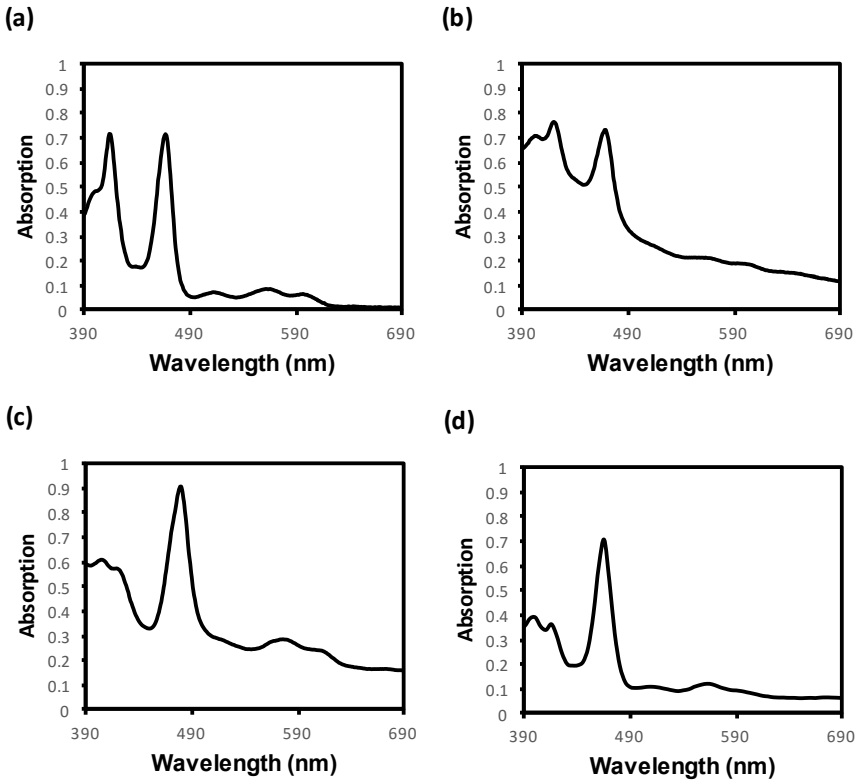

Figure 2. Absorption spectra of (a) [**4**] = 11.2 μM in methanol and (b) **4**@ICRM in methanol. w_0 = [H2O]/[surfactant] = 5. [**4**] = 20 μM. (c) [**5**] in methanol = 9.2 μM and (d) **5**@ICRM in methanol. w_0 = [H2O]/[surfactant] = 5. [**5**] = 24.2 μM.

Effect of loading:

The number of catalysts per ICRM can be easily varied by changing the catalyst/surfactant ratio during the ICRM synthesis. Catalyst/surfactant molar ratios of 1/50, 1/25, and 1/12.5 were chosen for the preparation of **4**@ICRM. These ratios translate to a number of catalysts per ICRM of 1, 2, and 4, respectively. These numbers were determined by dynamic light scattering experiment.

As expected with a higher loading, the 1:12.5 catalyst/surfactant ratio gave the highest yield (96%). We attributed this trend to a higher local concentration of the catalyst under a higher loading. Substrate entering the core has four times the probability of encountering the catalyst when catalyst/surfactant ratio is 1/12.5 than 1/50. In the ICRM-supported gold catalysts, we also observed a similar behavior.

Table 1. Reaction yields at 2 h for the epoxidation reaction of styrene catalyzed by the **4**@ICRM under different conditions.

Entry	Solvent composition	w_0	Catalyst/ surfactant	Yield %
1	1/0	5	1/12.5	52
2	7/1	5	1/12.5	53
3	3/1	5	1/12.5	71
4	1/1	5	1/12.5	96
5	1/1	5	1/25	70
6	1/1	5	1/50	71
7	1/1	10	1/25	85
8	1/1	15	1/25	90

Reaction conditions: catalyst (0.0005 mmol), Styrene (0.150 mmol), (diacetoxy iodo)benzene (0.225 mmol) imidazole, (0.020 mmol) and solvent = chloroform/methanol (2 mL). The reactions conducted for 2 h at room temperature. Yields were calculated by GC-MS.

Effect of w_0

w_0 is the parameter that defines the ratio of water to surfactant ratio in the hydrophilic core. We studied the effect of w_0 on the reaction yields since a change of micro polarity was expected to have a significant effect on the reaction yields. We chose w_0 = 5, 10, and 15 for the study. To our surprise, no difference in reactivity was observed. Increasing the water content increases the number of surfactants per ICRM but at the same time, the catalyst to surfactant ratio remains the same. It is possible that, since the catalyst was at the bulk interface of the ICRM, w_0 did not play any role in the reaction.

Table 2. Reaction yields at 2 h for the epoxidation of various substrates under optimized condition.

		4		**5**	
entry	**Substrate**	**ICRM**	**Free**	**ICRM**	**Free**
1	Styrene	96	100	93	35
2	Stilbene	64	70	84	35
3	Cyclooctene	45	67	93	40
4	1-Decene	10	9	10	15
5	p-vinyl benzoic acid	25	50	13	40
6	3-methyl-3-butene-1-ol	20	30	17	35

Reaction conditions: catalyst (0.0005 mmol), (diacetoxyiodo)benzene (0.225 mmol), substrate (0.150 mmol). Solvent = 1.0 mL methanol + 1.0 mL chloroform. The reaction was conducted at room temperature for 2 h. Yields were calculated by GC-MS.

Substrate study:

We then explored the substrate scope of the reactions with both the encapsulated catalysts. Since the catalysts are close to the hydrophilic core, it would be more accessible to hydrophilic

substrates. This would result in rate acceleration when compared to hydrophobic substrates. Table 2 summarizes the reaction yields of different substrates under optimized condition. The two catalysts showed different behavior under free conditions. Catalyst **4** showed enhanced activity for hydrophobic substrates whereas catalyst **5** showed a similar activity for both the hydrophilic and hydrophobic substrates. Upon entrapment, both the catalysts showed similar trends in the activity. For the catalyst **4,** the activity was slightly lower when compared to its free counterpart. This could be because that catalyst was somewhat protected by cross-linking density. Surprisingly, catalyst **5** showed enhanced activity for hydrophobic substrates compared to its free counterpart. A likely reason is the formation of oxo-bridged Mn-O-Mn dimer by catalyst **5** under free conditions. Upon entrapment, this deactivation pathway is eliminated. The activity trends could be explained by the accessibility of the substrates. Hydrophobic substrates have more access to the catalysts than the hydrophilic substrates. The location of catalyst **5** is more towards the bulk interface than that for the catalyst **4** since the catalyst itself is hydrophobic. Also the hydrophilic substrates tend to stay in the bulk solvent since the reaction solvent is a polar chloroform/methanol mixture.

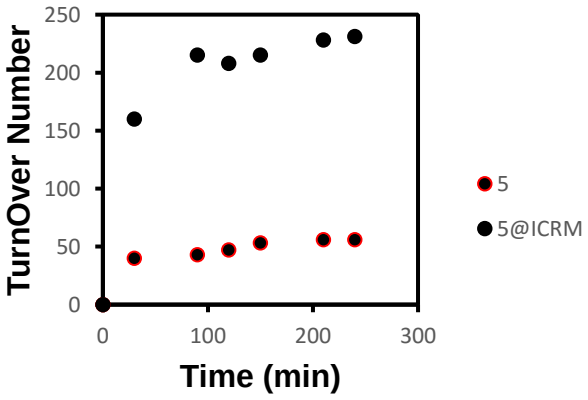

Fig. 3. Plot showing the enhancement of catalyst activity and stability in the epoxidation of styrene upon entrapment of **5** in ICRM (in terms of TON).

Effects of site isolation:

Table 3 summarizes the turnover number of the catalysts after 4 h using iodosobenzene as the oxidant. Catalyst **4** gave similar turn over number upon encapsulation as its free counterpart. This suggests that oxidation was the main deactivation pathway. To our delight, **5** gave 5 times greater turnover number upon encapsulation than its free counterpart. This suggests the catalysts was deactivated both by dimerization and oxidation. Kinetic studies were performed to investigate further the deactivation pathway. Figure 3 shows the kinetic profiles of the free and encapsulated **5**. Clearly, the catalyst lost its activity within 30 minutes of the reaction in the free state. Since entrapped catalyst was precluded from dimerization, it's only deactivation pathway was irreversible oxidation.

Table 3. Turn over number at 4 h for the epoxidation reaction by iodosobenzene.

Catalyst		**Turn over number**
4	free	145
	1/12.5	172
5	free	56
	1/25	231

Reaction conditions: catalyst (0.0005 mmol), iodosobenzene (0.309 mmol), substrate (0.300 mmol). Solvent = 1.0 mL methanol + 1.0 mL chloroform. The reaction was conducted at room temperature for 4 h. Yields were calculated by GC.

Conclusion

In summary, manganese porphyrins catalysts were encapsulated in the core of interfacial cross-linked reverse micelles. The encapsulated catalyst system resembles the natural heme moiety

present in the active site of cytochrome P450 in its structure and function. Since the rate of the reaction was not diffusion-controlled, hydrophobic and hydrophilic substrates showed a similar trend as in the free catalysts. In future work, we will explore the encapsulation of other catalysts and their applications.

Experimental Section

General method

All reagents and solvents were of ACS-certified grade or higher and used as received from commercial suppliers. Routine ^{1}H and ^{13}C NMR spectra were recorded on a Bruker DRX-400 or on a Varian VXR-400 spectrometer. HR-MS mass was recorded on Shimadzu LCMS-2010 mass spectrometer. Dynamic light scattering (DLS) was performed on a PD2000DLS+ dynamic light scattering detector. For the catalysis the products were analyzed on a HP 5890 gas chromatograph equipped with a HP-5 capillary column (30 m × 0.32 mm × 0.25 μm) with a flame ionization detector and SHIMADZU 5050A GC-MS equipped with a HP-5ms capillary column (30 m × 0.32 mm × 0.25 μm). The response factors of each component were determined with standard samples and were used to calculate the conversion and selectivity.

Syntheses

Syntheses of compound **2**[14] was reported in the literature and **3** was reported in the previous chapter 3.

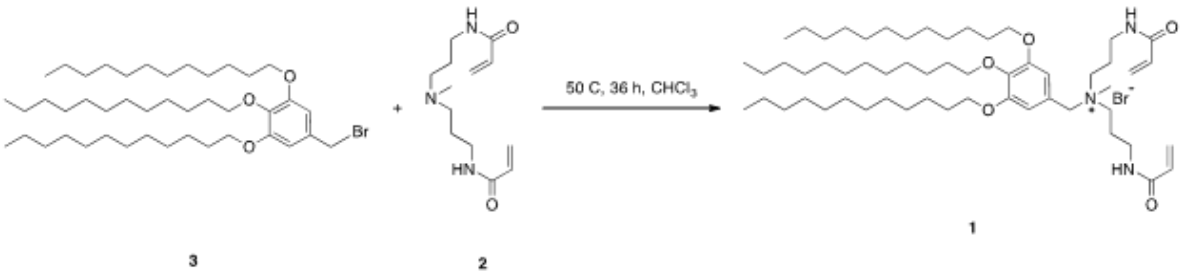

Compound 1: *N*,*N*'-((methylazanediyl)bis(propane-3,1-diyl))diacrylamide (**2**)[1] (0.75 g, 3.0 mmol) was dissolved in solution of compound **3** (2.5 g, 3.5 mmol) in $CHCl_3$ (30 mL). The reaction mixture was stirred at 50 °C for 36 h. The organic solvent was removed *in vacuo.* and the residue was purified by column chromatography over silica gel using CH_2Cl_2 /MeOH=20/1 to 10/1 as the eluent to give white solid (2.43 g, 72 %). ^{1}H NMR (400 MHz, $CDCl_3$, δ): 8.13 (t, *J* = 4.0 Hz, 2H), 6.59 (s, 2H), 6.48-6.44 (dd, *J* = 11.3 Hz and 6.8 Hz, 2H), 6.33-6.30 (dd, *J* = 1.2 Hz and 11.2 Hz, 2H), 5.65-5.63 (dd, *J* = 13.6 Hz and 6.4 Hz, 2H), 4.34 (s, 2H), 3.98 (t, *J* = 4.0 Hz, 6H), 3.61-3.42 (m, 8H), 2.95 (s, 3H), 2.23-2.06 (m, 4H), 1.82-1.72 (m, 6H), 1.50-1.45 (m, 6H), 1.37-1.26 (m, 48H), 0.88 (t, *J* = 4.0 Hz, 9H) ^{13}C NMR (100 MHz, $CDCl_3$, δ):166.72, 153.72, 140.51, 131.03, 126.52, 120.42, 111.16, 73.62, 69.67, 67.37, 59.11, 48.20, 35.88, 31.94, 30.37, 29.77, 29.76, 29.74, 29.71, 29.67, 29.61, 29.50, 29.41, 29.39, 26.16, 26.09, 22.70, 14.13. ; ESI-MS (*m*/*z*): $[M+H]^+$ calcd for $C_{56}H_{102}N_3O_5$, 896.7814; found 896.7819.

Preparation of 4@ICRM and 5@ICRM:

Millipore water (1.8 μL) was added to a solution of **1** (23 mg, 0.02 mmol), **4** (0.5 mg, 0.00048 mmol) in heptane (10 mL) and $CHCl_3$ (0.5 mL). The mixture was hand shaken and sonicated at room temperature for 4 min to give an optically clear solution. After addition of 2, 2-dimethoxy-2-phenylacetophenone (0.5 mg, 0.002 mmol) the mixture was irradiated in a Rayonet photoreactor for ca. 12 h until most alkenic protons were consumed. The organic solvents were removed by rotary evaporation. The residue was dissolved in 0.3 mL chloroform and precipitated upon addition of 10 ml of acetone. It was centrifuged and the residue was washed with methanol/acetone (4 mL/6 mL) 3 times and dried to give 22 mg (98 %).

Millipore water (1.8 μL) was added to a solution of **1** (23 mg, 0.02 mmol), **5** (1 mg, 0.00096 mmol) and p-styrene benzoic acid (0.57 mg, 0.0038 mmol) in heptane (10 mL) and $CHCl_3$ (0.5 mL). The mixture was hand shaken and sonicated at room temperature for 4 min to give an optically clear solution. After addition of 2, 2-dimethoxy-2-phenylacetophenone (0.5 mg, 0.002 mmol) the mixture was irradiated in a Rayonet photoreactor for ca. 12 h until most alkenic protons were consumed. The organic solvents were removed by rotary evaporation. The residue was dissolved in 0.3 mL chloroform and precipitated upon addition of 10 ml of acetone. It was centrifuged and the residue was washed with methanol/acetone (4 mL/6 mL) 3 times and dried to give 22 mg (98 %). and used for photophysical experiments. Absorbance of supernatant liquid was measured and amount of catalyst was measured using calibration graph.

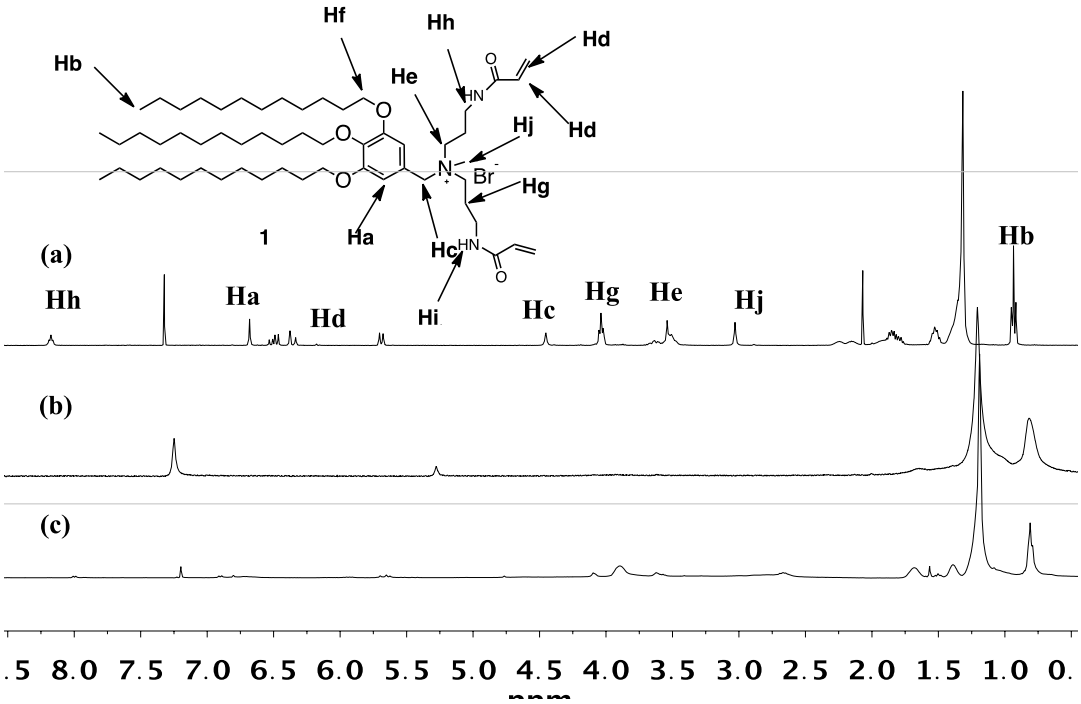

Figure 4. ^{1}H NMR spectra of in $CDCl_3$ (a) **1,** (b) **4**@ICRM and (c) **5**@ICRM

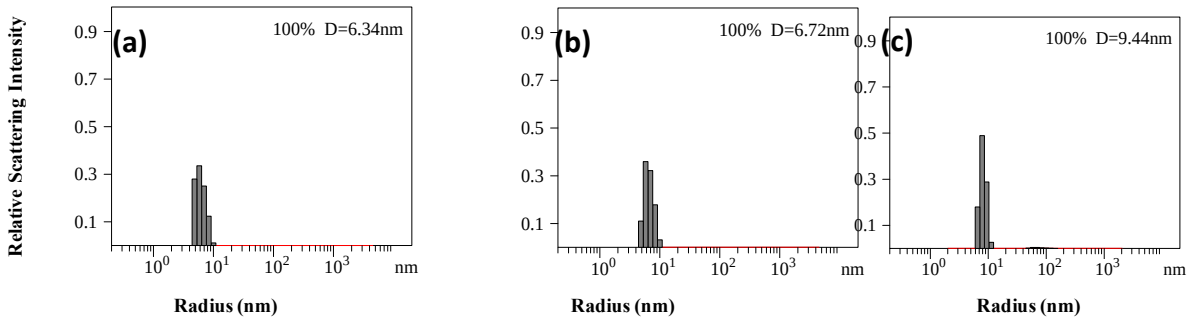

Figure 5. Distribution of the diameters of the nanoparticles in heptane as determined by DLS for **4**@ICRM (a) w_0 = 5 (b) w_0 = 10 and (c) w_0 = 15.

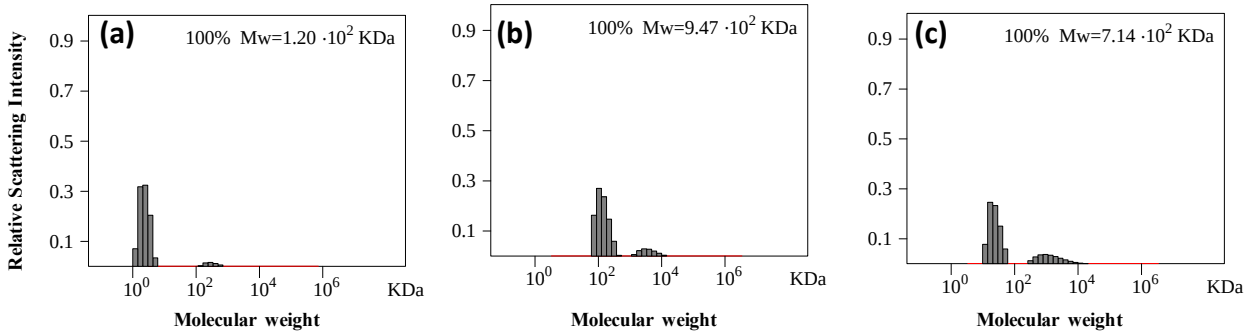

Figure 6. (a) Distribution of the molecular weights of the **4**@ICRMs w_0 = 5 and the correlation curve for DLS. The molecular weight distribution was calculated by the PRECISION DECONVOLVE program assuming the intensity of scattering is proportional to the mass of the particle squared. If each unit of building block for the **4**@ICRM is assumed to contain one molecule of compound **5** (MW = 975 g/mol), and 5 molecules of water (MW = 18 g/mol), the molecular weight of the **4**@ICRM translates to **112** [= 51,000/(975+ 5×18)] of such units. **(b)** Distribution of the molecular weights of the **4**@ICRMs w_0 = 10 and the correlation curve for DLS. The molecular weight distribution was calculated by the PRECISION DECONVOLVE program assuming the intensity of scattering is proportional to the mass of the particle squared. If each unit of building block for the **4**@ICRM is assumed to contain one molecule of compound **1** (MW =

975 g/mol), 10 molecules of water (MW = 18 g/mol), the molecular weight of the **4**@ICRM translates to **801** [= 934000/(8975+10×18)] of such units. **(c)** Distribution of the molecular weights of the **4**@ICRMs w_0 = 15 and the correlation curve for DLS. The molecular weight distribution was calculated by the PRECISION DECONVOLVE program assuming the intensity of scattering is proportional to the mass of the particle squared. If each unit of building block for the **4**@ICRM is assumed to contain one molecule of compound **1** (MW = 975 g/mol) and 15molecules of water (MW = 18 g/mol), the molecular weight of the **4**@ICRM translates to **700** [= 985000/(975+15×18)] of such units.

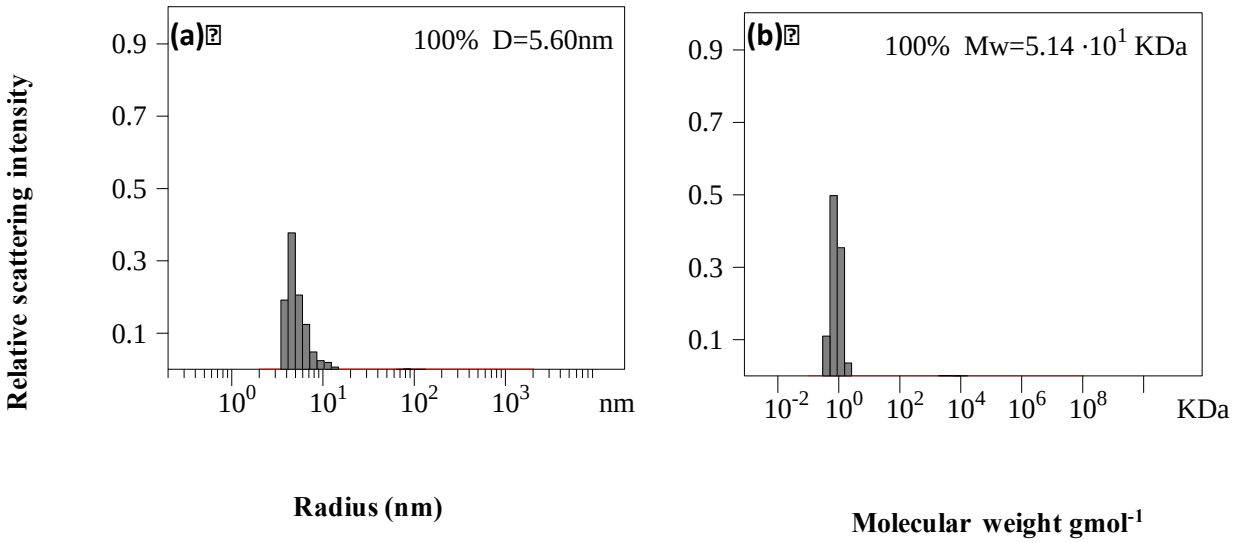

Fig 7. Distribution of the diameters of the nanoparticles in heptane as determined by DLS for **5**@ICRM (a) w_0 = 5. **(b)** Distribution of the molecular weights of the **5**@ICRMs w_0 = 10 and the correlation curve for DLS. The molecular weight distribution was calculated by the PRECISION DECONVOLVE program assuming the intensity of scattering is proportional to the mass of the particle squared. If each unit of building block for the **5**@ICRM is assumed to contain one molecule of compound **1** (MW = 975 g/mol), 10 molecules of water (MW = 18 g/mol), the molecular weight of the **5**@ICRM translates to **81** [= 934000/ (8975+10×18)] of such units.

^{1}H and ^{13}C NMR spectra of compound 1

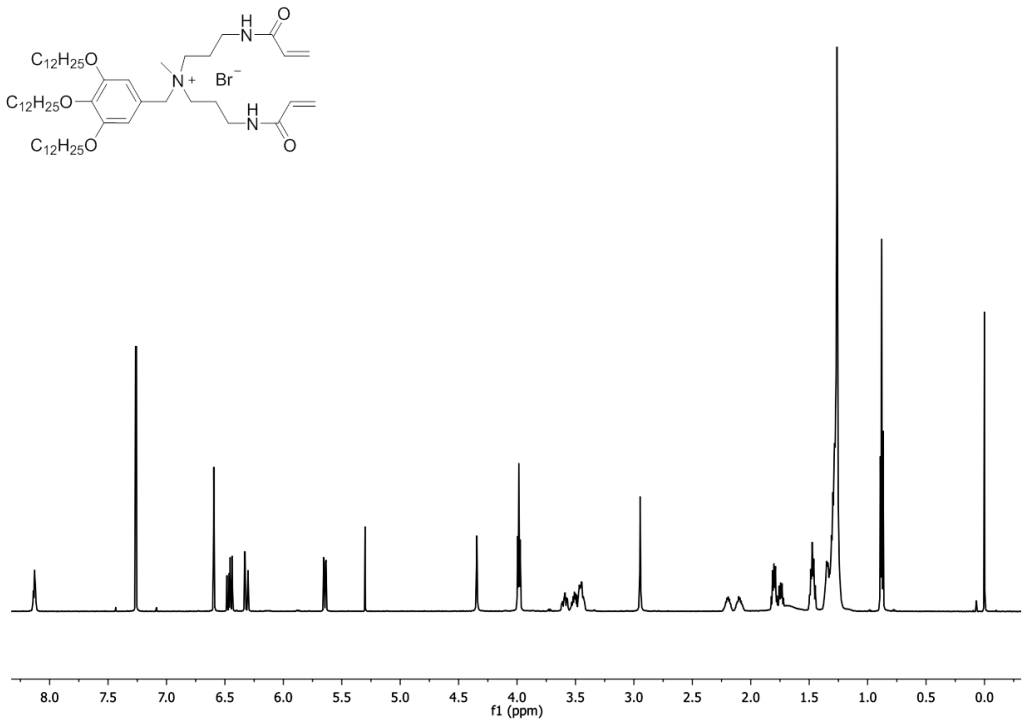

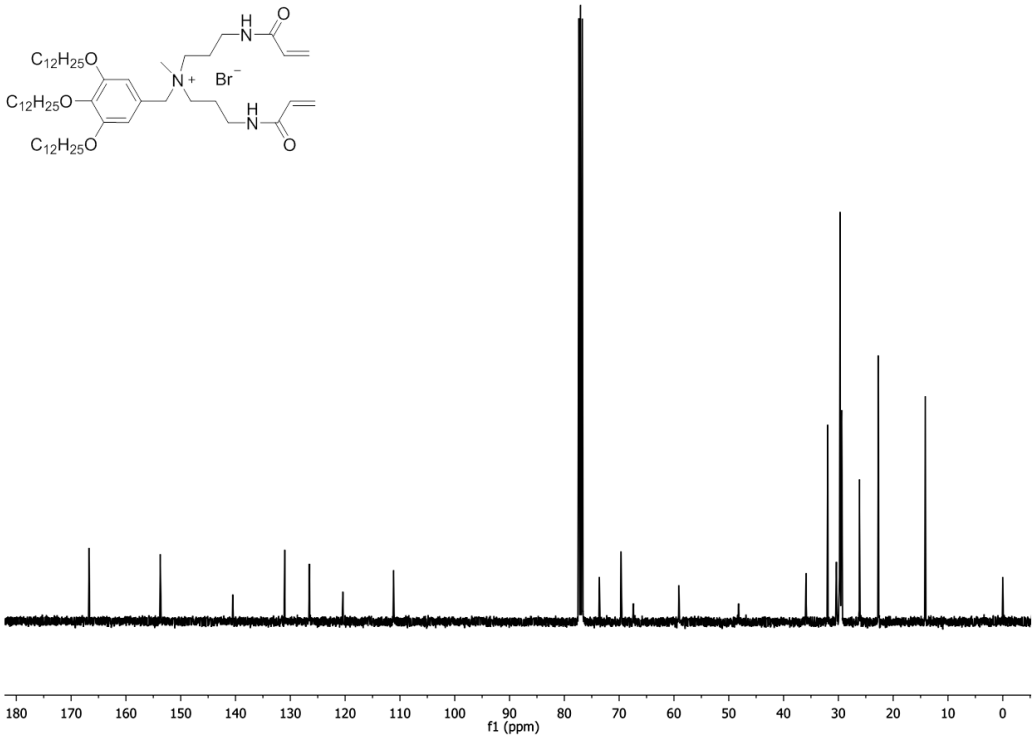

References

1. Helms, B.; Guillaudeu, S. J.; Xie, Y.; McMurdo, M.; Hawker, C. J.; Fréchet, J. M. J., One-Pot Reaction Cascades Using Star Polymers with Core-Confined Catalysts. *Angewandte Chemie International Edition* **2005,** *44* (39), 6384-6387.

2. Chen, Y.-Z.; Chen, P.-Z.; Peng, H.-Q.; Zhao, Y.; Ding, H.-Y.; Wu, L.-Z.; Tung, C.-H.; Yang, Q.-Z., Water-soluble, membrane-permeable organic fluorescent nanoparticles with large tunability in emission wavelengths and Stokes shifts. *Chemical Communications* **2013,** *49* (52), 5877-5879.

3. Tanabe, K. K.; Siladke, N. A.; Broderick, E. M.; Kobayashi, T.; Goldston, J. F.; Weston, M. H.; Farha, O. K.; Hupp, J. T.; Pruski, M.; Mader, E. A.; Johnson, M. J. A.; Nguyen, S. T., Stabilizing unstable species through single-site isolation: a catalytically active TaV trialkyl in a porous organic polymer. *Chemical Science* **2013,** *4* (6), 2483-2489.

4. Huang, Y.; Xu, S.; Lin, V. S. Y., Bifunctionalized Mesoporous Materials with Site-Separated Brønsted Acids and Bases: Catalyst for a Two-Step Reaction Sequence. *Angewandte Chemie International Edition* **2011,** *50* (3), 661-664.

5. Pollak, K. W.; Leon, J. W.; Fréchet, J. M. J.; Maskus, M.; Abruña, H. D., Effects of Dendrimer Generation on Site Isolation of Core Moieties: Electrochemical and Fluorescence Quenching Studies with Metalloporphyrin Core Dendrimers. *Chemistry of Materials* **1998,** *10* (1), 30-38.

6. Srirambalaji, R.; Hong, S.; Natarajan, R.; Yoon, M.; Hota, R.; Kim, Y.; Ho Ko, Y.; Kim, K., Tandem catalysis with a bifunctional site-isolated Lewis acid-Bronsted base metal-organic framework, NH2-MIL-101(Al). *Chemical Communications* **2012,** *48* (95), 11650-11652.

7. Merlau, M. L.; del Pilar Mejia, M.; Nguyen, S. T.; Hupp, J. T., Artificial Enzymes Formed through Directed Assembly of Molecular Square Encapsulated Epoxidation Catalysts. *Angewandte Chemie International Edition* **2001,** *40* (22), 4239-4242.

8. Zhang, S.; Zhao, Y., Facile Synthesis of Multivalent Water-Soluble Organic Nanoparticles via "Surface Clicking" of Alkynylated Surfactant Micelles. *Macromolecules* **2010,** *43* (9), 4020-4022.

9. Zhang, S.; Zhao, Y., Template Synthesis of Subnanometer Gold Clusters in Interfacially Cross-Linked Reverse Micelles Mediated by Confined Counterions. *Langmuir* **2012,** *28* (7), 3606-3613.

10. Zhang, S.; Zhao, Y., Effects of Micelle Properties on the Conformation of Oligocholates and Importance of Rigidity of Foldamers. *The Journal of Organic Chemistry* **2012,** *77* (1), 556-562.

11. Lee, L.-C.; Zhao, Y., Interfacially Cross-Linked Reverse Micelles as Soluble Support for Palladium Nanoparticle Catalysts. *Helvetica Chimica Acta* **2012,** *95* (6), 863-871.

12. Lee, L.-C.; Zhao, Y., Room Temperature Hydroamination of Alkynes Catalyzed by Gold Clusters in Interfacially Cross-Linked Reverse Micelles. *ACS Catalysis* **2014,** *4* (2), 688-691.

13. Lee, L.-C.; Zhao, Y., Metalloenzyme-Mimicking Supramolecular Catalyst for Highly Active and Selective Intramolecular Alkyne Carboxylation. *Journal of the American Chemical Society* **2014,** *136* (15), 5579-5582.

CHAPTER 5. ENHANCEMENT OF CATALYTIC ACTIVITY AND SELECTIVITY OF $Pt(TPPTS)_2Cl_2$ IN INTERFACIALLY CROSS-LINKED REVERSE MICELLES

Premkumar Rathinam Arivalagan and Yan Zhao

Abstract

$Pt(TPPTS)_2Cl_2$ was entrapped in the core of the interfacially cross-linked reverse micelle. It was used to catalyze hydration of hydroxyl alkynes. Activity of the catalyst was compared with that of the free catalyst and the catalyst solubilized in CTAB. Solvent effects, effects of the amount of water, and substrate scope were studied. $Pt(TPPTS)_2Cl_{2@}$ICRM was found to have higher activity and selectivity towards hydrophilic substrates. Inherent advantage of the ICRM over conventional reverse micelle was also demonstrated.

Introduction

Entrapping a catalyst in nano vessel offers protection and control of activity towards substrates. Activity and selectivity of the catalyst have always been important in catalysis. And for a supramolecular chemist, inspiration comes from the enzyme which uses molecular interactions and site isolation for activity and selectivity.[1] In heterogeneous catalysis, selectivity was achieved by trapping the catalyst in a porous material which allows only small molecules to diffuse in.[2-4] But when compared to the homogeneous catalysts, the trapped catalysts in these porous materials tend to have lower activity. Macrocycles were also employed to achieve selectivity but molecules are always in equilibrium with its free counterparts.

Recently, the Zhao group synthesized interfacially cross-linked reverse micelles based on reverse micelle self-assembly using cross-linkable surfactants. This material has many advantages over reverse micelle including enhanced stability irrespective of the solvent and amount of water

in the water pool. It was initially used as a template and soluble support for palladium and gold nanoclusters for catalytic applications.[2-5] It was then used to trap hydrophilic dyes to study the nature of the microenvironment and the location of the entrapped dyes. Site isolation property was then explored in the fourth chapter using manganese porphyrin catalysts known to get deactivated by dimerization under free condition. In this chapter, entrapped catalyst showed enhanced activity in the catalytic epoxidation of alkenes. But the solvent (chloroform/methanol) system that was used did not allow us to investigate selectivity and hydrophobic substrates showed good reactivity than hydrophilic substrates. From the entrapment of dyes and porphyrin catalysts, it was found that catalyst was at the interface and accessible to both the hydrophilic and hydrophobic substrates. We envisioned if the catalyst is very hydrophilic then it would be located in the water pool and would be accessible only to hydrophilic substrates. $Pt(TPPTS)_2Cl_2$ was chosen since it is very hydrophilic due to multiple anionic sulfonates and it is known to catalyze hydration of hydroxyl alkynes. Our aim was to demonstrate that ICRM can concentrate high local concentration of substrates and has selectivity towards hydrophilic substrates.

Results and Discussion:

Entrapment of the catalyst:

Entrapment of the catalyst in the core of the ICRM was performed using the procedure previously reported in the fourth chapter. Briefly, the catalyst with multiple anionic ligands was readily solubilized in reverse-micelle solution of surfactant **1** by electrostatic interaction in a heptane/chloroform mixture. Photo initiator was added followed by photo crosslinking, yielding $Pt(TPPTS)_2Cl_2$@ICRM. It was used for the catalytic study.

Table 1. Reaction yields at 6 h for the hydration reaction of 4-pentyne-1-ol catalyzed by the $PtCl_2(TPPTS)_2$@ICRM under different conditions.

entry	THF/Methanol/Chloroform	w_0	Amount of water eq.	Yield %
1	1/0/0	5	5	24
2	1/0/1	5	5	4
3	0/1/1	5	5	17
4	0/0/1	5	5	trace
5	1/0/0	10	5	37
6	1/0/0	15	5	49
7	1/0/0	5	15	78
8	1/0/0	10	15	100
9	1/0/0	15	15	100
10	1/0/0	15	5	26
11	1/0/0	TBAB	15	0
12	1/0/0	1	15	0
13	DMSO		15	0
14	1/0/0	4	15	50
15	1/0/0	CTAB	15	100

Substrate (0.120 mmol), catalyst (0.001 mmol), 6 h RT. Yields were calculated by ^{1}H NMR using bistrimethylsilylmethane as internal standard. [a]surfactant /catalyst ratio =40/1. [b,c,d]Reaction was performed in reverse micelle condition with TBAB, compound **1** and **4** as surfactants. Entry 13 was performed in DMSO without surfactants.

Solvent effects:

Table 1 summarizes the yields of hydration of 4-pentyne-1-ol under different conditions. Solvents affect the rate of the reactions by either stabilizing or destabilizing the transition state, reactants, and products. In reverse micelles, solvents also influence the distribution of the solute between the mesophase and bulk solvent. A nonpolar solvent increases the distribution of the substrates towards micellar interface which results in a high local concentration of the substrate at the interface. Since water is the reactant in this reaction, using a nonpolar solvent should play a significant role in the kinetics. Four different solvent ratios with different polarity were chosen to study the solvent effects.

The solvent polarity was increased by increasing the amount of methanol in the THF, methanol and chloroform mixture. As expected, increasing the polarity of the solvent decreased the yield of the reaction. When the solvent composition THF/methanol/chloroform was changed from (1/0/0) to 0/1/1, the reaction yield fell from 24% to 17%. At the same time, decreasing the polarity also affected the yield since that would decrease the solubility of water. When the solvent composition THF/Methanol/chloroform was changed from 1/0/1 to 0/0/1, the reaction yield fell from 4% to 0%.

Effect of w_0

w_0 is a parameter defined as the ratio of amount of the water to the amount of surfactant. It determines the size of the water pool in the reverse micelle and ICRM. In this reaction, since water is a reactant, changing the w_0 should have a considerable effect on the activity of the catalyst. As expected, when the w_0 was increased from 5 to 10 and 15, the yield increased from 24% to 37%

and 49% respectively. It can be concluded that increasing the size of water pool increases the amount of water around the catalyst and results in rate acceleration.

Effects of amount of water:

The inherent advantage of ICRM over reverse micelles is its stability irrespective of the parameters like w_0. A highly polar solvent is important for the self-assembly to form, whereas w_0 is important for the monodispersity of the self-assembly. To demonstrate this fact, we changed the amount of water in the reaction. As expected, CTAB was insoluble in THF if the amount of water was reduced to 5 equivalents with respect to the substrate and surfactant **1** was insoluble in THF under any of the given conditions. But ICRM was found to be soluble and stable irrespective of the amount of water. Thus, CTAB formed reverse micelle in THF only when $w_0 = 72$, whereas ICRM was found to be stable even for $w_0 = 0$. However, catalytic activity of the CTAB was found to be equivalent to ICRM which indicates that the catalytic activity is due to the high local concentration of water and substrates.

Table 2. Effects of amount of water.

Entry	Support	Water eq.	Yield %
1	CTAB	10	Precipitation
2	CTAB	30	100
3	**2**	10	Precipitation
4	**2**	30	Precipitation
5	ICRM $w_0 = 15$	10	49
6	ICRM $w_0 = 15$	30	100

Reaction conditions: Substrate (0.120 mmol), catalyst (0.001 mmol), 6 h RT. Yields were calculated by ^{1}H NMR using bistrimethylsilylmethane. surfactant /catalyst ratio =20/1.

Table 2. Substrate study

Reaction yields at 6 h for the hydration reaction of various alkynes catalyzed by the $PtCl_2(TPPTS)_2$@ICRM under different conditions.

Entry	Substrate	CTAB	ICRM	FREE
1	4-pentyne-1-ol	100	100	100
2	3-pentyne-1-ol	100	100	100
3	5-hexyne-1-ol	16	20	100
4	3-nonyne-ol	0	0	100

Reaction conditions: Substrate (0.120 mmol), catalyst (0.002 mmol), 6 h RT. Yields were calculated by ^{1}H NMR using bistrimethylsilylmethane. surfactant /catalyst ratio =20/1.

Substrate study:

Substrates selectivity in the literature is mostly based on either size or shape and reactivity of the functional groups. Recently, Frechet reported polarity mediated selectivity. Substrates with different polarity were programmed to give selective products based on their accessibility to the catalytic site.[6] In this work, since the core of the ICRM is very hydrophilic, entrapping the catalyst in the core makes the catalyst selective towards hydrophilic substrates. Four substrates were chosen, 4-pentyne-1-ol and 5-hexyne-1-ol are terminal alkynes, 3-pentyne-1-ol and 3-hexyne-1-ol are internal alkynes. Under free condition in methanol, all the substrates gave quantitative yields. Interestingly upon entrapment, the reaction yield of 5-hexyne-1-ol dropped down to 16% in yield with CTAB-entrapped catalyst and to 20% with ICRM-entrapped catalyst. For the 3-nonyne-1-ol,

no reaction was observed. These two substrates are hydrophobic and hence they cannot have access to the catalyst entrapped in the hydrophilic core of the CTAB reverse micelles and ICRM.

Conclusion

In conclusion, $Pt(TPPTS)_2Cl_2$ was entrapped in the core of the ICRM and was used to catalyze hydration of hydroxyl alkynes. Catalysts upon entrapment showed good activity due to a high local concentration of water and the substrates at the interface. The inherent advantage of the ICRM over conventional reverse micelle was also demonstrated by varying the amount of water used in the reaction. Finally, the catalyst was found to be highly selective towards hydrophilic substrates.

Experimental Section

General Method

Methanol, methylene chloride, and ethyl acetate were of HPLC grade and were purchased from Fisher Scientific. All other reagents and solvents were of ACS-certified grade or higher, and were used as received from commercial suppliers. Routine ^{1}H and ^{13}C NMR spectra were recorded on a Bruker DRX-400 or on a Varian VXR-400 spectrometer. ESI-MS mass was recorded on Shimadzu LCMS-2010 mass spectrometer. Dynamic light scattering (DLS) was performed on a PD2000DLS+ dynamic light scattering detector.

Syntheses of compound **1**[1] was previously reported.

Preparation of $Pt(TPPTS)_2Cl_2$@ICRM: Millipore water (1.8 μL) was added to a solution of **1** (23 mg, 0.02 mmol), $Pt(TPPTS)_2Cl_2$ (2 mg, 0.00048 mmol) in heptane (10 mL) and $CHCl_3$ (0.5 mL). The mixture was hand shaken and sonicated at room temperature for 4 min to give an

optically clear solution. After addition of 2, 2-dimethoxy-2-phenylacetophenone (0.5 mg, 0.002 mmol) the mixture was irradiated in a Rayonet photo reactor for ca. 12 h until most alkenic protons were consumed. The organic solvents were removed by rotary evaporation. The residue was dissolved in 0.3 mL chloroform and precipitated upon addition of 10 ml of acetone. It was centrifuged and the residue was washed with methanol/acetone (4 mL/6 mL) 3 times and dried to give 22 mg (98 %).

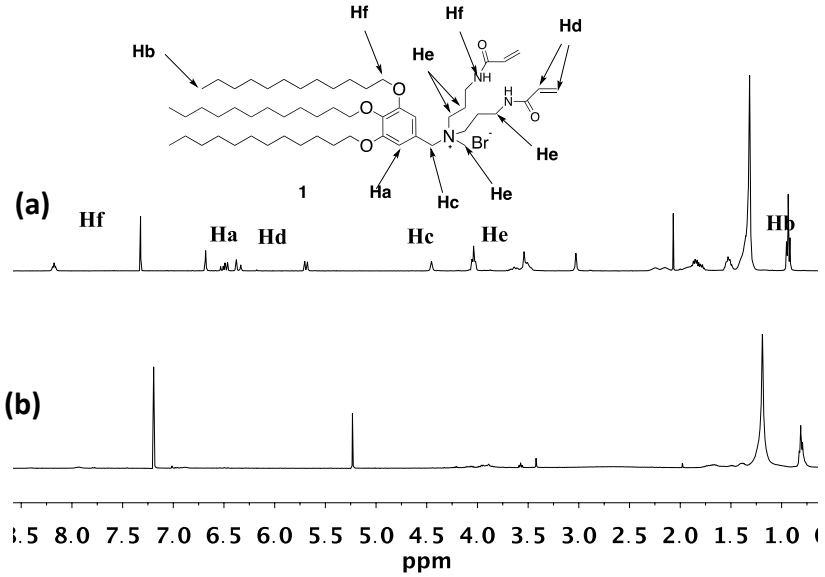

Figure 1. ^{1}H NMR spectra of (a) **1** and (b) $Pt(TPPTS)_2Cl_2$@ICRM (red).

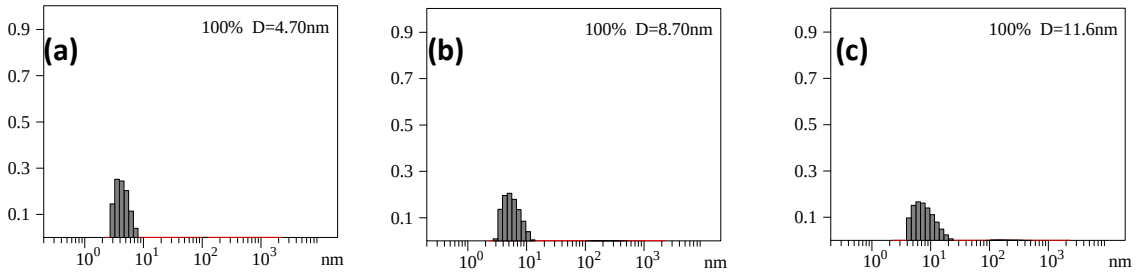

Figure 2. Distribution of the diameters of the nanoparticles in heptane as determined by DLS for $PtCl_2(TPPTS)_2$@ICRM (a) w_0 = 5 (b) w_0 = 10 and (c) w_0 = 15.

References

1. Merlau, M. L.; del Pilar Mejia, M.; Nguyen, S. T.; Hupp, J. T., Artificial Enzymes Formed through Directed Assembly of Molecular Square Encapsulated Epoxidation Catalysts. *Angewandte Chemie International Edition* **2001,** *40* (22), 4239-4242.

2. Lee, L.-C.; Zhao, Y., Interfacially Cross-Linked Reverse Micelles as Soluble Support for Palladium Nanoparticle Catalysts. *Helvetica Chimica Acta* **2012,** *95* (6), 863-871.

3. Lee, L.-C.; Zhao, Y., Room Temperature Hydroamination of Alkynes Catalyzed by Gold Clusters in Interfacially Cross-Linked Reverse Micelles. *ACS Catalysis* **2014,** *4* (2), 688-691.

4. Lee, L.-C.; Zhao, Y., Metalloenzyme-Mimicking Supramolecular Catalyst for Highly Active and Selective Intramolecular Alkyne Carboxylation. *Journal of the American Chemical Society* **2014,** *136* (15), 5579-5582.

5. Zhang, S.; Zhao, Y., Template Synthesis of Subnanometer Gold Clusters in Interfacially Cross-Linked Reverse Micelles Mediated by Confined Counterions. *Langmuir* **2012,** *28* (7), 3606-3613.

6. Scroggins, S. T.; Chi, Y.; Fréchet, J. M. J., Polarity-Directed One-Pot Asymmetric Cascade Reactions Mediated by Two Catalysts in an Aqueous Buffer. *Angewandte Chemie International Edition* **2010,** *49* (13), 2393-2396.